

ALMA MATER STUDIORUM · UNIVERSITÀ DI
BOLOGNA

SCUOLA DI INGEGNERIA E ARCHITETTURA

CORSO DI LAUREA MAGISTRALE IN INGEGNERIA ENERGETICA

TESI DI LAUREA IN

TECNOLOGIE INNOVATIVE PER LA PRODUZIONE, IL TRASPORTO E
L'ACCUMULO DELL'ENERGIA ELETTRICA M

**MELANIN BIOPIGMENTS FOR EMERGING SUSTAINABLE
TECHNOLOGIES: OPTICAL ABSORPTION AND
ELECTRICAL RESPONSE**

RELATORE:
**Chiar.mo Prof. Ing.
Davide Fabiani**

CANDIDATO:
Matteo Camaggi

CORRELATORI:
**Prof. Clara Santato
Ing. Eduardo Di Mauro**

SESSIONE III
ANNO ACCADEMICO 2016/2017

Contents

1	Introduction	7
1.1	Chemical Aspects	8
1.1.1	Notions on Polymers	8
1.1.2	Molecular Aspects of Melanins	10
1.2	Electrical and Optical Aspects	14
1.2.1	Notions of Solid State Band Gap Theory	14
1.2.2	Dye-Sensitized Solar Cells Structure and Operating Principle	18
1.2.3	Melanin Electrical and Optical Properties	24
1.3	UV-Visible Absorption Properties of Polymers Blended with Melanins	29
1.4	Biodegradability Aspects	31
2	Experimental and Methods	35
2.1	Electrical Properties	35
2.1.1	Substrate Fabrication	35
2.1.2	Melanin Deposition	38
2.1.3	Electrical Measurements	43
2.2	UV-Visible Absorption	45
2.2.1	Sample Fabrication	45
2.2.2	UV-Visible Absorption Analysis	51
2.2.3	UV Aging Chamber	54
2.3	Biodegradability Test	56
2.3.1	Experimental Setup	56

2.3.2	Analysis Procedure	58
3	Results and Discussion	63
3.1	Electrical Response	63
3.2	UV-Visible Absorption	69
3.2.1	Effects of Polymer, Additives and their Concentration .	69
3.2.2	UV Exposure Effects	90
3.3	Biodegradability Analysis	93
4	Conclusions and Perspectives	103

Abstract

Le melanine sono biopigmenti di colore marrone-nero presenti in natura comunemente nei mammiferi (ma anche nelle seppie, in funghi e alghe), notoriamente conosciute come le responsabili della colorazione della pelle e dei capelli. Le loro interessanti proprietà, come fotoprotezione, conduttività elettrica e chelazione metallica, hanno suscitato un grande interesse da parte dei gruppi di ricerca per comprenderne eventuali applicazioni in campo tecnologico. Nell'ambito del progetto di seguito illustrato, le proprietà di conduzione e foto-sensibilizzazione della melanina sono analizzate sia da un punto di vista elettrico, utilizzando la melanina come semiconduttore tra due elettrodi di oro a differenti voltaggi in condizioni di buio e di irraggiamento, sia da un punto di vista di affinità con polimeri, studiando se la proprietà di assorbimento della radiazione nell'intervallo UV-visibile possa essere sfruttata come filtro UV con particolare interesse nel settore del packaging. Inoltre, uno studio sulla biodegradabilità della melanina è stato affrontato, per verificare se gli standard normativi per definire la molecola come biodegradabile siano effettivamente rispettati.

Chapter 1

Introduction

The project described in this thesis has been developed at the Engineering Physics Department of *École Polytechnique de Montréal* in collaboration with Prof. Clara Santato. One of the main topic of research of the group is the study of the properties melanin, an organic biopigment, which has attracted more and more interest in the last years for promising use in technological applications.

Melanin is an ubiquitous biopolymer commonly found in mammals, bird feathers, cuttlefishes, squids, octopuses, but also plants, fungi and algae. Eumelanin and pheomelanin are the two common forms of melanin in human beings and originate from melanocytes in the basal stratum of the skin. The former is a brown-black pigment while the latter is red. This coloration arises from the different building block monomers taking part to the polymerization process: indole-units and benzothiazine-units respectively in eumelanin and pheomelanin. It is well known that the concentration of melanins in the skin determines its color. The level of UV radiation is the main factor in determining this phenomenon: for example, people who live close to the equator developed a dark constitutive, photoprotective, eumelanin-rich pigmentation to protect themselves from the high UVA and UVB loads. On the other hand, populations who live close to the poles, have a light constitutive pigmentation to promote seasonal UVB-induced photosynthesis of vitamin D₃.¹



Figure 1.1: *Example on natural presence or absence of melanins in the hair.*

Particularly, eumelanin features fascinating optical, electronic and chemical properties such as broadband UV-vis absorption, photoprotection, mixed protonic-electronic transport, resistive switching, metal chelation and radical scavenging.

It is important to consider that the study on this field is in continuous evolution, therefore the definitions and the properties described in this thesis are actually the state of the art, but it is possible that some of them would be proved wrong or integrated with new models in the future.

1.1 Chemical Aspects

1.1.1 Notions on Polymers

In order to understand better the processes and the topic of the following project, the main properties and behavior of polymers are summarized.

First of all, a *polymer* is a compound made up from many single units called *monomers*, which are the repetitive building blocks in a polymer chain. When two monomers are coupled they are known as *dimers*, when there are a

few units added together the system is called *oligomer*. For example, regarding the synthetic polymers, *acetylene* monomer is repeated to obtain *polyethylene*, or *poly- ϵ -caprolactone* is the polymer formed by the monomer *ϵ -caprolactone*. The physical properties of monomers are different from their macroscopic counterparts.

The process of formation of the polymers from monomer units is known as *polymerization*. The physical characteristics of polymer materials depend not only on the molecular weight and shape, but also on molecular structure:

- *Linear* polymers, with Van der Waals bonding between chains (for example polyethylene)
- *Branched* polymers, in which the chain packaging efficiency is reduced compared to linear polymers, leading to a lower density compared to the linear ones
- *Cross-linked* polymers, in which chains are connected by covalent bonds. Often achieved by adding atoms or molecules that form covalent links between chains. Many rubbers have this structure
- *Network* polymers, 3D network made from trifunctional monomers

It is possible to find polymers (or even monomers) with the same composition, but different atomic arrangements: this behavior is called *Isomerism*, which can modify the physical properties of the molecule. It is possible to distinguish two types of isomerism:

1. *Stereoisomerism*: atoms are linked together in the same order, but can have different spatial configuration (Figure 1.2), defined as:
 - i) *Isotactic* configuration, if all side groups R are on the same side of the chain
 - ii) *Syndiotactic* configuration, if side groups R are alternate sides of the chain
 - iii) *Atactic* configuration, if there is a random orientation of groups R along the chain

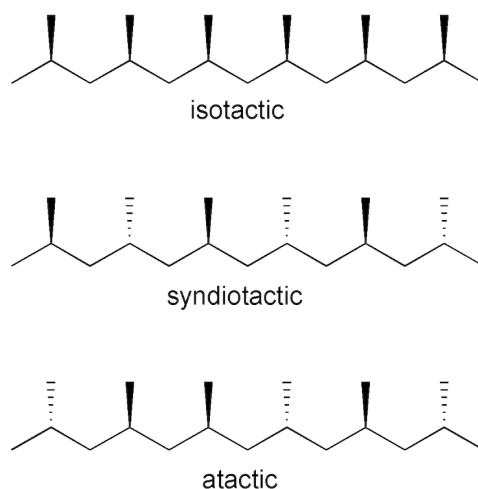


Figure 1.2: *Three types of Stereoisomerism*

- Geometrical Isomerism:* a form of isomerism displayed by unsaturated or ring compounds where rotation about a carbon bond is restricted. It is defined *cis*-configuration when the bounds are on the same side of the molecule, and *trans*-configuration if they are on opposite sides.

It is also possible to define *Copolymers* as polymers in which there is not a single type of monomers, but at least two different types of monomers.

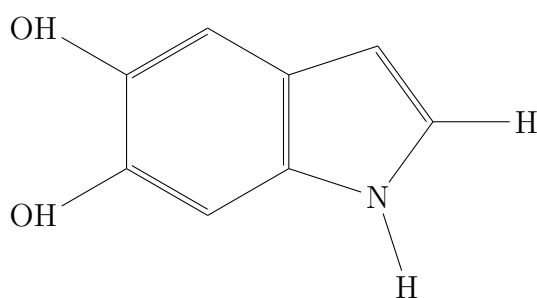
1.1.2 Molecular Aspects of Melanins

Melanins are pigments of diverse structure and origin derived by the oxidation and polymerization of tyrosine (one of the twenty-two amino acids which the cells use to build proteins) in animals or phenolic compounds in lower organisms.

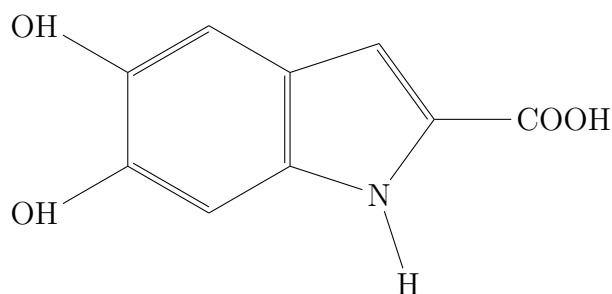
As mentioned before, eumelanins are the black to brown insoluble group of melanin pigments derived in part from the oxidative polymerization of L-dopa via 5,6-dihydroxyindole intermediates.² It is possible to find examples of natural eumelanins (like Sepia Melanin contained in the ink sac of a cuttlefish or in human black hair), but there are also synthetic ones. Since the early study of this pigment, synthetic eumelanin featuring physicochemical

properties of the natural one has been successfully synthesized.

Eumelanin consists of two building blocks show in the following structures:



5,6-dihydroxyindole (DHI).



5,6-dihydroxyindole-2-carboxylic acid (DHICA).

These two building blocks can polymerize into structurally different eumelanins due to the presence of several molecular sites of the monomers. The presence of two building blocks, different sites for polymerization and redox states (as shown in Figure 1.3) co-existing in the pigment results in the chemical heterogeneity of eumelanin.³

The process of polymerization of eumelanins can be summarized by the Figure 1.4: in human melanocytes, eumelanin synthesis involves enzymatic oxidation of tyrosine or dopa to give dopachrome, which undergoes isomerization in presence of the enzyme *Tyrp2* to DHICA. In absence of the enzymatic assistance, a spontaneous decarboxylation occurs, therefore DHI is produced instead of DHICA. For that reason, while natural melanins con-

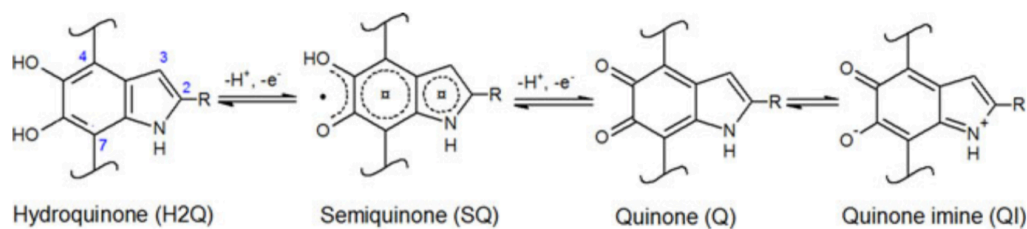


Figure 1.3: Redox forms of DHI and DHICA (R is $-H$ in DHI and $-COOH$ in DHICA): hydroquinone (H2Q), semiquinone (SQ), quinone (Q) and quinone imine form (QI). The numbers (2,3,4,7 on H2Q) indicate the different molecular sites.³

sists of DHICA-derivated units of more than 50%, synthetic dopa melanin contains mainly DHI, with only 10% of DHICA.⁴

Currently, Prof. Pezzella's group⁵ has access to a method for fabricating powder of solely DHI and DHICA monomers building blocks. This is paving the way toward the elucidation of the biopolymer structure in correlation with its optical properties.

The polymerization mechanism of the two building block monomers during the initial stage of oxidative polymerization are different for DHI and DHICA melanin. TEM images of DHICA polymers taken after a reaction time of two hours revealed relatively large elongated structures that are more than 100 nm long and significantly different from the onion-like aggregates with an approximate diameter of 50 nm that were generated by the DHI polymer and other typical eumelanins. The presence of carboxyl groups in the DHICA building blocks causes DHICA to polymerize into non-planar structures, differently from the DHI case. The negative charge, possibly present in the deprotonated carboxyl groups, can induce a twist in the polymer chain, leading to rod-shaped assemblies in DHICA-melanins, while DHI-melanins (composed of solely DHI monomers) show a π -stacking planar structure as it is possible to observe in Figure 1.5.^{3,4}

Nevertheless, nowadays the second level structure organization of melanin is still not clear. There is not a common agreement among the different research groups on this topic, therefore the real structure of the polymer is probably the biggest challenge in the scientific community.

Therefore, the great chemical and geometrical disorder (due to the different

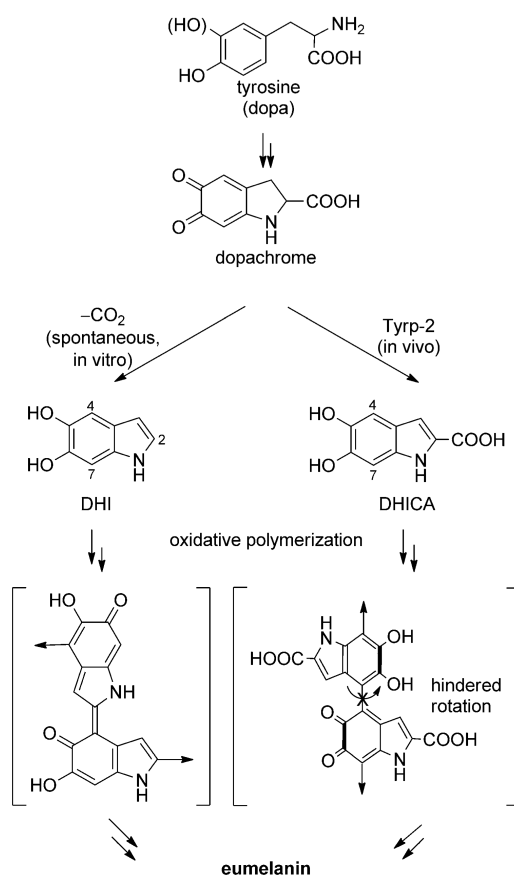


Figure 1.4: Scheme of eumelanin synthesis process.⁴

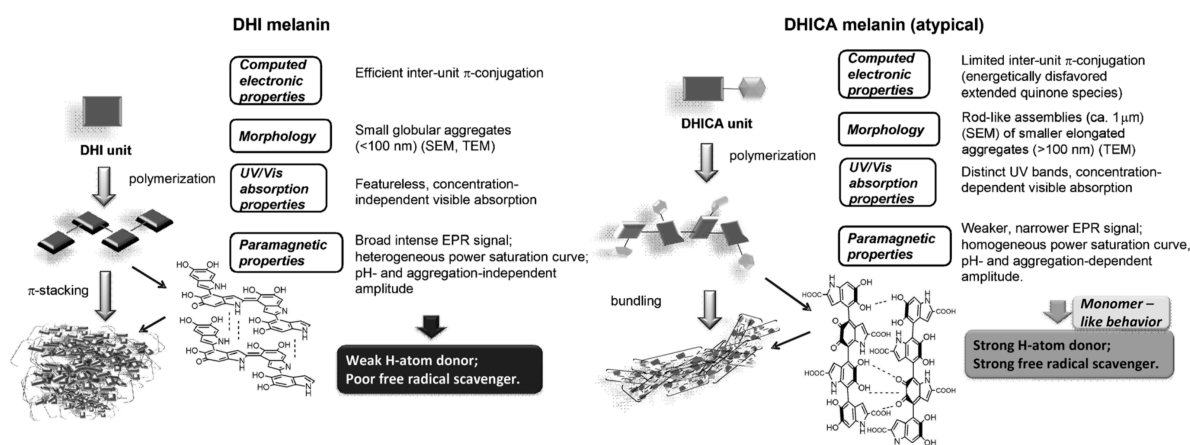


Figure 1.5: Different supramolecular organization of DHI and DHICA melanins.^{3,4}

number and ratio of DHI and DHICA monomers and different polymerization sites in each sheet) leads to the presence of many chemically different species which are the responsible of the properties listed above. In this thesis, the properties of photoconductivity, broadband absorption, photoprotection and biodegradability are investigated.

1.2 Electrical and Optical Aspects

1.2.1 Notions of Solid State Band Gap Theory

Electrical and optical properties of materials (i.e. photoconduction and optical absorption) are closely connected because they depends on the electronic structure of the materials, thus on the position and the type of atoms in the material.

Advanced quantum mechanics provides the motion and energy states of electrons in periodic lattices, which differ from those of a hydrogen atoms. For instance, in hydrogen atoms the Schrödinger Equation is solved taking the potential energy as the contribution of the electric and centrifugal potential. This effective potential is a central one, means that it depends only on the absolute value of the binding distance. This turns out into a system of discrete energy level for the electron: the ground state and the excited states form the well known hydrogen atom spectrum. The excitation to the higher energy levels is then triggered by the absorption of a photon with a given frequency ν and energy $h\nu$.

In structures like crystals, the Schrödinger Equation is periodic. Periodicity naturally comes out from the definition of a crystal as the combination of lattice and basis. The lattice is an ensemble of point that appears to have the same structure and orientation from each point of the lattice. To each point of the lattice a basis of atoms is associated. Solutions to the periodic equation brings about periodic wavefunctions and eigenvalues $E(\bar{k})$ (energy states) dependent on a continuum set of wavenumber \bar{k} .

The tight binding model in approximation of first neighbors predicts the energy levels to be so dense and packed in k to be assumed as a continuum

and a model of electronic energy bands is thus assumed. For example, in a silicon crystal there are approximately 10^{23} *atoms/cm*⁻³, so that the individual energy levels are no longer distinguishable from each other and thus form broad energy ranges. The width of the energy bands is a consequence of how strong the interatomic interactions are.

An important energy level in solids is *Fermi Level*, (E_f) which is defined as the energy of the highest occupied level at $T = 0$ K. In a probabilistic view, at that temperature, the probability to find occupied energy states with energy $E < E_f$ is 1, while it is 0 for $E > E_f$. When $T > 0$ K, the probability (P) that an electron will occupy a level at energy E at the temperature T is given by the *Fermi-Dirac* distribution:

$$P(E, T) = \frac{1}{1 + \exp\left(\frac{E - E_f}{kT}\right)} \quad (1.1)$$

where k is the Boltzmann constant. Therefore from the Equation (1.1) it is possible to understand that the probability to find an electron in states with $E > E_f$ increases with the temperature T .

All the important energy levels are the following (and summarized in Figure 1.6):

- *Valence Band*, E_v : the highest filled band at $T = 0$ K
- *Conduction Band*, E_c : the lowest empty band at $T = 0$ K
- *Ionization Energy*, E_i : energy to bring an electron from the valence band to the vacuum
- *Bond Energy*, E_b : energy to bring an electron from the valence band to the Fermi level
- *Extraction Potential*, Φ : energy per unit of charge to remove an electron from the Fermi level to the vacuum. It is more often used the *Work Function*, that is the energy of extraction, $e\Phi$
- *Electron Affinity*, χ : energy between the vacuum level and the conduction band edge. It defines either the Escape Condition of an electron

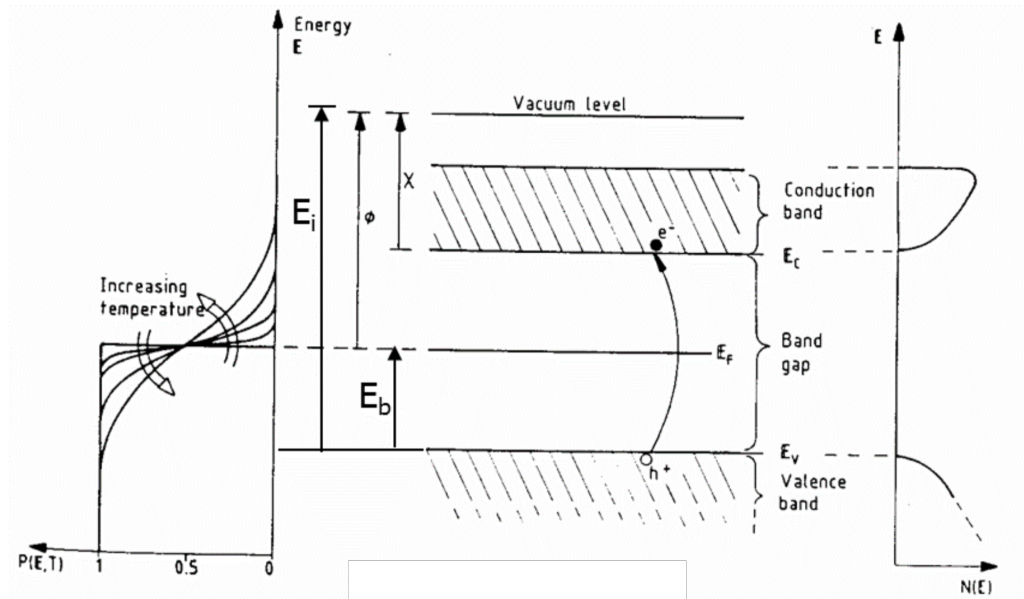


Figure 1.6: Important energetic quantities for the energy levels which an electron can approach.

from a negatively charged atom or the energy released when an electron is captured by a neutral atom.

The electronic band structure is an energy scheme that allows to describe the conductivity of conductors, insulators and semiconductors, graphically explained also in Figure 1.7:

- *Conductors*, such as metals which, with their metal bonding, are characterized by conductivity based on free electrons. In conductors, the valence band is either not fully occupied with electrons, or the filled valence band overlaps with empty conduction band. In general, both states occur at the same time, the electrons can therefore move inside the partially filled valence band or inside the two overlapping bands. In conductors there is no band gap between the valence band and the conduction band and thus, the Fermi level E_f is placed in the valence band and they need a very small energy to bring the electrons in the vacuum level (work function $e\Phi$ really small), so to bring them available for the conduction.

- *Insulators*, materials with no free charge carriers and, consequently, they are non-conductive. In insulators the valence band is fully occupied with electrons due to the covalent bonds. The electrons can not move because they are trapped between the atoms. To achieve a conductivity, electrons from the valence band have to move into the conduction band, crossing the band gap between them. Therefore, in insulators, only with a considerable energy expenditure ($E > 9 \text{ eV}$) the band gap can be overcome.
- *Semiconductors*, solids whose conductivity behavior is intermediate between that of conductors and insulators. Unlike metals, the conductivity increases with the rising of temperature because it leads to broken bonds and free electrons are generated. Even in semiconductors there is a band gap, but compared to insulators it is so small ($E \simeq 1 \text{ eV}$) that even at room temperature electrons from the valence band can be lifted into the conduction band. The electrons can move freely and act as charge carriers. In addition, each electron also leaves a hole in the valence band behind, which can be filled by other electrons in the valence band. Thus one gets wandering holes in the valence band, which can be viewed as positive charge carriers. There are always pairs of electrons and holes, so that there are as many negative as positive charges, the semiconductor crystal as a whole is neutral. An undoped semiconductor is known as intrinsic semiconductor and the number of charge carriers (electron with $E \geq E_g$) depends on the temperature T with the relation $n = n_0 \exp(-\frac{E_g}{kT})$. At a certain temperature an equilibrium is arranged between the electrons promoted to the conduction band and the electrons recombining with holes. With the increase of temperature, the number of electrons that can leap the band gap is increased with positive effects on the conductivity.

When the couple hole-electron is generated (*Exciton* state), it is necessary to bring the electrons and holes towards two different electrodes to avoid recombination of them: this separation is obtained by an electric field. Since the electrons always assume the energetically lowest state,

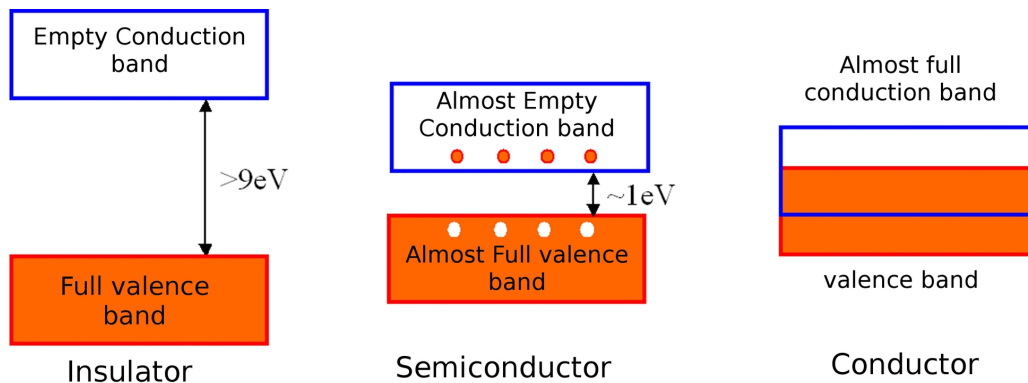


Figure 1.7: Band gaps configuration for conductors, semiconductors and insulators.

they recombine with the holes if there is no energy supply.

It is important to notice that the bands theory is valid only for crystalline solids, but when the structure of the material lacks of long range periodicity, only localized electronic orbitals are present. In this case, the gap is considered between the *Lowest Unoccupied Molecular Orbital*, *LUMO* and the *Highest Occupied Molecular Orbital*, *HOMO*.

The solar cells contain usually two materials: metals (conductors) as electrodes and semiconductors as the responsible of light absorption and generation of mobile charge carriers.

The utilization of melanin in some particular configurations of solar cells (like *Dye Sensitized Solar Cells*, *DSSC*) was investigated in order to replace the ruthenium dye currently the most used one.

1.2.2 Dye Sensitized Solar Cells Structure and Operating Principle

The dye-sensitized solar cell contains five fundamental components as shown in Figure 1.8:

- a mechanical support coated with Transparent Conductive Oxide
- the semiconductor film, usually TiO_2 , due to its several advantages. It is low cost, widely available and non-toxic

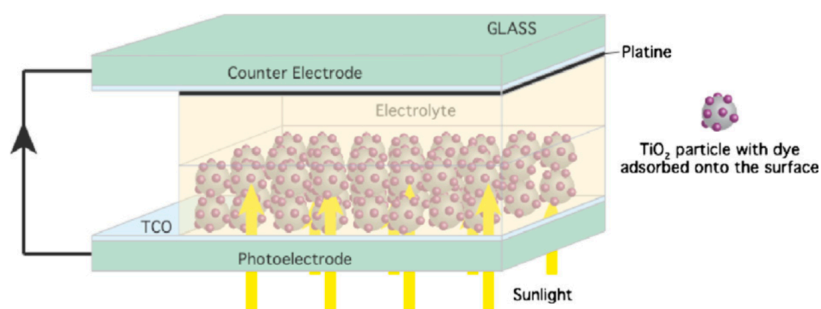


Figure 1.8: Representation of a dye-sensitized solar cell.⁹

- a sensitizer adsorbed onto the surface of the semiconductor. Ruthenium complexes were employed as sensitizer since Grätzel's article in 1991⁸, and still now they are the most commonly employed sensitizers. Recent studies with the aim to replace the common based ruthenium sensitizer with extract natural dyes were born, due to the advantageous features that they could offer, such as non-toxicity and complete biodegradation
- an electrolyte containing a redox mediator, commonly triiodide/iodine is used
- a counter electrode capable of regenerating the mediator, like platinum.

The first operating step is the absorption of a photon by the sensitizer, leading to the excited sensitizer which injects an electron into the conduction band of the semiconductor, leaving the sensitizer in the oxidized state. The injected electron flows through the semiconductor network to arrive at the back contact and through the external load to the counter electrode to reduce the redox mediator, which in turn regenerates the sensitizer. The complete circuit is shown in Figure 1.9, which also provide informations about energy levels.

The following equations explain the chemical behavior of the photosensit-

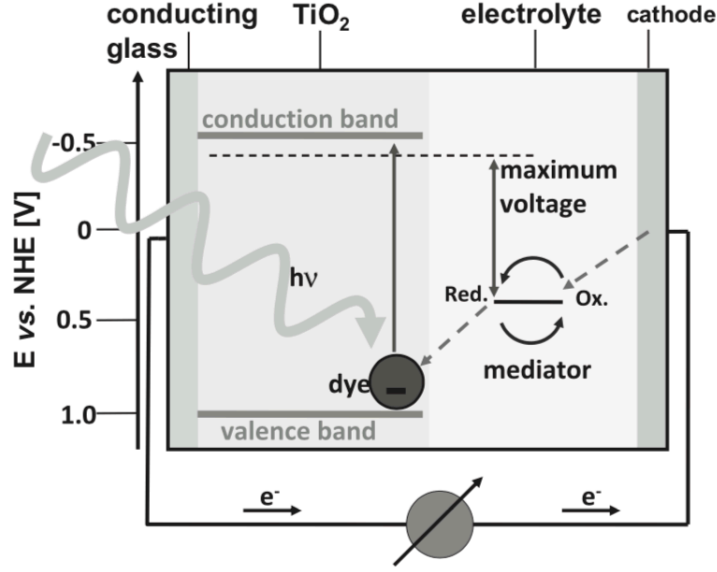
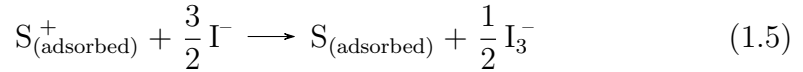
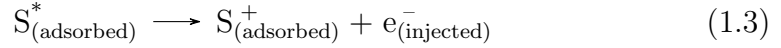
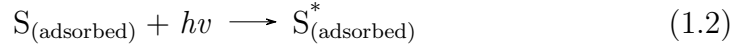


Figure 1.9: Operating principle and energy level diagram of dye-sensitized solar cell.⁹

ivity and electron transfer in the cell:



where S^* and S^+ are respectively the excited and the oxidized state of the sensitizer.

Some undesirable reactions result in losses in the cell efficiency. They are recombinations of the injected electrons either with oxidized sensitizer or with the oxidized redox couple at TiO_2 surface.

The total efficiency of a dye-sensitized solar cell depends on optimization and compatibility of each of these constituents, in particular on the semiconductor film along with the dye spectral responses. A very important factor is the high surface area and the thickness of the semiconductor film which leads to increased dye loading.

It's also important to specify some fundamental parameters to describe the cells performance like IPCE and η .

The incident monochromatic photon-to-current conversion efficiency (IPCE) allows to compare the light-harvesting performance of sensitizers in devices with the same architecture. It is defined as the number of electrons generated by light in the external circuit divided by the number of incident photons as a function of excitation wavelength.

$$\begin{aligned} IPCE(\lambda) &= \frac{\textit{Photocurrent density}}{\textit{Wavelength} * \textit{PhotonFlux}} = \\ &= LHE(\lambda) \phi_{inj} \eta_{coll} \end{aligned} \quad (1.6)$$

where $LHE(\lambda)$ is the light-harvesting efficiency at wavelength λ , ϕ_{inj} is the quantum yield for electron injection from the excited sensitizer in the conduction band of the TiO_2 , and η_{coll} is the efficiency for the collection of electrons.

The overall conversion efficiency η of a solar cell is determined by the photocurrent density (J_{sc}), the open circuit potential (V_{oc}), the fill factor (FF) of the cell and the intensity of the incident light (I_s).

$$\eta_{global} = \frac{J_{sc} V_{oc} FF}{I_s} \quad (1.7)$$

The open circuit voltage is determined by the energy difference between the Fermi level of TiO_2 and the Nernst potential of the redox couple in the electrolyte, as shown in Figure 1.9.

$$V_{oc} = \frac{kT}{q} \ln\left(\frac{\eta \phi_0}{n_0 k_{et} [I_3^-]}\right) \quad (1.8)$$

It is possible to observe from the Equation (1.8) that the open circuit potential is influenced by the quantum yield of photogenerated electron (η) for given incident flux (ϕ_0), by the electron density on the conduction band of TiO_2 in the dark (n_0) and by the recombination rate for the given triiodide concentration (k_{et}).

However, it was experimentally verified that V_{oc} for various sensitizers is

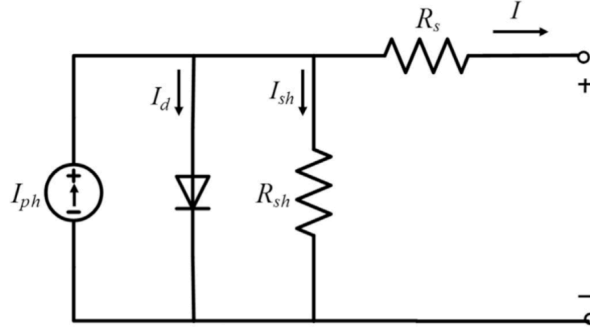


Figure 1.10: Schematic equivalent circuit of a solar cell.¹⁰

smaller than the difference between the conduction band edge and the redox couple, due to the competition between electron transfer and recombination mechanisms. It is important the rate of these phenomena for the design of efficient sensitizers, thus to improve the device.

J_{sc} could be calculated by the Equation (1.9), through the integration of the product of IPCE and incident photoflux (ϕ_0) over the spectral distribution:

$$J_{sc} = e \int IPCE(\lambda) \phi_0(\lambda) (1 - r(\lambda)) d\lambda \quad (1.9)$$

where e is the elementary charge and $r(\lambda)$ is the incident light loss.

The fill factor (FF) is defined as the ratio of the maximum power obtained with the device and the theoretical maximum power ($P_{th} = J_{sc} * V_{oc}$). This parameter is associated with the electron transfer process and internal resistance of dye-sensitized solar cells. There are a wide variety of equivalent circuits, such as the one illustrated in Figure 1.10. The study of these circuits shows that FF can be optimized by minimizing internal series resistance R_{sh} .

The Figure 1.10 shows the single diode model, largely used for silicon cells, and also applicable to dye-sensitized solar cells, in which the diode-like behavior is originated from charge transport at the TiO_2 / dye/ electrolyte interface. It is possible to write a relationship between the external current I and the voltage of the cell as:

$$I = I_{ph} - I_0 \left(e^{\frac{-q(V-IR_s)}{mk_bT}} - 1 \right) + \frac{V - IR_s}{R_{sh}} \quad (1.10)$$

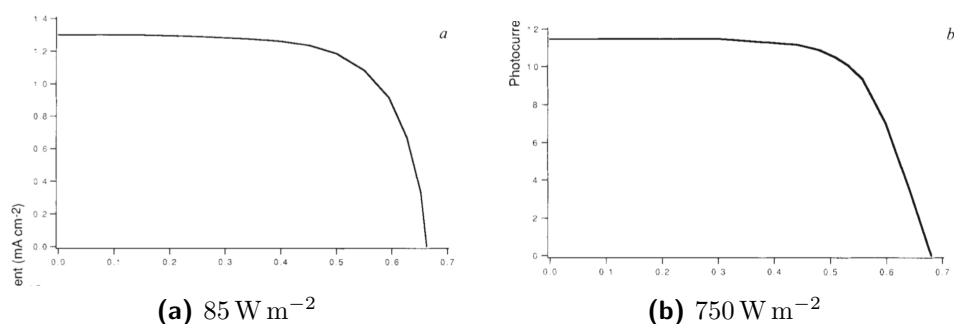


Figure 1.11: Current-voltage characteristic in a DSSC in different illumination conditions.¹⁰

where I_{ph} is the photogenerated current density, I_0 is the dark saturation current density, m the ideal factor, R_s the series resistance, R_{sh} the shunt resistance, k_b the Boltzmann's constant, q the elementary charge and T the absolute temperature.

One of the major advantages of equivalent circuit model is that it avoids the cumbersome use of a number of physical and chemical parameters, but instead projects the photovoltaic system as a combination of minimal number of electrical circuit elements. Each element implicitly reflects a physicochemical process in the cell.

O'Regan and Grätzel show in their first article in 1991⁸ the current-voltage characteristic obtained with the thin layer cell under illumination by simulated AM1.5 solar light. The two curves are reported in Figure 1.11 in which is shown that the photocurrent under diffuse daylight (*a*) is higher than under full sunlight (*b*). This phenomenon leads to an increase of efficiency in diffuse daylight, indicating that DSSCs performances are better than that of conventional silicon devices in these conditions.

Ruthenium complexes have been used as efficient photosensitizers because they have wide absorption bands, long lifetimes and long-term chemical stability. However, the critical disadvantages such as the high cost and lack of environmental safety of the inorganic dyes hinder its further development. On the other hand, the use of natural extracts as photosensitizers is an attractive alternative to synthetic dyes, like melanin, because of their environmental friendliness, cost-effectiveness and relative abundance. The re-

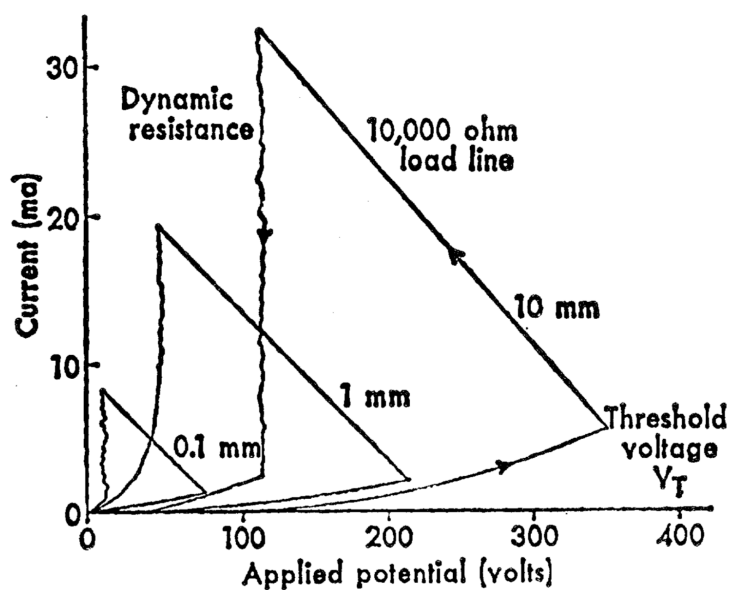


Figure 1.12: Melanin electrical switching properties.¹²

markable adhesion properties of melanine-like materials on surfaces, including metal oxides, is the underpinning for emerging applications, not only in energy fields, but also in biomedical and water treatment.

1.2.3 Melanin Electrical and Optical Properties

Since the late 1960s, electrical properties of melanins have fascinated a lot of scientists. McGinness¹¹ began to assert in 1972 that the electronic properties of melanins could have been explained in terms of a band model for semi-conduction in amorphous materials. It was observed how in melanins the conductivity increased with the absorption of light and also when a voltage was applied. This phenomenon was explained in terms of an increase of kinetic energy of the electrons with respect to potentials within which they trapped, leading to higher mobility and promotion of excited states, or field-assisted emission from acceptors, which produces exponential behavior in the current-voltage characteristic.

The same author published in 1974 an article in which the property of electric switching in melanins was investigated.¹²

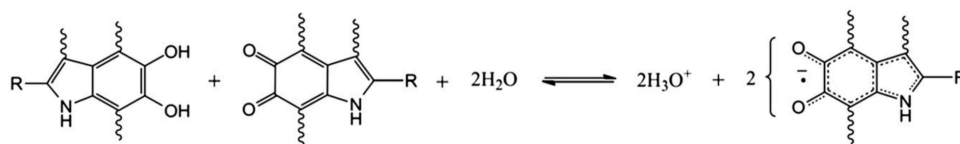


Figure 1.13: Equilibrium between the reduced (hydroquinone) and oxidized (quinone) forms of eumelanin to give two semiquinones (intermediate redox species) in high relative humidity conditions.¹³

The Figure 1.12 shows the typical electrical characteristics of a melanin samples in series with a load resistor and an applied potential. As the applied potential is increased, the current through the melanin sample increases monotonically up to a voltage V_T (threshold voltage), at which point the material switches. The same Figure 1.12 shows also how V_T is a function of thickness of the material, which indicates a strong dependence on the applied electrical field. But probably the most important factor is the presence of water: indeed dry samples would not switch until rehydrated, because water is capable of lowering the activation energy for conduction (hopping transport), apparently as a result of local modification of the dielectric constant of the material. These behaviors are currently studied in order to find applications of melanin in electronic devices.

Nevertheless, Mostert et al. in 2012 gave an another definition of melanin from the electrical properties point of view.¹³ They claimed that melanins cannot be considered as a amorphous organic semiconductor material, but an electronic-ionic hybrid conductor. The equilibrium of the hydroquinone, semiquinone and quinone species in the macromolecules, as shown in Figure 1.13, explains why melanin, at neutral pH, only conducts electricity when hydrated (thus there is not a modification of the local dielectric constant) and suggest that both carriers play a role in the conductivity.

In 2013, Wünsche et al.¹⁴ have been investigated the conduction in thin films of *Dopa melanin* spin coated, in a solution of *DMSO*, on *SiO₂* on *Si* substrates on which *Pt* electrodes were deposited by photolithography. Electrical measurements at biases of 0.2 V, 0.4 V, 0.6 V, 0.8 V and 1.0 V were conducted at different levels of relative humidity ($RH = 50\%$, 60%, 70%, 80% and 90%). As it is possible to observe from the graph in Figure 1.14, the

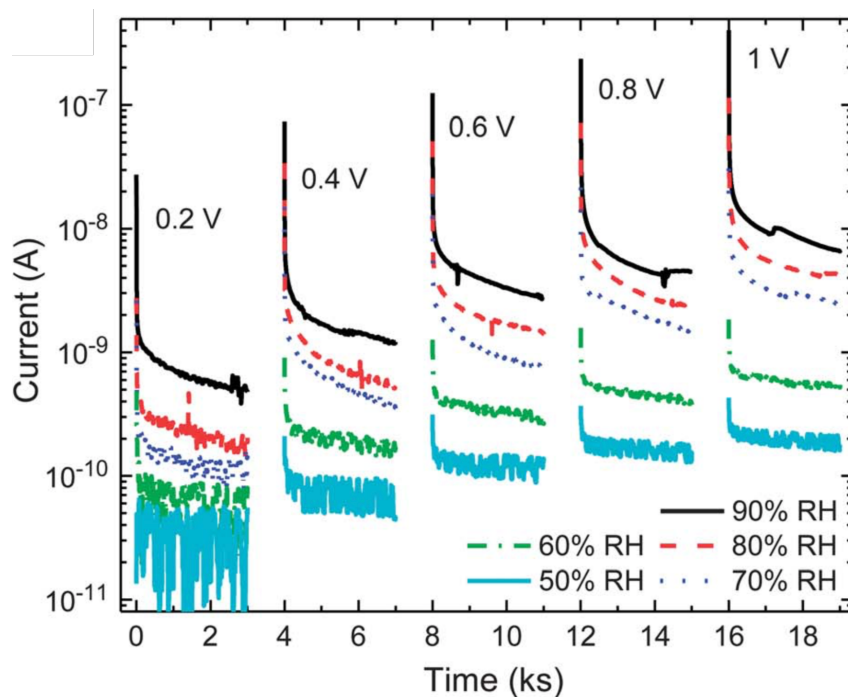


Figure 1.14: Transient current measurements of Sigmmelanin film for 3000 s long voltage pulses from 0.2 V to 1.0 V at relative humidity (RH) varied between 90% and 50%.¹³

conductivity on the sample is dependent on the water amount on the surface, suggesting that the two contribution to the electrical current (ionic and electronic currents) are both increasing with the weakly absorbed water content of the sample. The ionic current became increasingly dominant at higher sample hydration.

Another behavior which has been investigated in last years is the photoconductivity of melanin polymers. Jastrzebska et al. studied the photoconductivity effect in pellets of synthetic dopa-melanin polymer when radiated with a VIS-IR light source (400-800 nm) at different temperature (in a range of 293-326 K) and the steady-state photocurrent as a function of the wavelength.¹⁵ The authors explain how the higher temperatures causes a decrease of the time-constants (τ_r and τ_d) in the exponential behavior of rising and decreasing of the current (I_r and I_d) as in the following equations:

$$I_r = I_s - \sum_{i=1}^n A_{ri} e^{-\frac{t}{\tau_{ri}}} \quad (1.11)$$

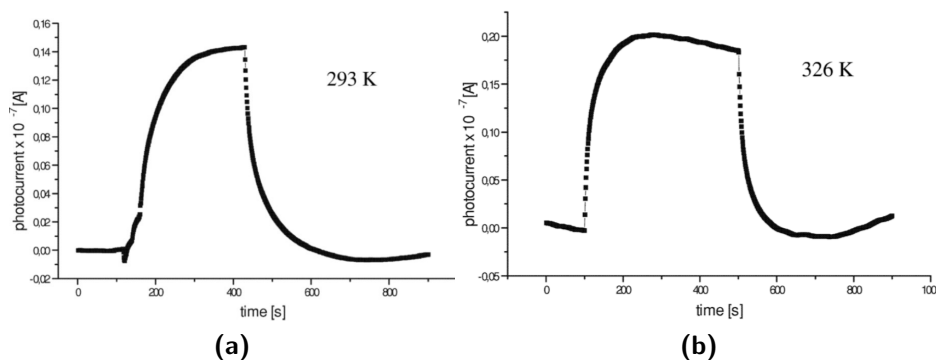


Figure 1.15: Rise and decay of photocurrent during switching on and off the radiation source at different temperature conditions.¹⁵

$$I_d = \sum_{i/1}^n A_{di} e^{-\frac{t}{\tau_{di}}} \quad (1.12)$$

The time-constants of photocurrent rise and decay are proportional to the trap concentration, which decreases as the the temperature increased. For that reason the photocurrent approaches more rapidly to the steady stationary value at higher temperatures, as shown in Figures 1.15a and 1.15b, also because changes in hydration state of melanin occurs during heating.

The melanin property of absorption in the range of UV-vis spectra has been observed from many research groups. Tran et al. in 2006 supported the theory that the broadband monotonic absorption of melanins is a consequence of the superposition of a large number of non-homogeneously broadened Gaussian transition associated with each of components of the eumelanin ensemble, thus the chemical disorder of the molecule is the responsible of the absorption behavior.¹⁶ As it is possible to notice in the absorbance trends in Figure 1.16, this behavior is confirmed. Furthermore, the photoconductivity spectrum shows significant departures from the optical spectra: the photocurrent curve shows a minimum at the wavelengths of 600-700 nm and tend to rise in the UV and near-IR regions. The authors explained that the mechanism of trap emptying seems to determine the spectral range of photoconductivity of melanins. Carriers captured by traps can be released by the radiation of the UV-vis and IR ranges: this results in

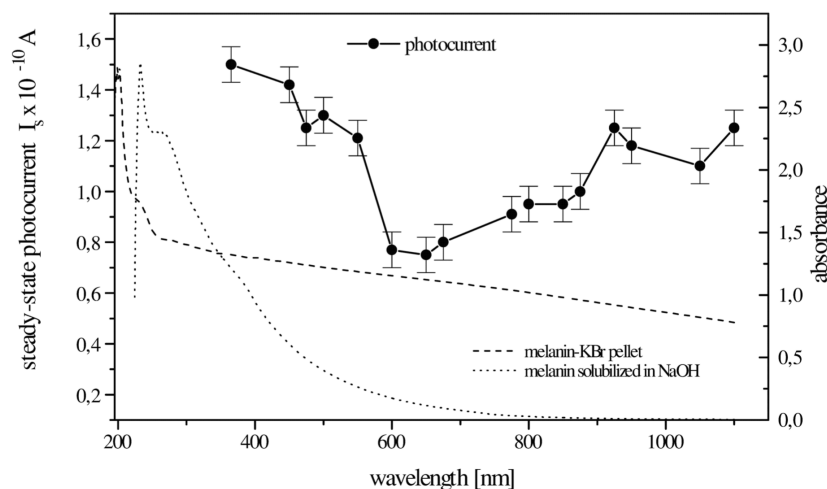


Figure 1.16: Optical absorption and steady-state photocurrent in melanin pellet and melanin solubilized in NaOH.¹⁵

the appearance of photocurrents which depend on the concentration and the degree of filling of the traps.

Furthermore, they asserted that the traditional model of melanin as an amorphous organic semiconductor is not required to explain its optical properties and suggested a reexamination of that definition.

What makes melanins interesting in application of energy conversion/storage, is also the interface behavior with metal oxides, such as TiO_2 . Recently, many research groups tried to replace the ruthenium sensitizer of DSSCs with melanins compounds. In 2013, Lee et al. used purified squid ink (whose main component is eumelanin) to build a DSSC in which the purified ink is coated on TiO_2 nanotubes or nanoparticles.¹⁷ The overall performance are rather modest (light-to-electric efficiency around 0.7, $V_{oc} = 0.74$ V, $J_{sc} = 1.6$ mA cm⁻² and $FF = 0.7$), but the promising properties and characteristics of melanins are a motivation to continue investigating it in order to utilize this natural pigment in technological applications. Its metal chelation, photoconductivity and ion-electron hybrid conduction properties, combined to its natural origin, are very promising base on which build future projects. In conclusion, melanins seem to have the same electrical behavior of an organic amorphous semiconductor, but recently this theory was questioned in

order to explain the role of water in the conductivity. The Prof. Santato's group is actually performing experiments on this aspect, trying to give an answer to this phenomena.

1.3 UV-Visible Absorption Properties of Polymers Blended with Melanins

How the UV absorption properties of melanin are linked with electrical properties was discussed in the Paragraph 1.2.3, but the interaction of these behavior with polymers could have a great interest also in different applications, i.e. in packaging area. There are actually materials UV absorbents (mainly inorganic compounds, like TiO_2 or Al_2O_3) utilized in this field, but the substitution of these compounds with organic biomolecules could be an interesting prospect for the future.

The absorption spectra of DHI, DHICA and dopa melanins are reported by Panzella et al. in the Figure 1.17, in which it is possible to observe the different profiles of absorption, in particular between DHI and DHICA melanins.⁴ Whereas the DHI melanin gave a typical monotonic profile, the DHICA polymer is characterized by an intense absorption band in the UV region around 320 nm. This behavior is attributed by the authors to reduced monomer-like chromophoric components that co-exist with quinonoid units, and persisting during the polymerization process as a consequence of hindered inter-unit π -electron delocalization within oligomer/polymer scaffolds. The small but distinct peak of absorption in the spectrum of dopa-melanin around 320 nm again, can be attributed to the minor DHICA-derived component.

An experiment with Sepia Melanin (SE) extract added to a poly(vinyl alcohol) (PVA) film was performed by Wang et al.¹⁸ The authors illustrated how even a low concentration of Sepia Melanin (0.5%wt.) in PVA blocked most of UV light below 300 nm, but maintaining high transparency in visible spectrum. Figure 1.18 shows UV-visible transmittance spectra of PVA and PVA/SE nanocomposites in the wavelength range from 200 to 800 nm.

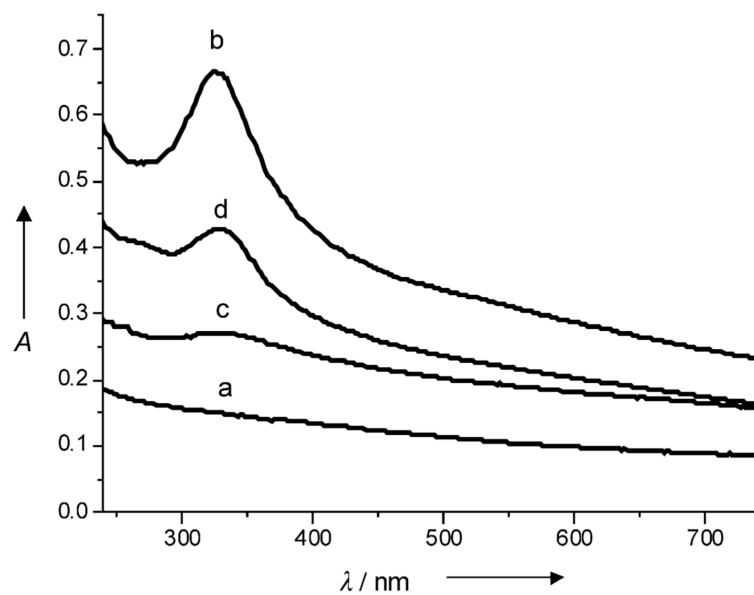


Figure 1.17: UV/Vis spectra of synthetic eumelanins, as suspensions in Tris buffer (2.5 mg/100 ml, pH 7.5). a) DHI melanin; b) DHICA melanin; c) dopa melanin. d) DHICA melanin (acetate buffer, pH 3).⁴

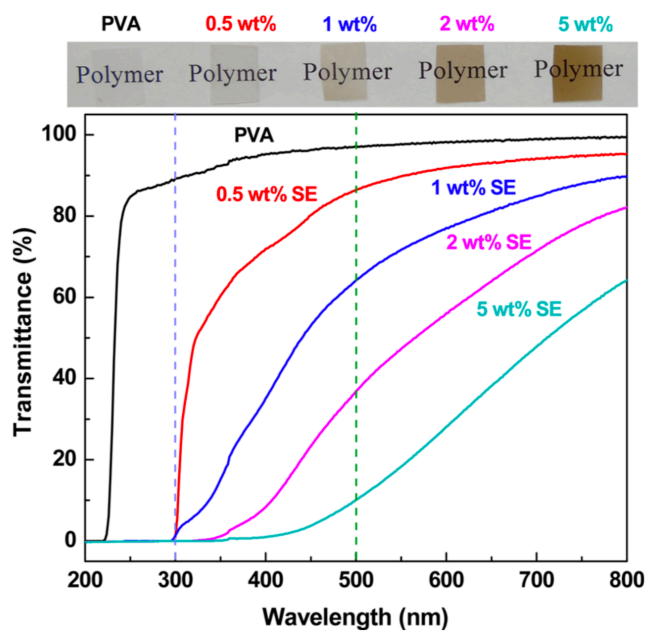


Figure 1.18: UV/Vis light transmittance spectra (bottom) and optical images (top) of PVA and PVA/SE nanocomposites.¹⁸

The neat PVA was nearly transparent for 220 – 800 *nm* wavelength of light. In contrast, the PVA/SE films could block light below 300 *nm* with only 0.5% *wt.* SE. With increasing of SE concentration, the UV shielding performance of PVA/SE films increased until nanocomposites with a percentage of 2% *wt.* of Sepia Melanin, in which the UV light was almost completely shielded under 340 *nm*, whereas the transparency decreased.

1.4 Biodegradability Aspects

The interest of the research on sustainable materials increased in last years. The main goal is to find out compounds which guarantee an higher compatibility of bio-based polymers (polymers synthesized by biomass or renewable resources) with the environment.

A large part of the groups defines melanin as *biodegradable*. But is the melanin actually biodegradable? To define a polymer biodegradable, two items need to be satisfied, as the ASTM 6400-12, D5338-15 and D883-17 require:

1. It has to be a polymer in which degradation results from the action of naturally-occurring microorganisms such as bacteria, fungi and algae.
2. In absolute terms or with respect to a positive control, 90% of its Carbon is digested by microorganisms and transformed into CO_2 .

From this definition, it is possible to understand that biodegradability depends on the environment.

It is important not to mix the different definitions of *Biodegradable polymer* and *Bio-based polymer*: it is possible to have bio-based but non-biodegradable polymers (such as Nylon 9 and Nylon 11), and, on the other hand, biodegradable petroleum-based polymers (like Poly- ϵ -caprolactone, PCL).

Furthermore, ASTM D6400-12 gives definitions in order to distinguish similar concepts, but not synonyms:

- *Compostable* plastic: a plastic that undergoes degradation by biological processes during composting to yield CO_2 , water, inorganic compounds

and biomass at a rate consistent with other known compostable materials and leave no visible, distinguishable or toxic residue

- *Degradable* plastic: a plastic designed to undergo a significant change in its chemical structure under specific environmental conditions, resulting in a loss of some properties that may be measured by standard test methods appropriate to the plastic and the application in a period of time that determines its classification

The method to evaluate the biodegradability of a compound is entirely explained in ASTM D5338-15, from which the more important points are reported. From the title *Standard Test Method for Determining Aerobic Biodegradation of Plastic Materials Under Controlled Composting Conditions, Incorporating Thermophilic Temperatures* the operating conditions for evaluation of the biodegradability of a material are easily deducible:

- i) Aerobic Conditions, presence of molecular O_2 , minimum 6%
- ii) Controlled composting conditions, therefore it is necessary to control $H_2O\%$ wt., pH , C/N Ratio etc.
- iii) Thermophilic temperatures, the microorganisms require a temperature between 45–80 °C to thrive

Therefore, it is clear how this is not a test in which biodegradability is evaluated in ambient conditions, but in specific conditions that are used by the systems of appropriate companies.

As explained before, also the compost has to satisfy standard conditions. The Table 1.1 synthesizes the characteristics that the compost needs.

The ASTM D5338 gives also all the indications to install the setup, the procedure and the elaboration of the data. The information about the experimental setup will be explained better in the Paragraph 2.3.1 on page 56.

Table 1.1: *Requirements for the compost*

Parameter	Minimum	Maximum
Origin	Organic fraction of municipal solid waste, <i>or</i> compost from plants, treating green, <i>or</i> yard waste, <i>or</i> mixtures of green waste and municipal solid waste	
Age (months)	2	4
Sieve	10 <i>mm</i>	
Organic Matter (wt. %)	30	N/A
pH	7	8.2
Water Content (wt. %)	45	50
C/N Ratio	10	40
Production of CO_2 per gram of volatile solid (mg)	50	150

Chapter 2

Experimental and Methods

2.1 Electrical Properties

2.1.1 Substrate Fabrication

The main idea behind this experiment is to understand the behavior of DHI-melanin and DHICA-melanin polymers when exposed to a light source in presence of an applied bias. In order to perform that measurements, a patterned substrate with electrodes is requested on which a spin coating process takes place to deposit melanins on it.

A photolithography process was used to obtain the mark of the electrodes on the silicon wafer (SiO_2/Si , thermally grown $0.25 \mu\text{m}$ of SiO_2 on Si) layer and, subsequently, through metal evaporation deposition (electron beam evaporator) the electrodes were printed on the substrate. In order to obtain the correct pattern, the procedure had to be developed into a clean room and the following steps (resumed in Figure 2.1) have been applied:

1. Open the N_2 , the vacuum and the compressed air valves. Switch on the lamp of the photolithography equipment and, after a couple of minutes, start it.
2. *Cleaning of the mask*: the mask is a transparent quartz plate with opacity zones in correspondence with the geometric pattern to be reproduced. Put it into the mask holder and dip them into the photo-

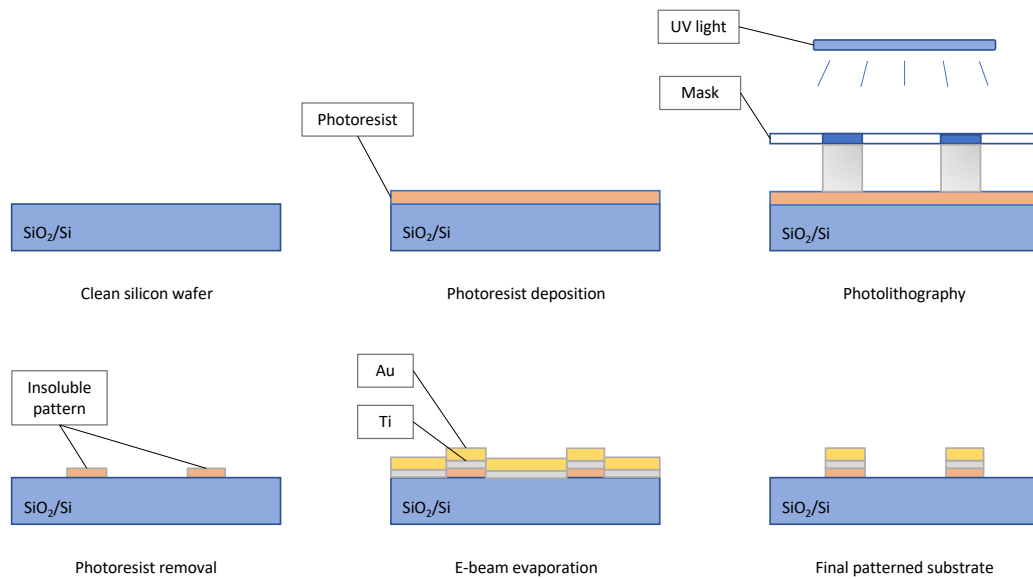


Figure 2.1: Main steps of photolithography and e-beam evaporation microfabrication processes to pattern the electrodes on the substrates.

remover solution under the hood for about 15min. After the treatment, wash the mask with DI water and IPA (Isopropyl Alcohol) and dry it by the nitrogen gun.

3. *Cleaning of the substrate:* after a first cleaning with the nitrogen flow, the silicon wafer has to be process in the oven (*Yes Oven*), where the water vapor is removed thanks to the high temperature and low pressure (used program #4, in which values of time, temperature and pressure were preset). After the treatment, remember to press the reset button in order to leave the internal pressure of the oven to 100 mbar.
4. *Spin coating* of the resist on the wafer. Put the sample on the centre of the spin coater, push the vacuum button and verify that the substrate is well centered. Take the photoresist *AZ 5214* (a positive photoresist) and pour it with a pipette on the surface of the wafer until it is completely covered. Close the lid of the machine and run it with a speed of 4000 rpm for 30 s. The rotation allows the complete and homogeneous (except for the edges) overlay of the surface with the photoresist, reaching a final thickness between 1.4-1.68 μm .

5. *Thermal treatment* is requested in order to evaporate the excess solvents. Put the wafer on a hot plate (with an extremely precision of temperature control) maintained at a $T = 110^{\circ}\text{C}$ for 50 s.
6. *Photolithography*: verify with a power meter the value of the power of the UV lamp (it depends on its life, thus it is important to verify that value every time the machine is used) and compute the time of exposure by dividing the value of energy requested (it depends on the mask, in this case 55 mJ) by the value of the power measured.
Change the mask on the mask holder and fix it properly with the pins and the vacuum button and centre it under the light source. Place properly the wafer in the substrate holder and start the exposition. After that, pour the developer (726, AZ 351B) in a large container and water in a second one. Dip the wafer in the developer and gently agitate the container for 1 min; after that put the sample in the container with water and, again, gently agitate it. Lift the wafer, rinse it with DI water and dry it with the nitrogen gun. In this procedure, as written before, a positive photoresist was used: this material is originally not soluble in the developer, but the UV radiation turns it from insoluble to soluble in the exposed zones. During the treatment with the developer, the portions of the substrate covered by the pattern of the mask during the photolithography keep the insolubility property, thus it is possible to see the pattern on the substrate.
Switch off the lamp of the machine.

After the printing of the pattern, the process of electron beam evaporation is performed in order to make a metal deposition on the selected portion of the surface. This method allows to have a precise deposition of materials that are difficult, or even impossible, to process using standard resistive thermal evaporation. During an e-beam evaporation process, current is first passed through a tungsten filament which leads to joule heating and electron emission. High voltage is applied between the filament and the hearth to accelerate these liberated electrons towards the crucible containing the material to be deposited. A strong magnetic field focuses the electrons into a

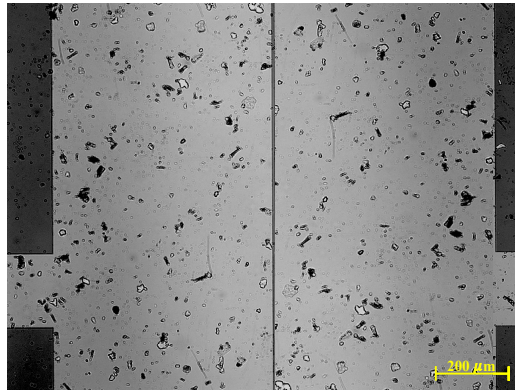


Figure 2.2: $10\ \mu\text{m}$ gap (central line) substrate before cleaning and melanin deposition processes. Optical images (Zeiss Axio), $10\times$ magnification factor, Reflectance mode

unified beam; upon arrival, the energy of this beam of electrons is transferred to the deposition material, causing it to evaporate (or sublime) and deposit onto the substrate. With a quartz balance it is possible to know exactly the amount of metal adhered on the substrate and therefore the thickness of the deposition. In this case of study, a first layer of $5\ \text{nm}$ of titanium is deposited and then $30\ \text{nm}$ of gold on it. The layer of titanium is fundamental in order to create adhesion between the substrate and gold electrodes.

After the metal deposition, a process of lift-off is necessary in order to remove the layer in the zone in which is not requested. The sample is left in a removal solution which remove the metal nanoparticles from the not patterned zones of the substrate. With a cutting machine with a diamond tip it is possible to cut singles sample from the initial wafer, which contains several specimens. The sample, shown in Figure 2.2, consists in two planar electrodes of $4\ \text{mm}$ width with a gap of $10\ \mu\text{m}$. The electrodes have a connection with a pad to allow to place better the pins of the measurement machine.

2.1.2 Melanin Deposition

After the production of the patterned substrate, where the electrodes were printed on a silicon wafer, the second step is the deposition of melanins on it.

First of all a procedure of substrate cleaning is mandatory to obtain a sample

completely free from any kind of dust particles or molecules on which make the melanin deposition. This is the procedure followed in this experiment.

1. Take four becker (at least of 200 *ml*) for the procedure, and a bigger one for the liquid waste.
2. Clean the first becker (for the first bath, in isopropanol (IPA)):
 - i) Take becker 1, clean with acetone and with the tissue
 - ii) Rinsing with acetone
 - iii) Rinsing with isopropanol
3. First ultrasonic bath, in IPA:
 - i) Put 100 *ml* of IPA in becker 1
 - ii) Take the sample holder in teflon
 - iii) Put water in the ultrasonic bath, at least 2/3
 - iv) Nitrogen gun to clean the specimen before putting it in the teflon container
 - v) Rinse the container+sample with acetone
 - vi) Rinse the container+sample with isopropanol
 - vii) Start the ultrasonic bath for 45 *min*
4. Clean the second becker (for the second bath, in acetone):
 - i) Isopropanol rinse
 - ii) Acetone Rinse
 - iii) Put 100 *ml* of acetone in becker 2
5. Second ultrasonic bath, in acetone:
 - i) Take out the container+sample from the becker with isopropanol
 - ii) Rinse the container+sample with acetone

- iii) Put the container+sample in becker 2 and start the ultrasonic bath for 10 *min*
6. Put back becker 1:
 - i) Empty becker 1 in the liquid waste
 - ii) Rinse it with acetone
 - iii) Rinse it with isopropanol
 - iv) Dry it with nitrogen gun
7. Clean the third becker (for the third bath, in isopropanol):
 - i) Acetone rinse
 - ii) Isopropanol rinse
 - iii) Put 100 *ml* of isopropanol in becker 3
8. Third ultrasonic bath, in isopropanol:
 - i) Take out container+sample from becker 2
 - ii) Rinse them with isopropanol
 - iii) Put container+sample in becker 3 with isopropanol and start the ultrasonic bath for 5 *min*
9. Put back becker 2:
 - i) Empty becker 2 in the liquid waste
 - ii) Rinse it with isopropanol
 - iii) Rinse it with acetone
 - iv) Dry it with nitrogen gun
10. Clean the sample holder in which store the specimen after the cleaning procedure:
 - i) Rinse with acetone and a tissue
 - ii) Rinse again with acetone

- iii) Rinse with isopropanol
 - iv) Rinse with water
 - v) Dry with nitrogen gun
11. Clean in the same way the tweezers
12. Fourth ultrasonic bath, in water:
- i) Rinse with DI water the fourth becker
 - ii) Put 100 *ml* of DI water in it
 - iii) Take the container+sample from becker 3, rinse them with DI water and put them in the becker 4
 - iv) Start the ultrasonic bath for 5 *min*
13. Put back becker 3:
- i) Empty becker 3
 - ii) Rinse with acetone
 - iii) Rinse with isopropanol
 - iv) Dry with nitrogen gun

After all this procedure, keep the clean substrate in the sample holder to avoid any contamination.

The successive step is to prepare the suspension of monomers of DHI and DHICA to make the deposition on the substrate by spin coating. Take the monomer powders from the refrigerator (where are stored to preserve them) and weight in a clean vial the amount of powder in order to obtain the desired concentration. In this case a quantity of around 10 *mg* of melanin powder was taken and consequently the right volume of Anhydrous Methanol was added in order to obtain a suspension with a concentration of 10 *mg/ml*.

The spin coating process (30 *s* at 2000 *rpm*) was performed the same sample in glovebox and, subsequently, an induced polymerization in ammonia environment (built with two becker and a glass lid as shown in Figure 2.3 was carried out to accelerate the process (DHICA need at least 16 *h* to obtain

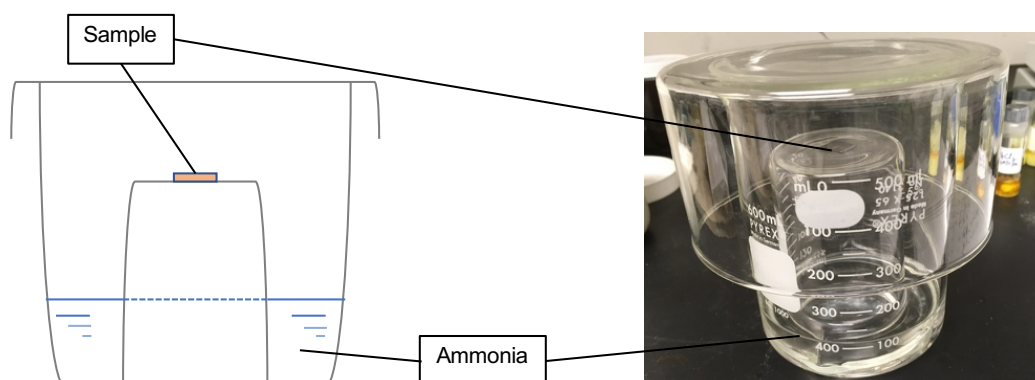


Figure 2.3: Ammonia chamber in which the sample is left to allow an induced polymerization.⁵

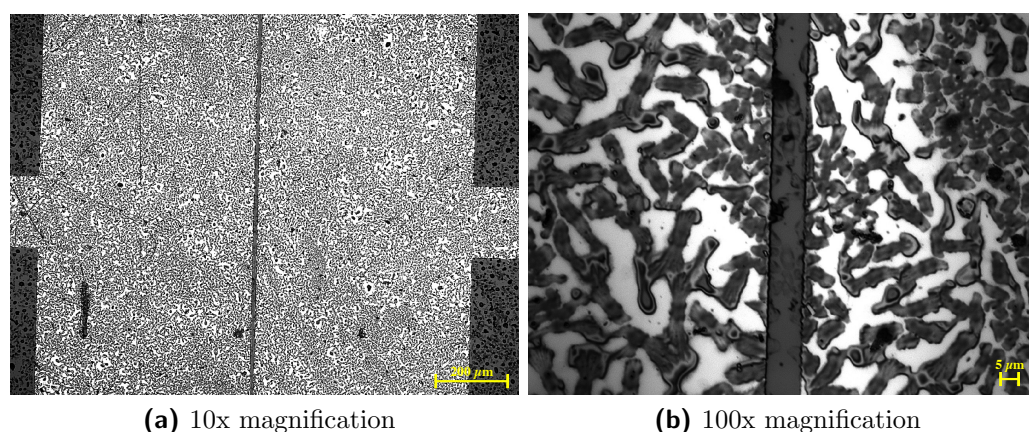


Figure 2.4: Optical microscope (Zeiss Axio) images in Reflectance mode of the substrate with $10\ \mu\text{m}$ gap (a,b) (central stripe) between two gold electrodes.

a complete polymerization, DHI at least $3\ h$). The results of the deposition and polymerization on the sample are reported in Figure 2.4.

The Figure 2.5 was taken with an *Atomic Force Microscope (AFM)* in Tapping Mode, which allows to analyze the morphology of the deposition of melanin in the gap between the electrodes. The film (around $79\ \text{nm}$ thick, has circular structures aggregate together, leaving zones apparently empty. A focus on one of these voids was studied, as it is possible to notice in the same Figure 2.5, demonstrating that actually there are structures not visible in the image with lower magnification.

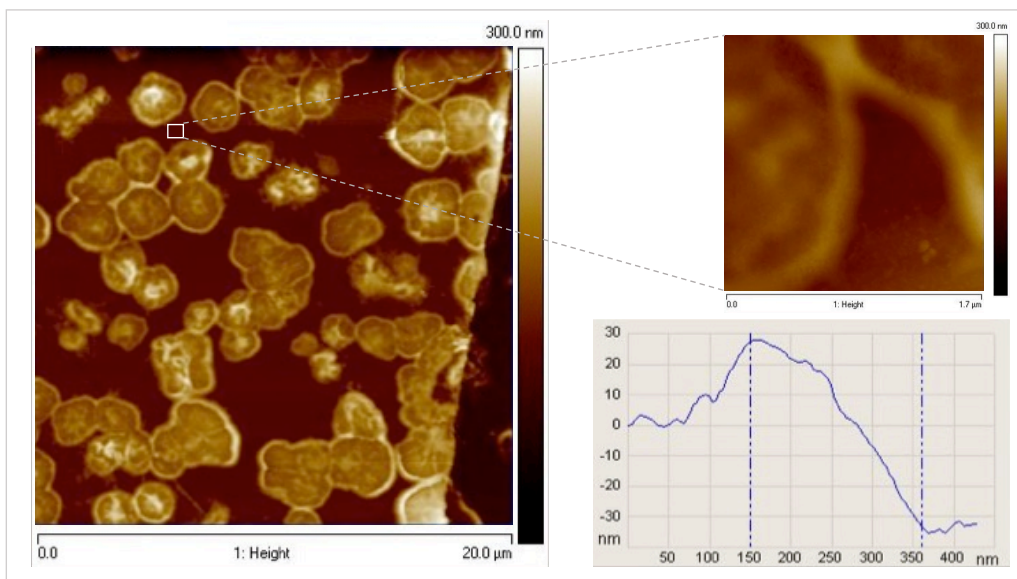


Figure 2.5: *AFM images 20 μm x 20 μm of DHICA melanin in the gap between the gold electrodes.*

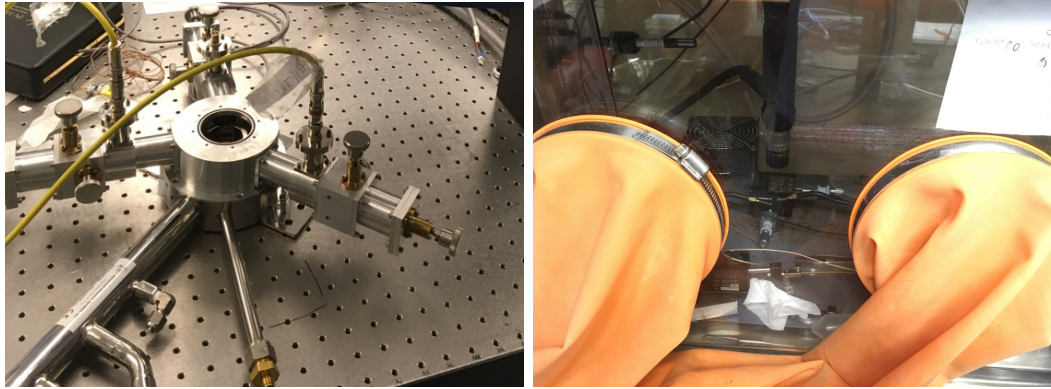
2.1.3 Electrical Measurements

Electrical measurements were performed both in ambient conditions, in open air, Figure 2.6a to evaluate the conductivity when the sample was at environment humidity conditions ($RH \approx 25\%$), and in a humidity chamber, Figure 2.6b, where it is possible to set the desired RH level.

The gold electrodes were contacted with micro-manipulated tungsten probes and a software-controlled source/measure unit (Agilent B1500A for open air and B2902A for humidity chamber) was used to apply voltage to the sample. A current-time characteristic was recorded under constant bias conditions every 30 *min*, considering the following applied voltage: 0.1 V, 0.3 V and 0.5 V.

The first measurement was taken in ambient conditions and subsequently the samples were stored in the humidity chamber at 90%RH for at least 24 *h* in order to equilibrate the hydration before the measurement. In order to evaluate the photo-response of melanin, two tests were performed on the same bias condition:

- *Dark*, in which the sample was tested in the humidity chamber with



(a) Micromanipulated electrical probe station for measurements in ambient conditions. (b) Micromanipulated probe station for measurements in high relative humidity conditions.

Figure 2.6: *Measurement stations for the conductivity tests on the samples.*

no light source added. It was not a completely black environment, but the Faraday cage around the chamber provides a quite dark one.

- *Light*, in which the light source, used to place the pins of the Agilent on the sample, radiates the substrate.

The light source in the humidity chamber was characterized in order to know the intensity of the light as a function the wavelength on the sample, through the utilization of a portable Integration Sphere system. The Irradiance is plotted in Figure 2.7, in which it is possible to observe that the light has emission basically only in Visible range, with a peak at 625 nm , in the orange-red zone.

It was chosen to radiate the sample after $7\text{ min }30''$, to evidence the transient of current increase, for a period of 15 min . After that, the light was chopped, in order to evaluate the transient of decrease of the current. The experiments under light conditions took 30 min for each sample, as the dark ones.

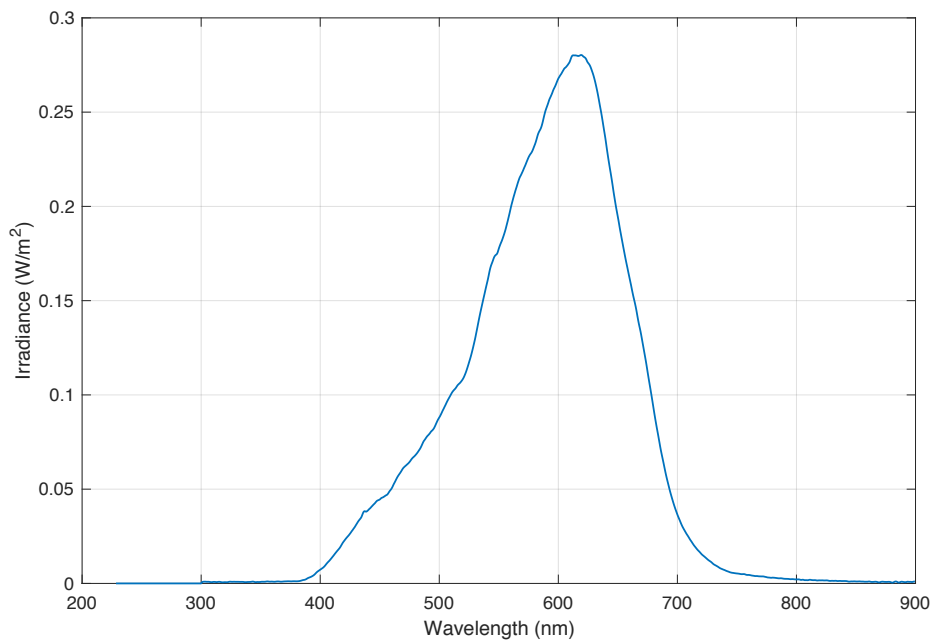


Figure 2.7: Irradiance of the light source in the humidity chamber for the photoconductivity test.

2.2 UV-Visible Absorption

2.2.1 Sample Fabrication

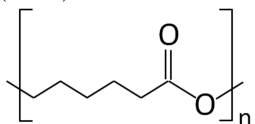
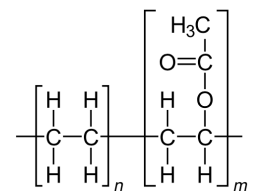
An organic sustainable additive like eumelanin would be really interesting in the packaging industry, with respect to the recent sensibility on the "green industry". The main idea behind this application is to find out if it is possible to exploit the behavior of UV-radiation protection of eumelanin by its addition to plastic polymers in order to develop UV-screening properties in the latter. Furthermore, the property of radical scavenger of eumelanin could give an enhancing thermal stability to the polymers because the melanin could act on the free radical that form during the thermal degradation of polymers.

In order to study these properties, polymers with different additives and different weight percentage were produced by thermo-mechanical process. Considering that eumelanin undergoes thermal degradation at temperature in the range of 130-170°C²², a processing temperature in this range was the

selective criterion for the packaging polymers used for this work.

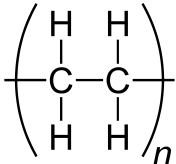
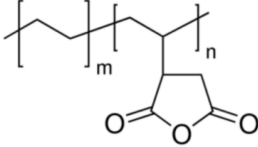
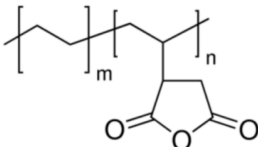
It has to be lower than the degradation temperature of melanin and higher than the melting temperature of the polymer in order to have proper viscosity of the melt during batch mixing. Therefore, important polymers ubiquitous on the market such as Polypropylene (PP) and Polyethylene Terephthalate (PET) had to be ruled out because their melting points are respectively 160-175°C and 245-265°C²³; however, polymers used to promote the adhesion of PP and PET in multilayer systems (like Bynel41, Bynel42, EPC, PEMA, PEEMA) could be investigated. In the following Table 2.1, the polymers investigated in this work and their characteristics are resumed.

Table 2.1: *Polymers utilized in the UV-vis absorption experiment*

Polymer and Repeating Unit	Commercial Grade	Category	Melting Point (°C)	Outstanding Properties
Poly(ϵ -caprolactone) (PCL) 	Capa™ 6800 from Perstorp	Polyester	58-60	Prepared from renewable resources, biodegradable ²³
Ethylene-vinyl acetate co-polymer (EVA) (9.3% of vinyl acetate) 	ELVAX 3128 from DuPont	Copolymer polyolefin- vinyl ester	99	Flexibility, Toughness and heat sealability ²³

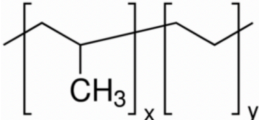
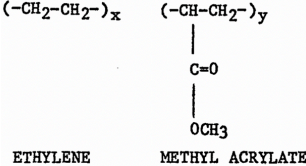
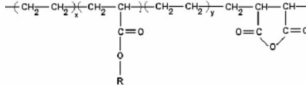
Continue on the next page

Continue from the previous page

Polymer and Repeating Unit	Commercial Grade	Category	Melting Point (°C)	Outstanding Properties
Linear Low-Density Polyethylene (LLDPE) 	LL 6407.67 from Exxon Mobil	Polyolefin	127	Improved mechanical properties, compared to LDPE at the same density, tear strength, toughness, processability and stiffness ²³
Anhydride-modified Linear Low-Density Polyethylene (LLDPE-MA) (Maleic Anhydride ≈ 0.4 – 0.5% wt.) 	Bynel 41E865 from DuPont	Polyolefin	109	Adherence to EVOH, polyamide, PE and Ethylene copolymers
Anhydride-modified Low-Density Polyethylene (LDPE-MA) (Maleic Anhydride ≈ 0.4 – 0.5% wt.) 	Bynel 42E703 from DuPont	Polyolefin	105	High interlayer adhesion between: EVOH, polyamide, PE, Ethylene copolymers and ionomers

Continue on the next page

Continue from the previous page

Polymer and Repeating Unit	Commercial Grade	Category	Melting Point (°C)	Outstanding Properties
Copolymer Ethylene-Propylene (EPC) (Ethylene=11%) 	Vistamaxx™ 3020FL from Exxon Mobil	Polyolefin	130	Moisture-barrier properties
Ethylene-Methyl Acrylate copolymer (PEMA) (Methyl Acrylate ≈ 27 – 31% wt.) 	<i>LOTRYL</i> ® 29MA03T from Arkema	Copolymer Polyolefin- acrylate polymer	92	Adhesion with Polyethylene Terephthalate (PET)
Random terpolymer of Ethylene, Ethyl Acrylate and Maleic Anhydride (PEEAMA) 	<i>LOTADER</i> ® 4700 from Arkema	TerPolymer Polyolefin- acrylate polymer- maleic anhydride	65	Adhesion with Polyethylene Terephthalate (PET)

Ends from the previous page

Three types of eumelanin were used in this study: two synthetic eumelanins (chemically controlled DHICA-melanin and DHI-melanin) and natural eumelanin extracted from the ink sac of a cuttlefish (*Sepia eumelanin*), following the procedure below, as reported in literature²⁴.

The extraction and purification of *Sepia Melanin* were performed in an acid medium. To 50 g of commercial cuttlefish ink were added 100 ml of HCl (in

Table 2.2: *Thermo-Mechanical conditions in the polymer production process*

Polymer	Melt Compounding		Thermoforming in the press			Cooling at 25°C		
	Batch mix rot.	time	Batch mix T	time	T	p	time	p
	rpm	min	°C	min	°C	MPa	min	MPa
PCL	50	20	105	15	75	1.58	3	0.43
LLDPE	50	20	140	10	135	1.01	3	0.43
EVA	50	20	135	15	115	1.58	3	0.43
LLDPE-MA	50	20	140	12	125	1.29	3	0.43
LDPE-MA	50	20	120	15	120	1.58	3	0.43
EPC	50	25	145	15	135	1.29	3	0.43
PEMA	50	25	125	12	115	1.01	3	0.43
PEEAMA	50	25	125	12	115	1.01	3	0.43

a range of molarities varying between 0, 0.5, 1.0, 2.0 and 3.0 M for each sample) in a dark container. The slurry was stirred for 30 min (magnetic or ultrasonic stirring) and kept for 24 h at 10°C. Solid is separated from the supernatant fluid by centrifugation (1000 rpm at 5°C for 15 min), washed-suspended three times with a 0.5 M HCl solution, water, acetone and finally water. After a 24 h lyophilization to remove all the solvent, a very thin black product was obtained at the end of the procedure.

To evaluate the UV-screening enhancement, eumelanin was added to the polymer by melt compounding in a batch mixer at 50 rpm . The temperature and melting times are reported in Table 2.2. Films were the obtained by thermoforming in a hot press and the stabilized with a pressa at room temperature. The result was a film of 20.1 cm x 15 cm as shown in Figure 2.8.

As eumelanin powders, added in the amount 1% wt., proved to have very poor dispersion properties giving to the final polymer macroscopically visible black dots (Figure 2.8), the melanin free acid treatment (MFA)²⁵ was deemed necessary prior to the addition to the polymer in order to homogenize the product obtained by melt compounding. MFA was obtained by solubilization of the granules at low concentrations of H_2O_2 (1%) in 0.5 M ammonia at pH

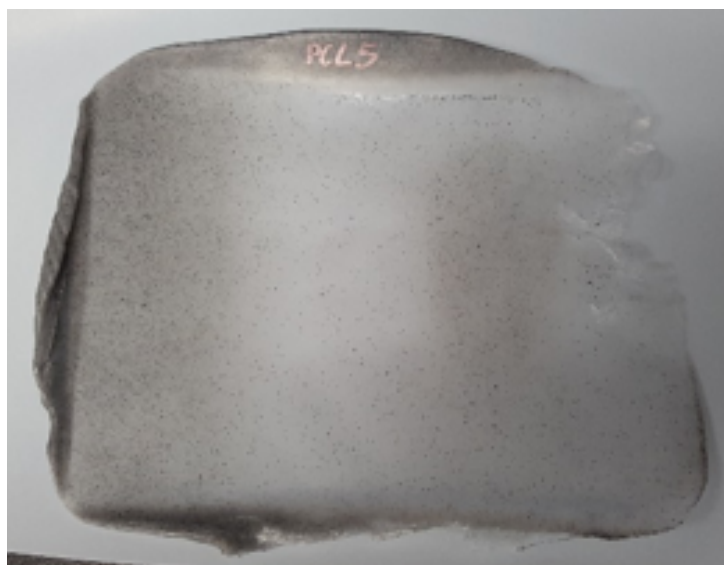


Figure 2.8: *PCL film melt-compounded with DHI-melanin powder (1% wt.).*

10 and 200:1 liquor ratio. Complete dissolution of melanin under these conditions took place within 60 *min* for DHI-melanin and DHICA-melanin, but it required 24 *h* for Sepia Melanin. At this point the peroxide was destroyed by borohydroxide, the water was removed by evaporation in a rotovapor starting from 40°C and the product was isolated as a water-soluble, high lustrous material. On acidification to pH 2, the solubilized melanin precipitated. This product was denoted as melanin free acid (MFA). Its solubility behavior is typical of a polymer containing few ionizable groups, dissociation of which forces the polymeric chain into solution. Thus MFA remains insoluble at low pH and dissolves rapidly when the pH of the system is raised above 4. However, once in the form of MFA, the biopigment proved to be so homogeneously dispersed that the polymer color turned black: the starting amount was then established to 0.2% wt. instead of 1% wt. For each polymer it was produced (as syntisized in Figure 2.9):

- A blank film as a control: the processing parameters (temperature, batch mixer rotation speed, pressing time and temperature) were the same used for samples with the additives in order to maintain the same thermo-mechanical story.

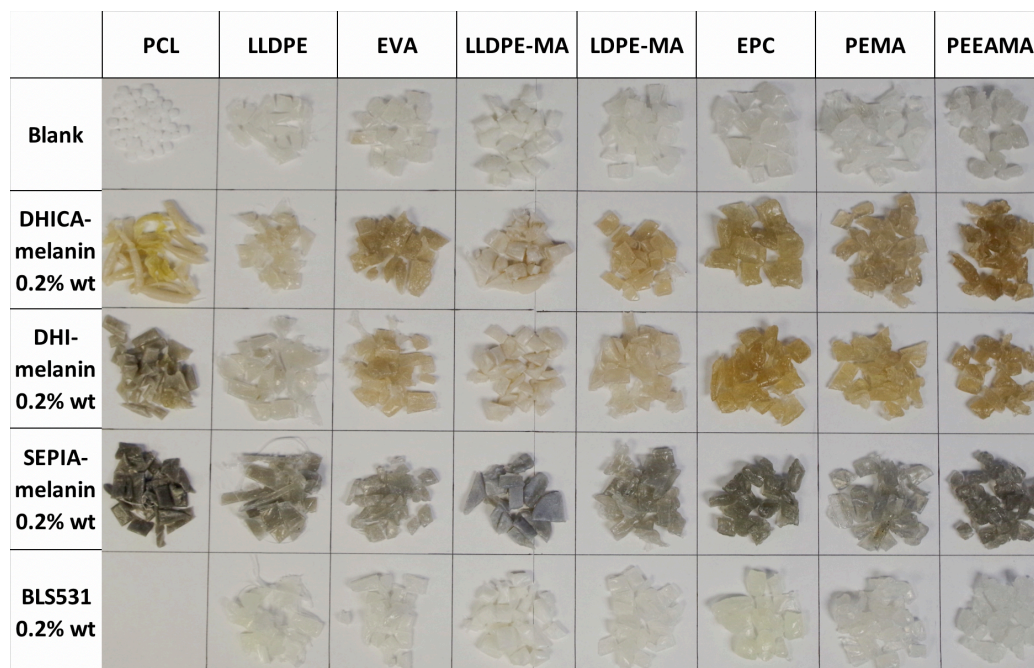


Figure 2.9: Pellets of different polymers with the additives analyzed.

- The samples with the three aforementioned type of eumelanin (DHI-melanin, DHICA-melanin and Sepia Melanin).
- A sample with a commercial additive, (2-Hydroxy-4-(octyloxy)benzophenone, commercial name BLS[®]531 from Mayzo), a toxic and non-biodegradable benzophenone molecule which absorbs in the UV.

2.2.2 UV-Visible Absorption Analysis

In order to verify the UV-vis absorption properties on the polymers, it was utilized a spectrophotometer *Lambda 1050* from *PerkinElmer*. This equipment allows to measure the Absorption (A), Reflection (R) and Transmission (T) of the radiation on a sample placed in an Integration Sphere. The sources of the light are two lamps (D2 Lamp and Tungsten Lamp) and the machine automatically select a specific wavelength to send to the sample. As a result, a plot is obtained, in which the chosen variable (A, T, R) is represented at each wavelength in the range that the operator had set. In this experiment,

the usual range is between 250 nm (in UV-C region) to 1400 nm (NIR region).

The first step to obtain information on the absorption of the film with the different additives was to choose the more suitable configuration of the sample placed in the sphere. Two configurations were analyzed:

1. *Spectralon*: configuration which implies to place the sample on the wall of the integration sphere and a lid of Spectralon (high reflective material) behind it. It allows to perform measurements of Transmission + Reflection (T+R) of the sample because the photons incident on the sample, were reflected by Spectralon back to the sphere. This method does not give negative absorption values, that should be physically meaningless, but, as it is possible to observe from the Figure 2.10, the radiation is transmitted twice through the sample, thus the absorption may be increased.
2. *Center Mount 20°*: configuration which implies to place the sample in the centre of the sphere, with an inclination of 20° between the direction of the front beam and the sample. This method allows to take the value of the Transmission + Reflection (T+R) too. This method does not amplify the value of absorption, but for thin samples of low absorbing and high reflectance materials it is not unusual to obtain negative values of absorption, mainly in the low wavelength region where the scattering becomes predominant in the integrations sphere.

After a first period of test with both configurations, it was decided to perform all the measurements with the *Center Mount 20°* method, because it is expected that the absorption values are closer to the real ones, but, at the same time, it's known that there would be the possibility to obtain some negative values.

It is important to notice that the software actually gives the values of Transmission + Reflection (T+R), not only the Transmission. That implies that the values of the coefficient of absorption (α) computed using the Lambert-Beer Law (2.1) is not the real one, but a different one that it was called *pseudo* α (2.2).

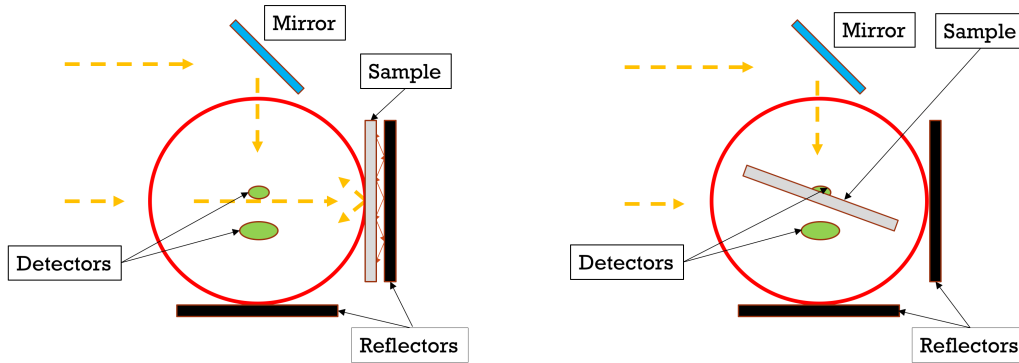


Figure 2.10: Configurations of the methods *Spectralon* (on the left) and *Center Mount 20°* (on the right) performed for the measurement of $T+R$.

$$\begin{cases} I = I_0 e^{-\alpha x} \\ T = \frac{I}{I_0} \end{cases} \longrightarrow \alpha = \frac{-\ln(T)}{x} \quad (2.1)$$

$$\text{pseudo } \alpha = \frac{-\ln(R + T)}{x} \quad (2.2)$$

To perform the measurement, samples with dimensions around $3 \text{ cm} \times 2 \text{ cm}$ have to be placed in the sample holder. Therefore some portions were cut from the original polymer fabricated. The Figure 2.11 show the configuration of the machine to reproduce the experimental setup used. It is important to set the right angle of the sample holder (on the right of the Figure 2.11) and that the lenses are placed in mode *C*, otherwise the light beam will not be collimated on the centre of the integration sphere.

To run the experiment, is enough to open the software and set, as said before, the range of analysis between 250 nm and 1400 nm with data interval of 1 nm .

From each sample, three portions (named with a progressive roman number index) from it were taken in order to have a triplicata of data and the same measurement was done on each one.

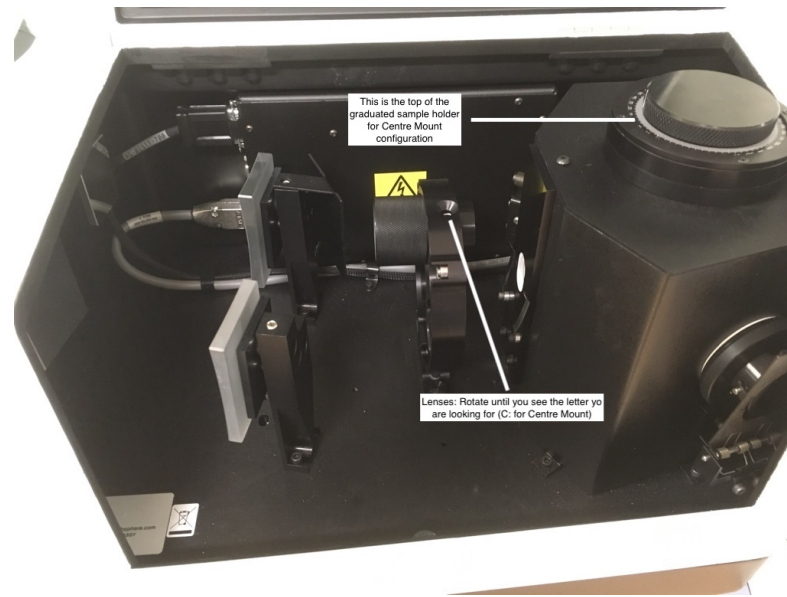


Figure 2.11: *Configuration of the machine to reproduce the experiment*

2.2.3 UV Aging Chamber

The second step of the experiment consist on figure out how the absorption properties of the samples change after a period of 48 days of UV radiation exposure.

A UV aging chamber was built as shown in Figure 2.12a. A UV lamp (Reptile UVB200, 26 W) is placed in a hole made on the lid of a plastic box and all its walls were covered by aluminum foil in order to minimize the UV radiation absorbed by the chamber and maximize the reflection. A sample holder, with a grid to identify the samples, is installed inside the box. The dimensions of the chamber do not allow to place all the 156 samples, consequently 64 were selected.

The main problem to solve is to make sure that all the samples were receiving the same quantity of radiation. A measurement of radiation intensity on each sample position was done twice in order to obtain an average of that values (the mean value of the intensities on the UV chamber is $1170 \mu\text{W}/\text{cm}^2$, but there were intensities between $400 \mu\text{W}/\text{cm}^2$ and $2300 \mu\text{W}/\text{cm}^2$). It was subsequently possible to compute an intensity map of the UV radiation on the sample holder, thereby a method of switching of the samples every 6 days

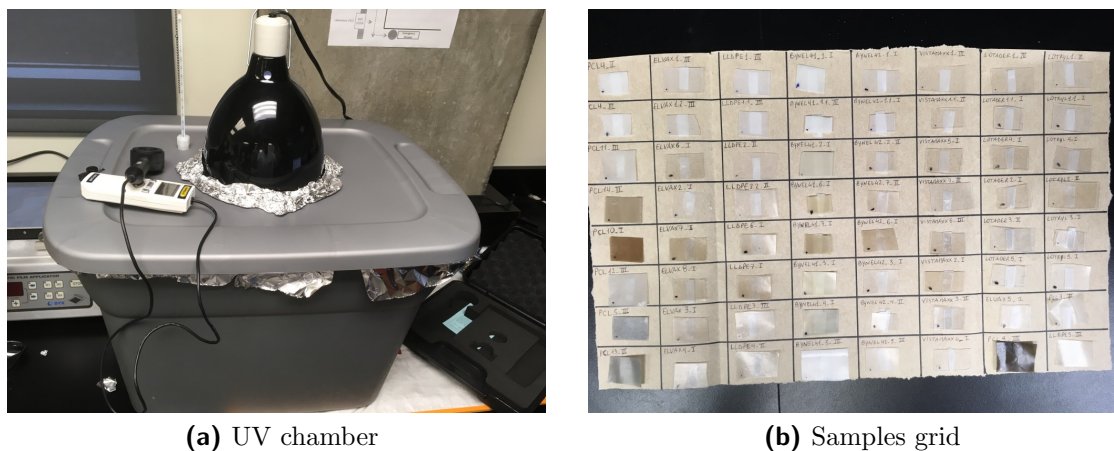


Figure 2.12: UV chamber and samples for the UV aging

was studied in order to radiate on average all the samples at the same way. In order to identify which side of the samples is the irradiated one, as it is possible to notice in Figure 2.12b, there is a black dot in the bottom left corner.

Furthermore, in order to evaluate the effect of the aging on the samples, FTIR (Fourier-Transform Infrared) spectroscopy was performed. Rather than shining a monochromatic beam of light on the sample (working principle of the absorption spectroscopy seen in Chapter 2.2.2 on page 51), the beam contains many frequencies of light at once and it is measured how much of that beam is absorbed by the sample. Subsequently the beam is modified to contain a different combination of frequencies, giving a second data point, and so on many times as chosen in the settings of the machine. The software computes all the data, through the Fourier-Transform algorithm, giving a graph which shows the absorption at each wavelength. Running this measurements before and after the aging allows to identify if the structure of the sample is changed through the peaks analysis.

2.3 Biodegradability Test

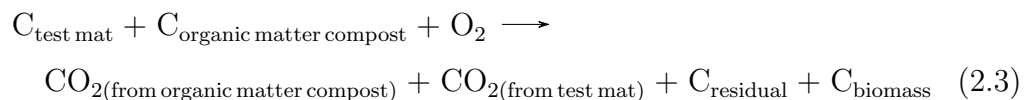
2.3.1 Experimental Setup

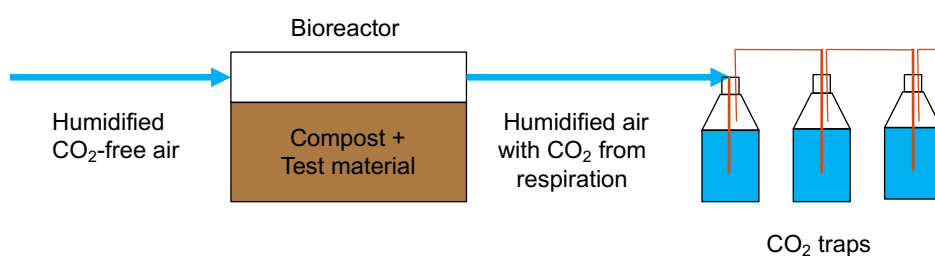
The method to evaluate the cumulative CO₂ developed and the percentage of biodegradation of the samples (or, in other words, mineralization) is the titration of Ba(OH)₂ (Barium Hydroxide) as suggested by ASTM D5338. The experiment was a hundred days long (precisely 98 days, from October 26th, 2017 to February 1st, 2018).

Test material (in this experiment Sepia Melanin, whose biodegradability is to evaluate), is put in a reactor (a glass bottle of 2l of capacity with three openings, two for the inlet and outlet air connection and a bigger one for the insertion of material) with a compost blend (250 g for each reactor), with bacteria and others microorganisms which are the responsible of digestion of the sample, as shown in Figure 2.13b. The reactors were stored at a temperature of $(58 \pm 2)^\circ\text{C}$.

Another item to consider is the selection of the compost: it has to respect the standard criteria reported in ASTM D5338 (Table 1.1 on page 33). The material from the company *Englobe* respects almost all the conditions, except for the size of the compost: it was necessary an operation of manual sieving to leave only matter under 10 mm of dimension.

Basically the setup for a single bioreactor could seem really simple: a CO₂ free air flow is forced to bubble in a column with water (with a pressure around 1.4 psi), in order to humidify the air and to provide the essential water for life. After that, the air is sent to the reactor with an air flow of 40 (arbitrary unit, only to know that all the reactors are receiving the same air flow), where the microorganisms in the compost use the O₂ in the air and the carbon present both in the test material than in the organic matter of the compost for the reactions of cellular respiration as shown in the equation (2.3).





(a) Schematic representation of a line for a single bioreactor



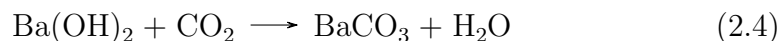
(b) Bioreactors in the oven



(c) Example of three series of traps

Figure 2.13: *Basic elements of the Biodegradability Test setup*

Downstream, the outlet air flow from the reactors is forced to bubble in a series of three traps (bottles of 1.8l of capacity each with inside a solution of Ba(OH)₂ and water 0.1M), Figure 2.13c, in which the reaction (2.4) takes place. The BaCO₃ (Barium Carbonate) is a very chemically stable white precipitate, from which CO₂ is not able to get away. After the first trap, the air is forced in a second and a third trap, where the probability to capture all the CO₂ developed in the reactors increase.



Therefore a single line for a single sample is schematize in Figure 2.13a.

The problem is that is not possible to know the quantity of CO₂ developed only with this configuration, because from the reaction (2.3) it is possible to notice two different components of carbon dioxide, because the microorganisms do not digest only the sample that was inserted, but also the organic

part of the compost. Thus:

1. $\text{CO}_2(\text{from organic matter})$ is the carbon dioxide developed from the digestion of the carbon presents in the compost matter;
2. $\text{CO}_2(\text{from test mat})$ is the carbon dioxide developed from the digestion of the carbon presents in the test material added.

Here it is the necessity to add a bioreactor with only compost. By this operation, it is possible to know the exact quantity of CO_2 developed from the degradation of the organic matter of the compost, hence, by difference, it is possible to compute the amount of carbon dioxide from the digestion of the samples.

In order to have a reference to compare the results, it was necessary to add two more samples:

- A *Positive Control* sample, a material which has a known biodegradability under the same experimental conditions. In this experiment *Cellulose* was used, which has a mineralization of 70% in 45 days of test (or 90% in 180 days).
- A *Negative Control* sample, a material with no biodegradation in this conditions. *Polyethylene* was used as negative control.

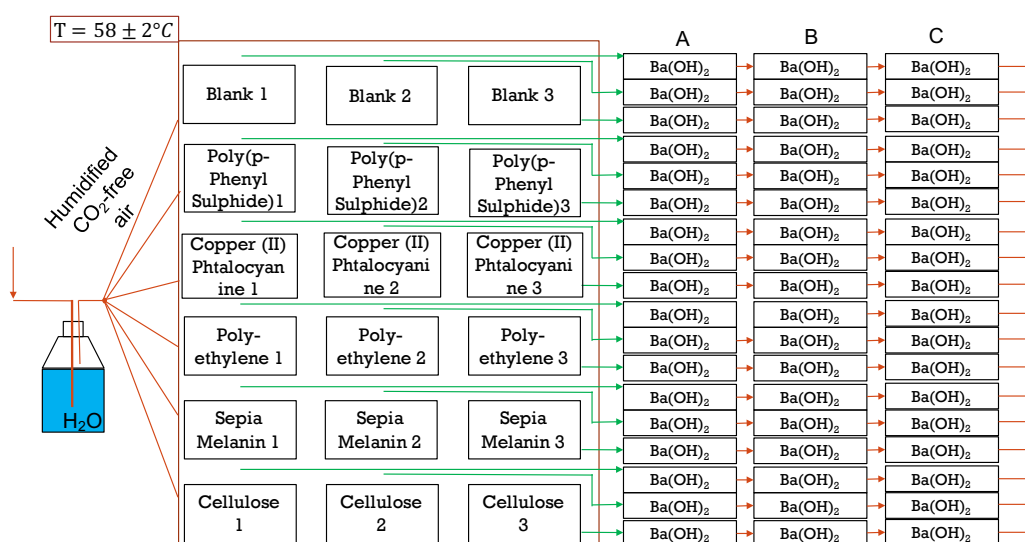
To complete the experiment, other two samples were utilized to understand effectively the biodegradation of two molecules of interest in green electronic field: *Copper (II) Phtalocyanine* and *Poly(p-Phenylene Sulphide)*. It's important to notice that, in order to have more data and reliability, three bioreactors for each sample were installed. In conclusion, the setup includes eighteen reactors with a series of three CO_2 traps each. Table 2.3 contains the convention used to identify the bioreactors during the experiment and the Figure 2.14 shows the complexity of the entire system.

2.3.2 Analysis Procedure

To evaluate the quantity of CO_2 captured, and then the mineralization, a titration is performed. A little quantity of solution in the traps is taken

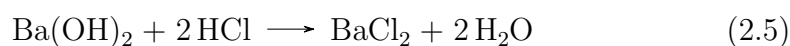
Table 2.3: Organization of the bioreactors

Bioreactor number	Content Material
1	Background 1
2	Background 2
3	Background 3
4	Poly(p-Phenylene Sulphide) 1
5	Poly(p-Phenylene Sulphide) 2
6	Poly(p-Phenylene Sulphide) 3
7	Copper (II) Phtalocyanine 1
8	Copper (II) Phtalocyanine 2
9	Copper (II) Phtalocyanine 3
10	Polyethylene 1
11	Polyethylene 2
12	Polyethylene 3
13	Sepia Melanin 1
14	Sepia Melanin 2
15	Sepia Melanin 3
16	Cellulose 1
17	Cellulose 2
18	Cellulose 3

**Figure 2.14:** Schematic representation of the entire setup

twice per week, and every time two different batches of vials were filled (one called *Sample α* and one *Sample β* . At the beginning, every week the solution in the traps was replaced with a new one, but it was realized that, analyzing the saturation of the traps, that action was not required so often. Every time that a new solution of $\text{Ba}(\text{OH})_2$ was prepared, two samples from that were taken, with the names *As Prepared α* and *As Prepared β* .

The titration automatic equipment (from the company *Metrohm*) has a rack with 34 sample holders and it is automatically managed by the software. The working principle of the titration is to add a quantity of HCl to the sample in order to obtain final pH equal to 7. The reaction in the chamber is as follows:



The procedure normally utilized for this measurements is:

1. Preparation of the station: fill with DI water the container for the chamber rinse and the bottle for the dilution, fill with HCl the appropriate bottle and empty the waste container.
2. Start the calibration of the machine: it needs three buffer solutions (pH 4, pH 7, pH 10) and DI water.
3. Validation of the machine with four samples with a solution of 2 ml of NaOH and 40 ml of DI water. This passage was considered not more significant after an maintenance action by an engineer of *Metrohm* in December.
4. Preparation of the samples: 2 ml of samples from the traps and 40 ml of DI water were put in a cup, labeled with the name of its own trap and covered with aluminium foil as it is possible to observe from the Figure 2.15a. It was realized that without any cover on the top of the cups, the $\text{Ba}(\text{OH})_2$ was capturing CO_2 from the air, therefore the results of the titrations of the samples which were exposed for a longer time to the air were not completely reliable.

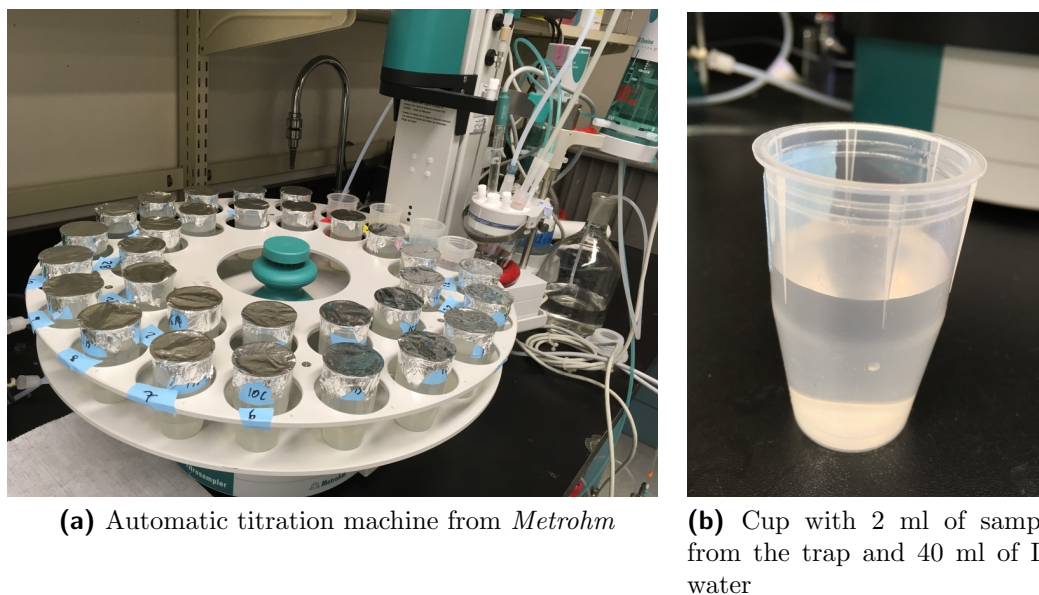


Figure 2.15: *Instrument and samples for the titration measurement*

5. Add to the software the following instructions:

- Method developed to perform the titrations
- Position and name of the samples
- Set 30 ml of the solution for the measurement

The machine returns the volume of the HCl utilized to neutralize the $\text{Ba}(\text{OH})_2$: this value was recorded in a file which contains all the informations and elaborations performed.

As written before, the solution on the traps was changed periodically every two or three weeks. But it does not mean that the bottles were not touched in the meanwhile. Indeed, there was a precise schedule to follow in order to avoid (or to solve) problems in the system.

- At least twice per day, a *Bubble Check* was performed. It was a procedure to make sure that everything was working in the right way. It meant to check the pressure in the water column and in the bioreactors (respectively 1.4 psi and 0 psi), to put the air flow to 40 units

Table 2.4: *Conventional symbols for the bubbling check*

Symbol	Meaning
•	Working
○	Slow Bubbling
X	Working after one shake
△	Working after two shakes
I	Working after an action was taken
ϕ	Manometer found to 0
M	Flexible tube fallen in the trap

for each reactor and to take note of the bubbling in the traps (by the conventional symbols in Table 2.4) and write every action taken.

- Verification of the reactors weight: with the temperature around 58 °C the evaporation is significant, therefore the compost was losing gradually water. In order to avoid to dry excessively it (because the absence of water would have slowed down the respiration by the microorganisms), once a week it was computed the quantity of water to add to reach the original weight of the reactors. After every opening operation of the reactors, a very accurate check of their caps was required: the higher temperature in the oven was the responsible of the thermal expansion of the plastic caps, therefore it was absolutely important to check several times if the bioreactors were well sealed to avoid air leakages.
- Substitution of the flexible tubes in the traps: these pipes allows the bubbling of the air in the Ba(OH)₂, allowing an intimate contact and the capture of CO₂, producing a white precipitate, BaCO₃. This barium carbonate was the responsible of the clog of the tubes, arresting the air flow in the traps. An operation of massaging or replacing of the them was required in order to avoid these problems.

Chapter 3

Results and Discussion

3.1 Electrical Response

The electrical and photoconductivity properties of DHICA-melanin were analyzed in ambient ($RH \approx 25\%$) and high humidity conditions ($RH \approx 90\%$). The first test performed in ambient conditions at different applied potentials confirmed immediately the hypothesis in Mostert and Wünsche^{13,14} articles, where it was demonstrated that the conductivity on melanin films is strongly dependent on the water quantity in it. Indeed, no current was detected in ambient conditions, neither in dark environment, nor in presence of light. The Figure 3.1 shows the transient of current in 30 min of test at different applied bias (0.1 V, 0.3 V and 0.5 V) in dark condition.

The trend of the graphs in dark conditions can be compared with the ones observed by Wünsche¹⁴ on the *Sigma Melanin* and reported in Figure 1.14 on page 26: the current is clearly dependent on the applied voltage, increasing its magnitude with the bias. But the most important property to observe is probably the characteristic shape of the graphs. In fact, it is clearly noticeable a fast decreasing on the first part, followed by a plateau with a slow, but persistent, decrease.

It is possible to explain this behavior with the coexistence of three mechanisms:

1. The first rapid decrease of the current could be ascribed to the ionic

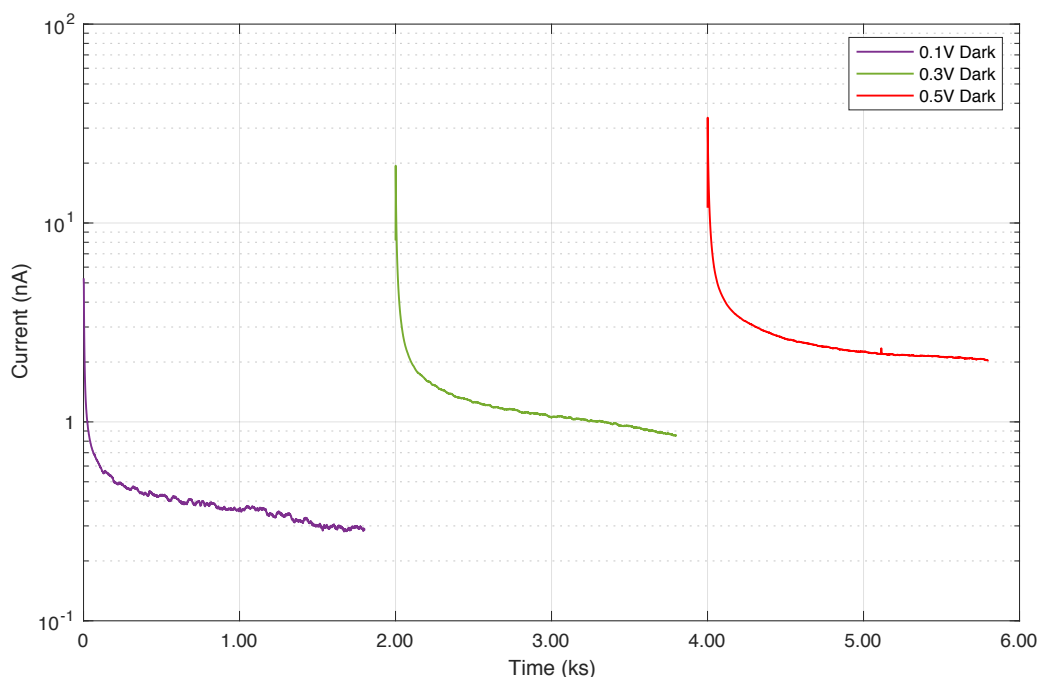


Figure 3.1: Transient current on the DHICA-melanin film deposited on gold electrodes with $10\ \mu\text{m}$ gap under different bias conditions, at $\text{RH} \approx 90\%$.

currents that are blocked at the gold electrodes (formation of electrical double layers). Ions are mainly H^+ and OH^- , but it is not excluded the presence of others anions and cations from the synthesizing process of melanin monomers, like Cl^- , Na^+ or other from melanin itself. The low mobility of the ions in absence of water can partially explain the absence of current in ambient conditions. Through the software *Origin* an exponential fit was performed (Figure 3.2) and the Equation 3.1 describes it, with coefficient of determination $R^2 = 0.986$.

$$y = A_1 * e^{-\frac{x}{t_1}} + A_2 * e^{-\frac{x}{t_2}} + y_0 \quad (3.1)$$

Where $A_1=4.01202\ \text{nA}$, $A_2=26.78915\ \text{nA}$, $y_0 = 2.21014\ \text{nA}$,
 $t_1 = 181.24902\ \text{s}$, $t_2 = 8.14799\ \text{s}$.

2. The electrons injected in the melanin due to the presence of the external

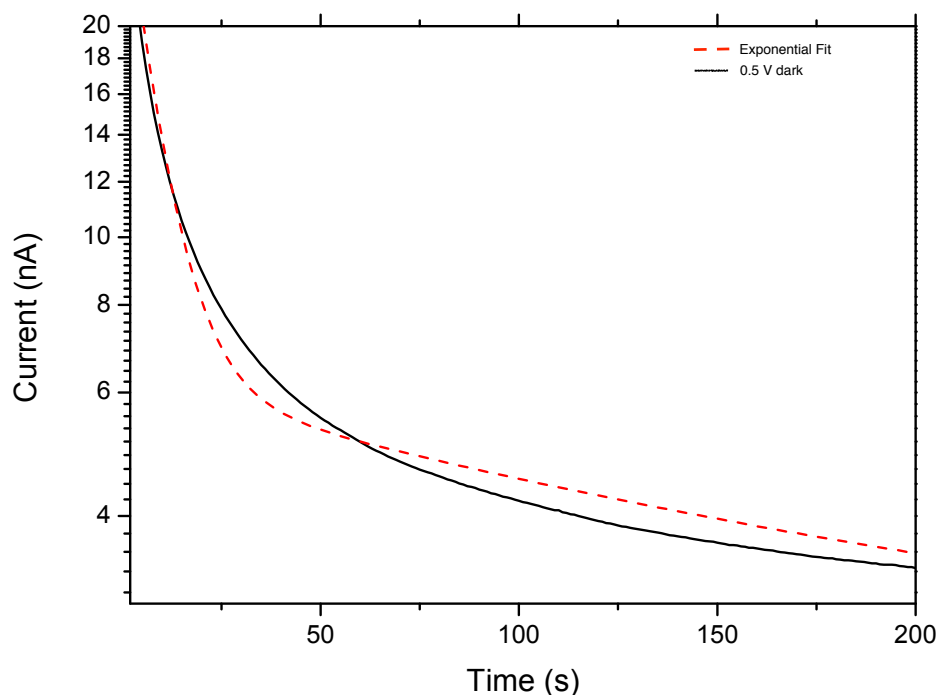


Figure 3.2: First 200 s of transient current in DHICA-melanin film deposited on gold electrodes with 10 μm gap at 0.5 V, RH \approx 90%, and its exponential fit.

electric field. It is probably the quasi-plateau zone, when probably they reach a sort of equilibrium.

3. It cannot be excluded an electrochemical contribution.

Figure 3.3 resumes the three conduction principles just mentioned. It is important to note that the three currents are influenced by the others: the mobile protons blocked at the negative electrode facilitate the electrons injection in the dielectric, but, on the other hand, the electrical double layer generate an electric field with opposite direction compared to the external one. The complexity of this model of charge transport in the melanin thin film requires for sure more efforts to understand the mechanisms, but according to the results of Wünsche¹⁴ on *Sigma Melanin*, the presence of a ionic and electronic conduction in DHICA-melanin films seems confirmed.

In order to investigate the photoconductivity property of melanin, a light source in visible range lit the sample, whose spectrum and intensity are specified in Chapter 2.1.3 on page 43. The photocurrent due to the exposure

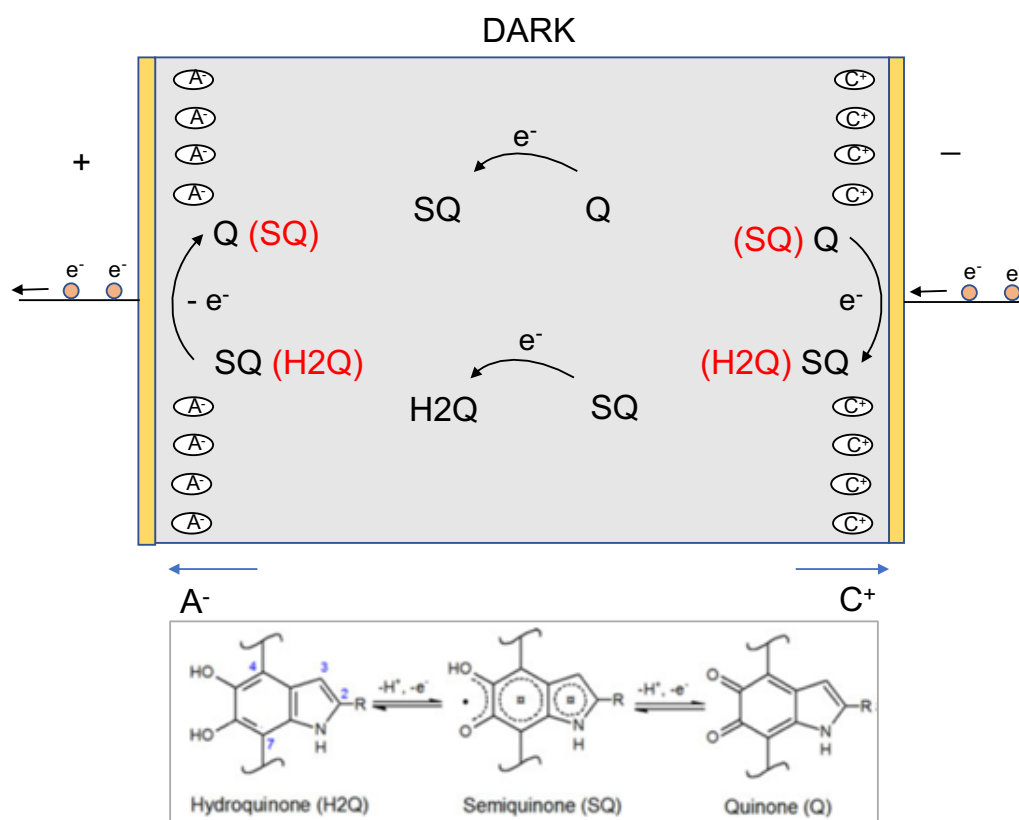


Figure 3.3: Conduction principles in DHICA-melanin thin film.

on a light source was already mentioned in Figure 1.15 on page 27. The results on the experiment conducted on DHICA-melanin film are shown in Figure 3.4, where a comparison between the dark and light trend is overlaid for each applied bias.

An increase of current is evident when the light is turned on, with an value between 4 – 5 times the dark one (before the radiation on the sample). It is possible to notice also a decrease when the light is chopped with a similar trend of the dark condition. The difference between the curves at the same bias can be ascribed to the *RH* fluctuations in the chamber: indeed, it was difficult to maintain exactly the same humidity percentage value during all the test time due to leakage in the sealing of it. The auto-regulation of water content in that environment provides to increase it if *RH* is lower than a preset value. It was considered and accepted $RH = 90 \pm 1\%$, but the test

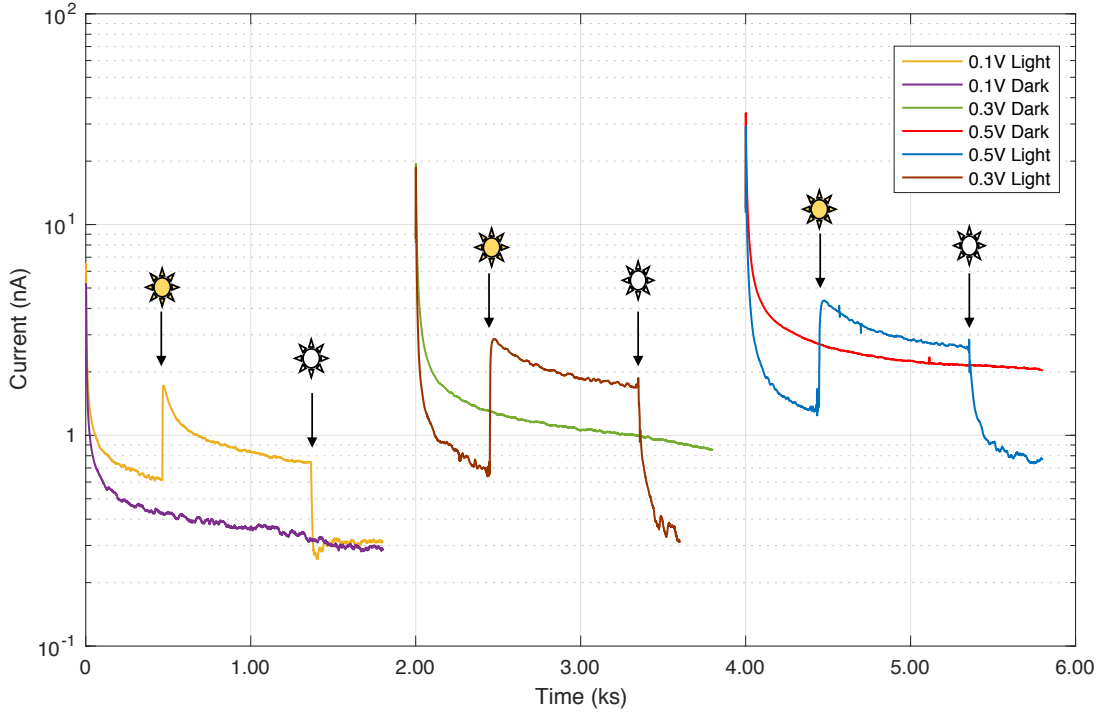


Figure 3.4: Comparison between transient current in light and dark condition on a DHICA-melanin deposited on gold electrodes with $10\ \mu\text{m}$ gap under different bias conditions, $RH \approx 90\%$.

performed in higher water content conditions presents higher currents, due to the higher mobility of the charge carriers in the DHICA-film.

Furthermore, it was used, as before, the software Origin in order to study the transient current immediately after the chop of the light, as shown in Figure 3.5. The software retrieves the equation of the fit (Equation 3.2), with a coefficient of determination $R^2 = 0.973$.

$$y = y_0 + A_1 * e^{-\frac{x-x_0}{t_1}} \quad (3.2)$$

Where $A_1 = 1.81897\ \text{nA}$, $y_0 = 0.80947\ \text{nA}$, $x_0 = 1349.1175\ \text{s}$, $t_1 = 38.089\ \text{s}$. The photosensitization of the DHICA-melanin thin film and the consequent photocurrent, can be explained as following: under light conditions, electron transfer processes are more probable since electrons have higher energy (or holes have lower energy) compared to the vacuum. There is a wide distribution of molecular energy states in melanin, due to chemical and physical

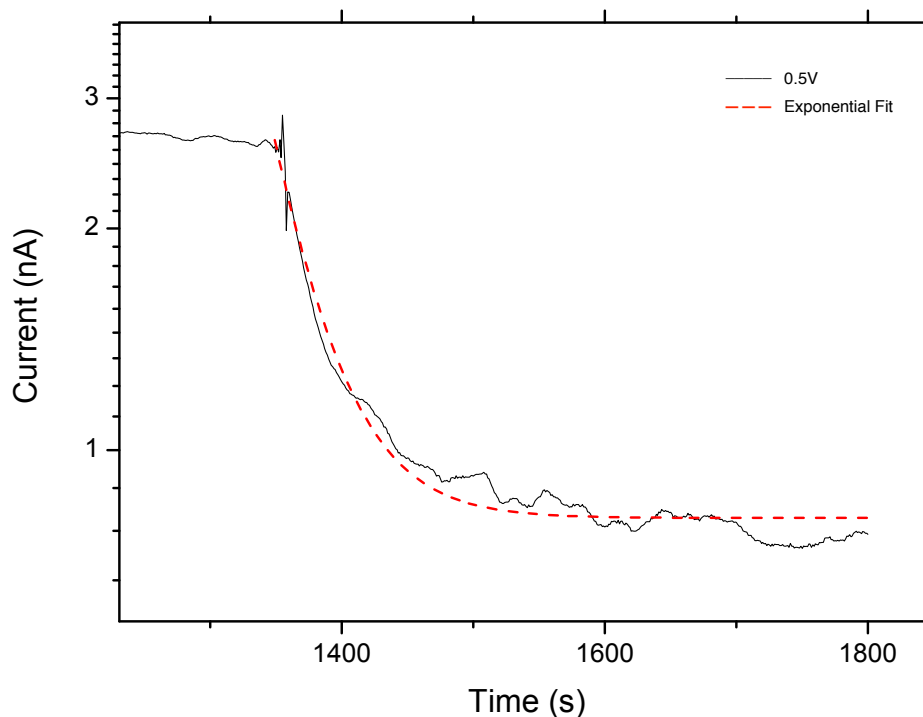


Figure 3.5: *Transient current after the chop of the light in DHICA-melanin film deposited on gold electrodes with $10\ \mu\text{m}$ gap at $0.5\ \text{V}$, $RH \approx 90\%$, and its exponential fit.*

disorder such that electron transfer processes are possible both in dark and light conditions.

The results of these tests gives important feedbacks on the electrical properties of melanin, also under light source. DHICA-melanin presents a peak of absorbance of the radiations for wavelength in the near-UV/UV region, thus the results obtained in this experiment are significant, considering that the radiation spectra of the light utilized is around $650\ \text{nm}$, far from the UV range (as it is possible to see from Figure 1.16 on page 28). A UV light source from a plasma device was also tested, but it was not possible to insert the fiber optic inside the chamber for the high humidity level. Further efforts are requested in order to understand this behavior in different light conditions, but also with DHI-melanin. The next step will be the study with the DHI-melanin (polymerized in the same way and same experimental conditions of the test just described) to understand if the different supramolecular structure influence the conduction and photo-conduction. Furthermore an

analysis on the monomers of DHI and DHICA will be interesting to have more information on the band gap.

3.2 UV-Visible Absorption

3.2.1 Effects of Polymer, Additives and their Concentration

The data acquired from the spectrophotometer were elaborated by means of Excel in order to reproduce the graphs and edit them. As previously explained in the Chapter 2.2.2, the equipment acquired the values of Transmission + Reflection together, thus the equations 2.1 and 2.2 on page 53 were considered to compute the values of the coefficient of absorption *pseudo* α . The general approach to understand the data was to show the *pseudo* α as a function of the wavelength (in the range 250 nm to 1400 nm) for the different polymers and analyze the effect of the different additives on each one. Considering the possible primary interest in packaging field, the ideal case would be a biopigment which increase the absorption of the polymer in the UV range (until $\approx 380\text{ nm} - 400\text{ nm}$) that leaves unaltered the visible absorption.

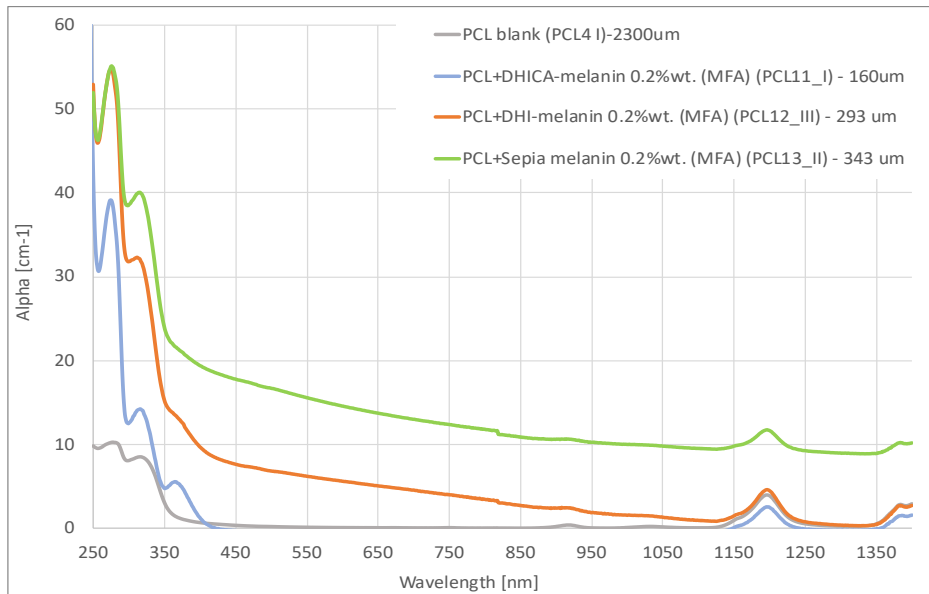
In Figures 3.6, the general influence of the the additives on the polymers is shown. On the y-axis the coefficient of absorption of the polymer with additive normalized on the one of the blank polymer ($\alpha_{pol+add}/\alpha_{blank}$) is reported as a function of the wavelength on the x-axis. The effect on the single polymer will be investigated in the next paragraphs where each polymer is analyzed separately to evaluate the influence of the additive and its concentration.

Poly(ϵ -caprolactone) (PCL)

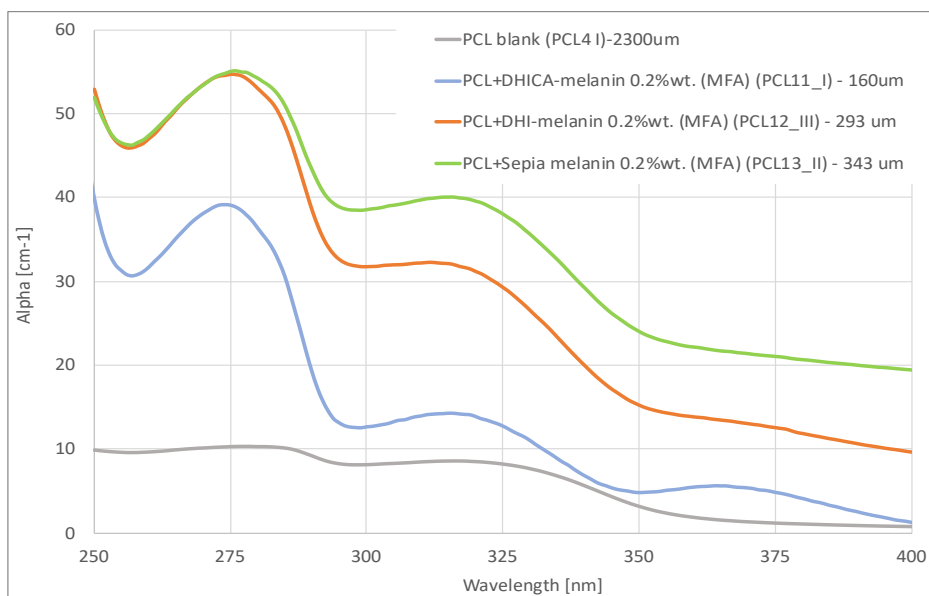
Graphs in Figure 3.7 show the influence of the different melanin additives (DHICA, DHI and Sepia Melanin) at the same weight concentration (0.2% wt.) in the polymer. From the Figure 3.7b is possible to notice that in the UVC (until 280 nm) and UVB (280 nm – 315 nm) regions, DHI-melanin



Figure 3.6: Influence of the melanin additives on the polymer analyzed in the UV range (on the left) and visible-NIR range (on the right).



(a) Entire spectra



(b) Focus on UV range, 250 nm – 400 nm

Figure 3.7: *Pseudo* α as a function of wavelength for PCL with the same weight concentration of melanin additives (0.2%wt.): a) in the entire analyzed spectra; b) in the UV range (250 nm – 400 nm)

and Sepia Melanin confer a 5 time increase of the absorption coefficient, while DHICA-melanin brings about a slightly inferior increase (3-4 times). However, in the near UVA (380 nm), the increase due to DHICA-melanin remains the same, whilst DHI-melanin and Sepia Melanin manage to confer a one order of magnitude increase. Such trend is confirmed also in the visible and near IR range.

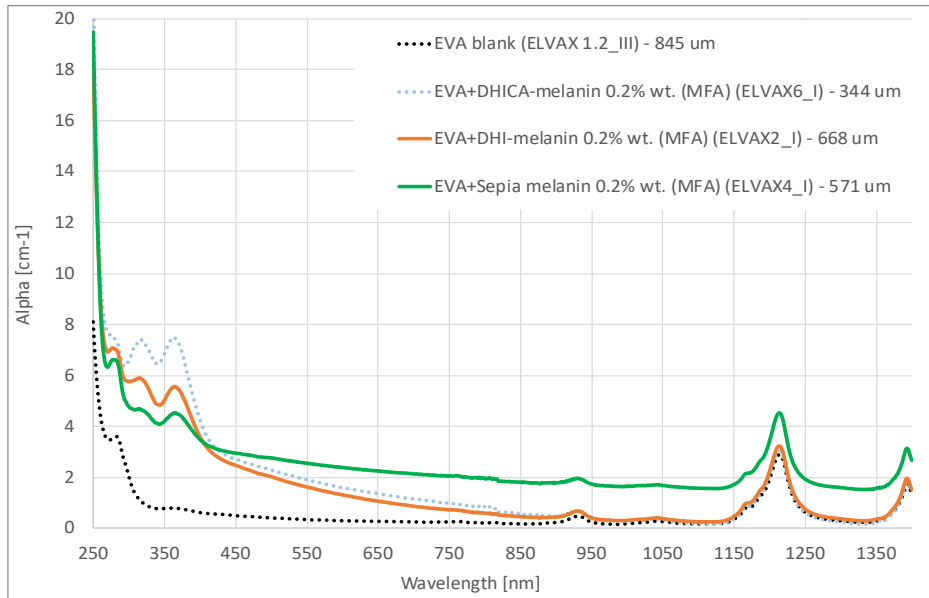
Only for the UV-absorption enhancement, DHI-melanin and Sepia Melanin seem to be the best options, but taking into account the visible too, DHICA-melanin preforms the best as it entails a lower decrease of transparency. Sepia Melanin, on the other hand, enhances the absorption in the visible up to 2 orders of magnitude.

Ethylene-vinyl acetate copolymer (EVA)

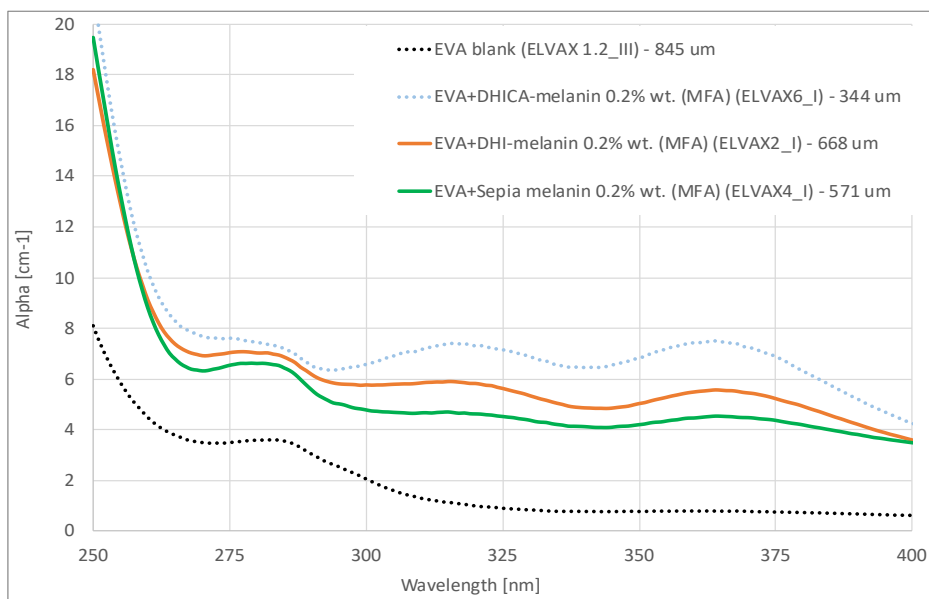
From the graphs in Figure 3.8 it is possible to notice that in the UVB and UVC ranges DHICA-melanin performs better than DHI-melanin and Sepia Melanin, with an increase of the value of α of 3 – 8 times for the DHICA-melanin compared to the 3 – 5 times for DHI-melanin and Sepia Melanin, as it is possible to see in the Figures 3.6 on page 70. From the graphs of visible-NIR range in the same of the same Figure, Sepia Melanin performs worse than synthetic melanins, as the ratio $\alpha_{pol+add}/\alpha_{blank}$ reaches a one order of magnitude increase. DHICA-melanin seems to give the best performance in terms of compromise between UV-shielding enhancement with limited visible absorption.

Ethylene-Methyl Acrylate copolymer (PEMA)

The three additives in PEMA manage to confer approximately one order of magnitude increase in the UVA and UVB regions, as represented in Figures 3.9, with DHI-melanin showing the best enhancement, reaching 15 time of increase compared to the blank one at 380 nm as shown in Figure 3.6c on page 70. While Sepia Melanin keeps this increase in the visible too, the synthetic ones gives a less evident contribution to the absorption.

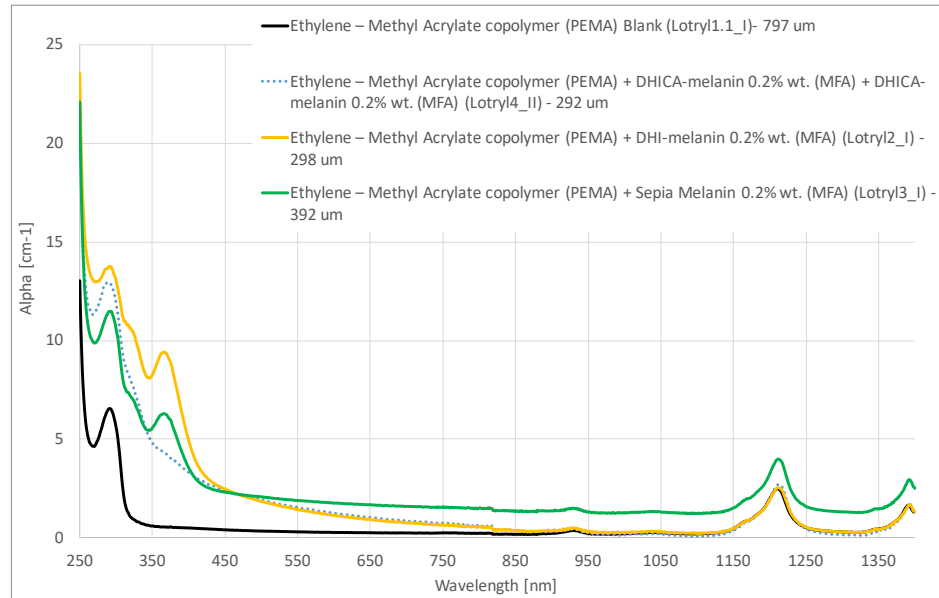


(a) Entire spectra

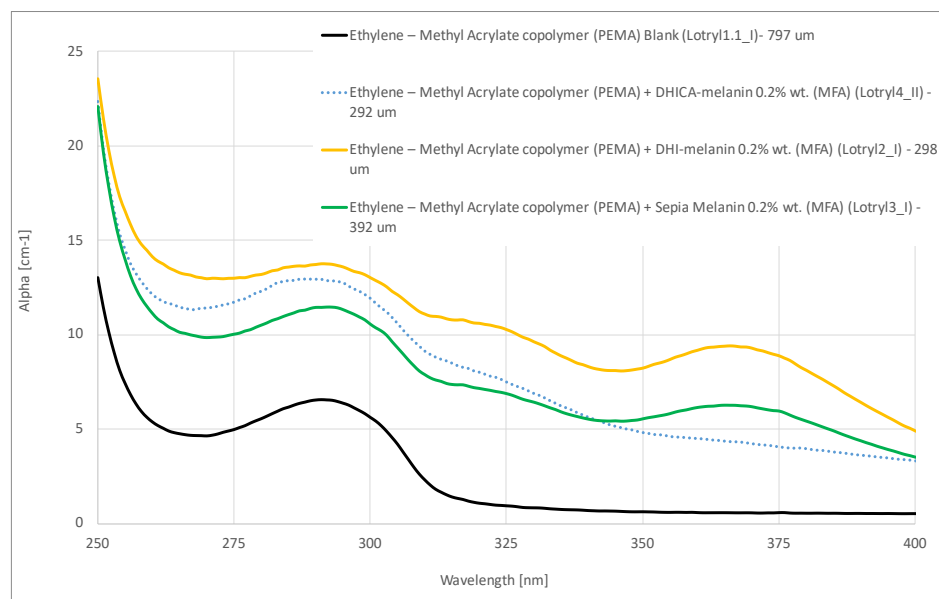


(b) Focus on UV range, 250 nm – 400 nm

Figure 3.8: Pseudo α as a function of wavelength for EVA with the same weight concentration of melanin additives (0.2%wt.): a) in the entire analyzed spectra; b) in the UV range (250 nm – 400 nm)



(a) Entire spectra



(b) Focus on UV range, 250 nm – 400 nm

Figure 3.9: Pseudo α as a function of wavelength for PEMA with the same weight concentration of melanin additives (0.2%wt.): a) in the entire analyzed spectra; b) in the UV range (250 nm – 400 nm)

Random Terpolymer of Ethylene, Ethyl Acrylate and Maleic Anhydride (PEEAMA)

The bar charts in the UV range of Figure 3.6 on page 70 indicate that the absorption enhancement in this region is limited for the PEEAMA with respect to the other polymers, with a maximum increase of 4 times of the ratio $\alpha_{pol+add}/\alpha_{blank}$. This very limited effect for the three additives could be ascribed to an intrinsic property of the polymer: the ethyl groups of the ethyl acrylate might have screened the polar part of the ethyl acrylate, preventing a good interaction between the additives and the polymer.

Linear Low-Density Polyethylene (LLDPE)

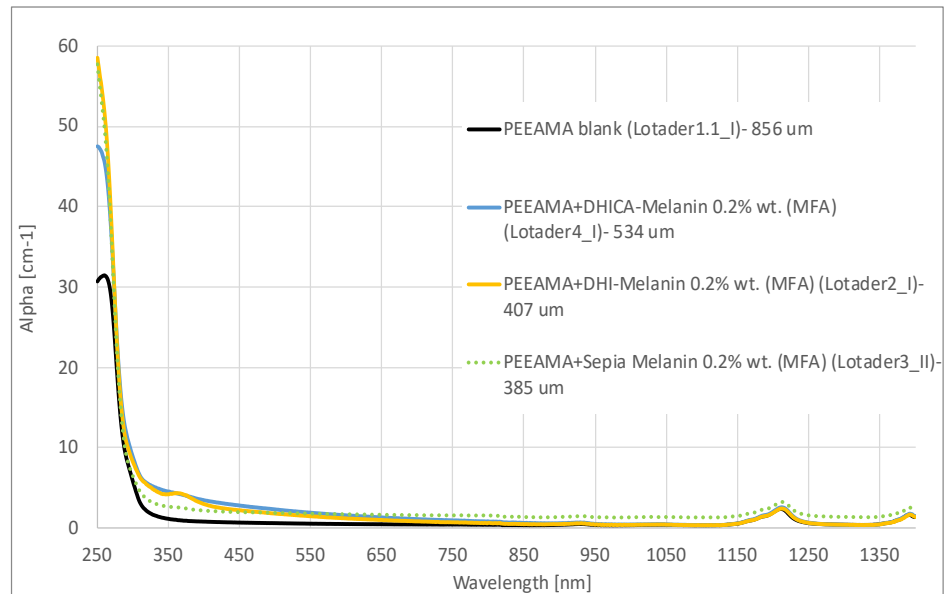
The LLDPE presents a negligible enhancement of the coefficient of absorption in the UVC and UVB ranges, considering that the blank polymer has its own peak of absorption between $270\text{ nm} - 320\text{ nm}$, as it is possible to deduce from Figures 3.11 on page 77 and 3.6 on page 70, while in the UVA zone there is an increase of 4 – 7 times. Considering the visible range the ratio $\alpha_{pol+add}/\alpha_{blank}$ has values between 5 – 10 for the three additives.

Anhydride-Modified Linear Low-Density Polyethylene (LLDPE-MA)

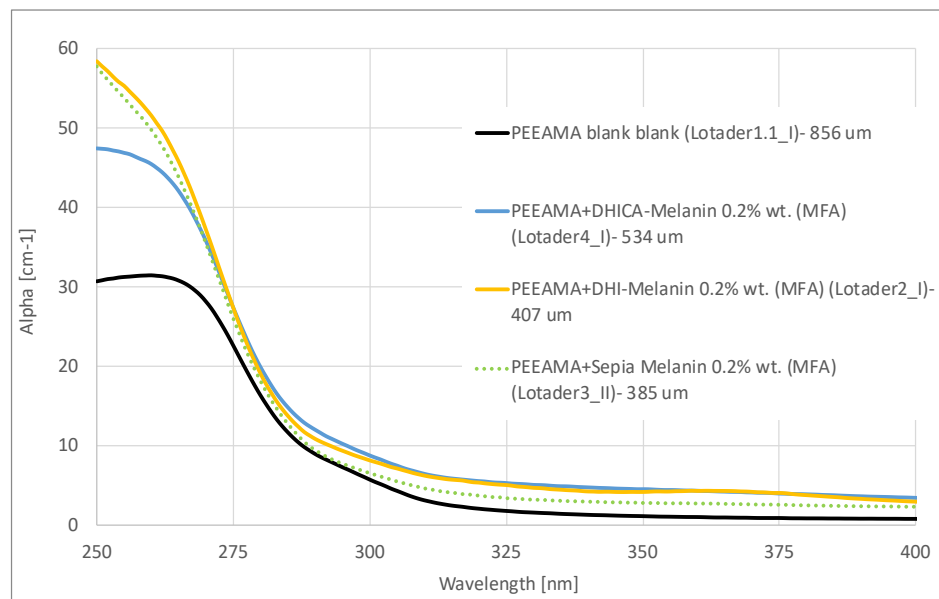
The trend of the coefficient of absorption in the UV is negligible as shown in Figure 3.12 on page 78: in UVA the blank LLDPE-MA present a peak of absorption, thus the enhancement for the polymer with additive is not relevant; in UVC and UVB the DHI-melanin and Sepia Melanin provide an increase about 3 – 4 times. In the visible Sepia Melanin confers up to 1 order of magnitude increase of the α .

Anhydride-Modified Low-Density Polyethylene (LDPE-MA)

From the charts in Figures 3.6 on page 70 and 3.13 on page 79 it is possible to see that the enhancement in UV region is negligible for all the three additives. This behavior may be due to a too low melt compounding temperature.

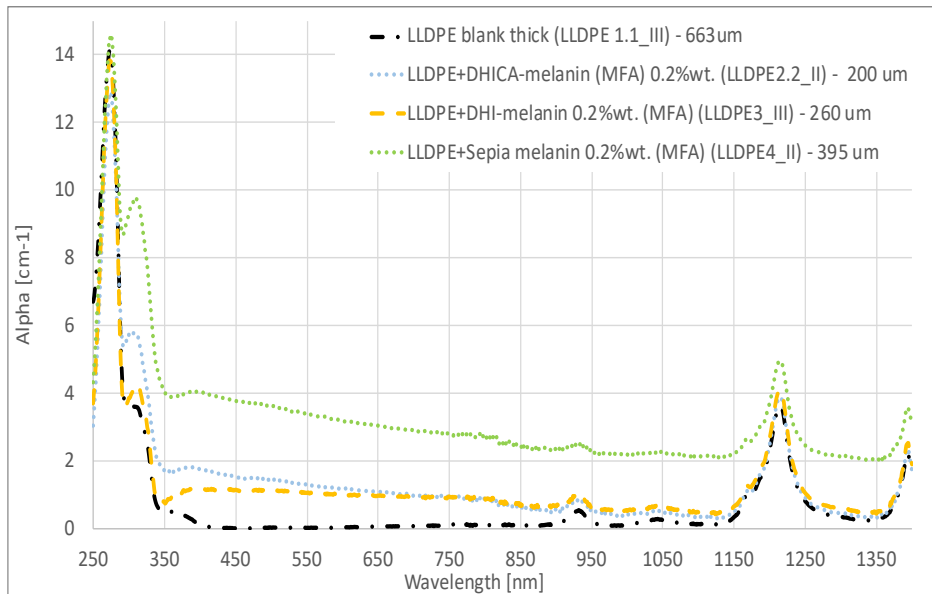


(a) Entire spectra

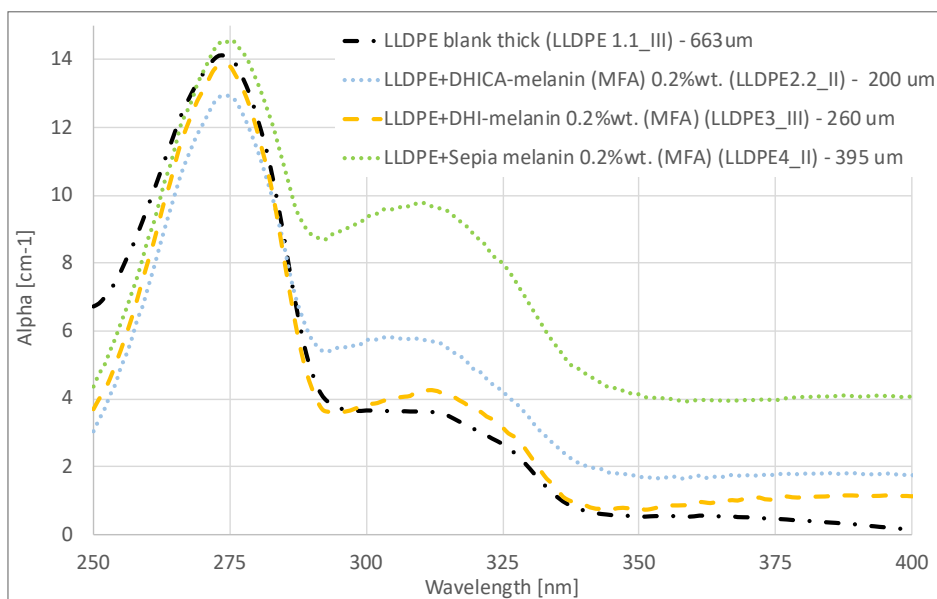


(b) Focus on UV range, 250 nm – 400 nm

Figure 3.10: *Pseudo* α as a function of wavelength for PEEAMA with the same weight concentration of melanin additives (0.2%wt.): a) in the entire analyzed spectra; b) in the UV range (250 nm – 400 nm)

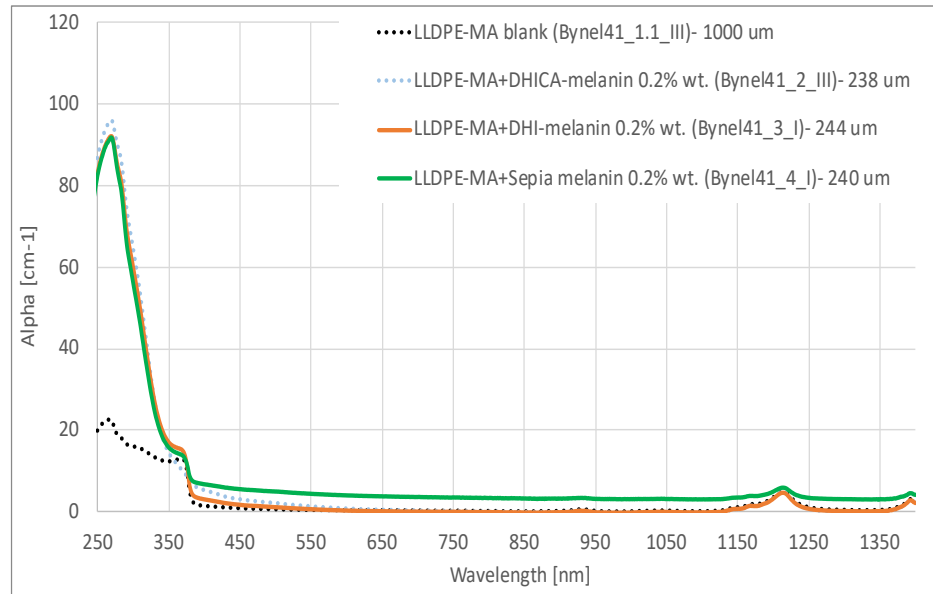


(a) Entire spectra

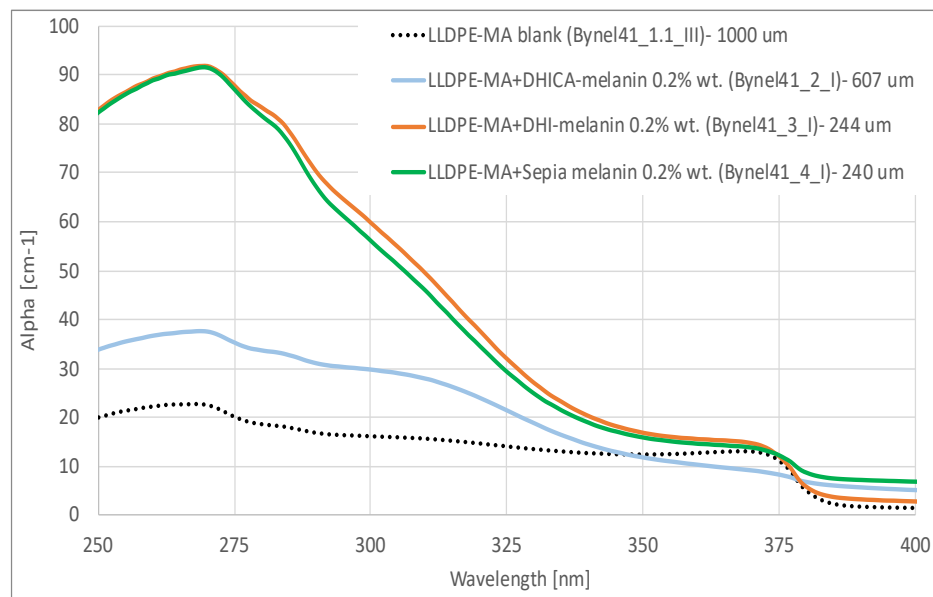


(b) Focus on UV range, 250 nm – 400 nm

Figure 3.11: *Pseudo* α as a function of wavelength for LLDPE with the same weight concentration of melanin additives (0.2%wt.): a) in the entire analyzed spectra; b) in the UV range (250 nm – 400 nm)

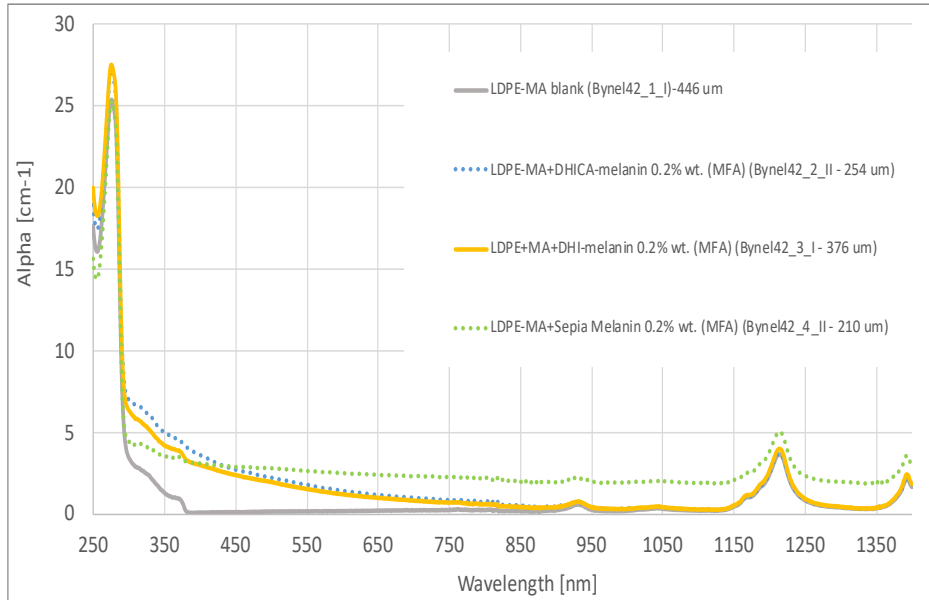


(a) Entire spectra

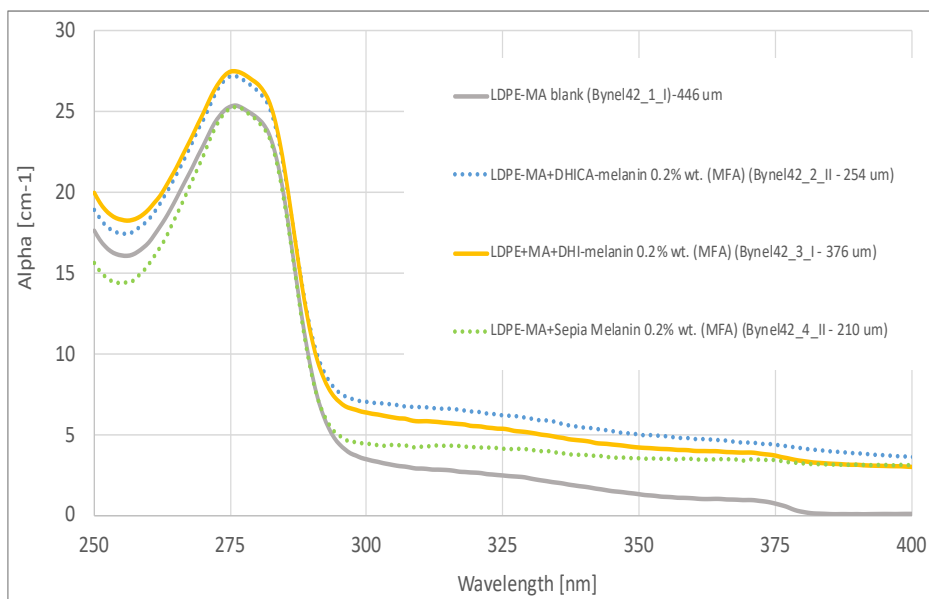


(b) Focus on UV range, 250 nm - 400 nm

Figure 3.12: Pseudo α as a function of wavelength for LLDPE-MA with the same weight concentration of melanin additives (0.2%wt.): a) in the entire analyzed spectra; b) in the UV range (250 nm - 400 nm)



(a) Entire spectra



(b) Focus on UV range, 250 nm – 400 nm

Figure 3.13: Pseudo α as a function of wavelength for LDPE-MA with the same weight concentration of melanin additives (0.2%wt.): a) in the entire analyzed spectra; b) in the UV range (250 nm – 400 nm)

Copolymer Ethylene-Propylene (EPC)

It is possible to observe in the Figure 3.14 on the next page and 3.6 on page 70 that DHICA-melanin provides an increase of 3 – 6 times if the absorption coefficient, DHI-melanin of one order of magnitude and Sepia Melanin in the range of 2 – 9 times. Also in this case the synthetic melanins perform better than the Sepia Melanin in the visible range as the latter brings about an increase of one order of magnitude compared to the blank coefficient of absorption over the entire visible spectrum.

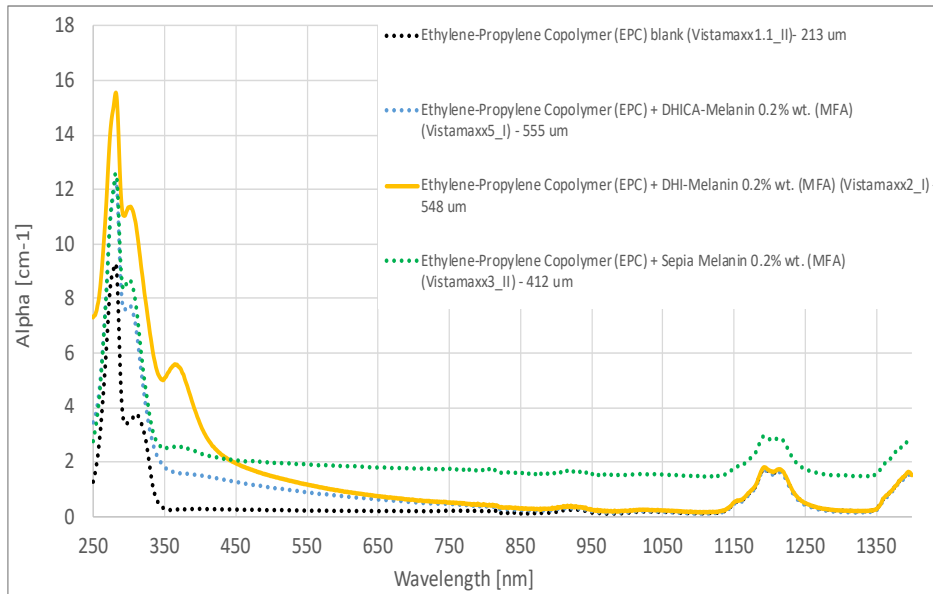
Table 3.1 on page 82 summarizes the values of the ratio $\alpha_{pol+add}/\alpha_{blank}$ at different wavelengths/range (UVC (250 nm), UVB (320 nm), UVC (380 nm), visible (590 nm and 800 nm)).

Observations

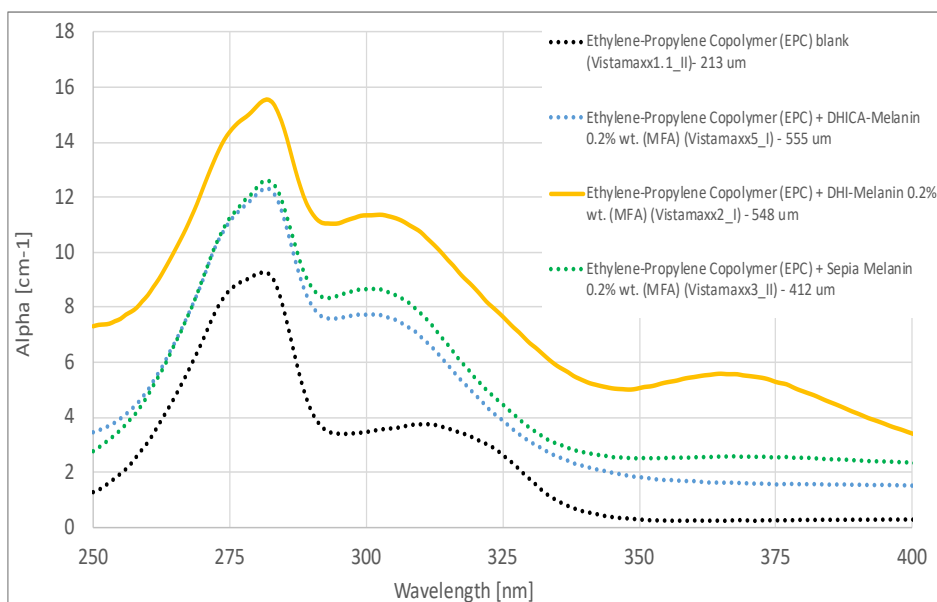
After this first analysis, it can be stated that only for the polymers EVA, PCL, PEMA and LLDPE-MA the addition of 0.2% *wt.* of Melanin Free Acid has really given a significant (at least 2 – 3 times with respect of the *psedo* α of the blank) UV-absorption enhancement. A possible explanation could be found in the presence of polar groups in the polymer structure, which are supposed to favor the interactions with the melanin biopigments.

The plastics analyzed in this project can be distinguished into two categories:

- Four of them contain a non-negligible percentages of polar groups on the main chain or side groups (PCL is a polyester, with oxygen atoms on the main chain; EVA contains 9.3% *wt.* of vinyl acetate; PEMA contains 27 – 31% *wt.* of ethyl acrylate and PEEAMA contains 29% *wt.* of ethyl acrylate and 1.3% *wt.* of maleic anhydride). Three of them are polymers with UV-absorption enhancement provided by eumelanin (the exception of PEEAMA was aforementioned).
- The other four are polyolefins with no (as LLDPE and EPC) or very negligible (like LLDPE-MA and LDPE-MA) percentage of polar groups. Among those, LLDPE and LDPE-MA show in the previous analysis a negligible enhancement by 0.2% *wt.* Melanin Free Acid. The polymer



(a) Entire spectra



(b) Focus on UV range, 250 nm – 400 nm

Figure 3.14: Pseudo- α as a function of wavelength for EPC with the same weight concentration of melanin additives (0.2%wt.): a) in the entire analyzed spectra; b) in the UV range (250 nm – 400 nm)

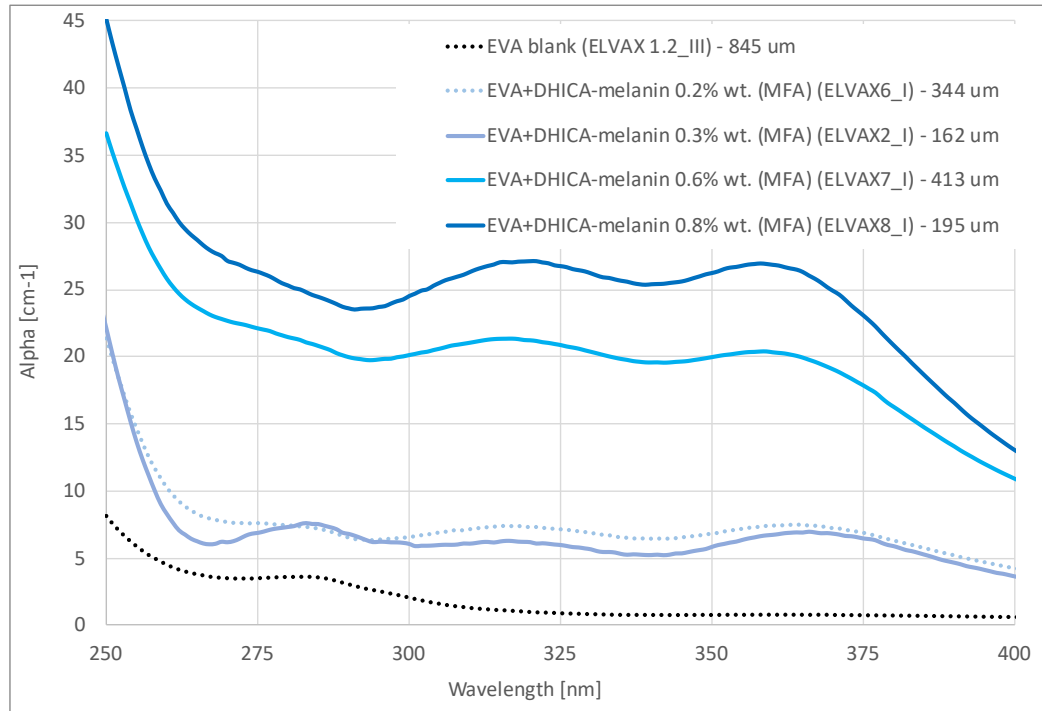
Table 3.1: Ratios $\alpha_{pol+add}/\alpha_{blank}$ for an additive amount of 0.2% wt. at different wavelengths in UV and visible regions.

Polymer	Additive 0.2 % wt.	$\alpha_{pol+add}/\alpha_{blank}$				
		UVC 250 nm	UVB 320 nm	UVA 380 nm	Visible 590 nm 800 nm	
PCL	DHICA-melanin	4	2	4	5	2
	DHI-melanin	5	4	10	30	30
	Sepia Melanin	5	5	20	85	100
EVA	DHICA-melanin	3	7	8	5	4
	DHI-melanin	2	7	7	4	3
	Sepia Melanin	2	5	6	7	7
PEMA	DHICA-melanin	2	8	7	5	3
	DHI-melanin	2	10	15	4	2
	Sepia Melanin	2	7	10	6	6
PEEAMA	DHICA-melanin	2	3	5	3	2
	DHI-melanin	2	3	4	3	2
	Sepia Melanin	2	2	3	4	4
LLDPE-MA	DHICA-melanin	4	3	1	2	1
	DHI-melanin	4	3	1	1	1
	Sepia Melanin	4	2	2	7	9
LDPE-MA	DHICA-melanin	1	1	1	1	2
	DHI-melanin	1	1	1	1	2
	Sepia Melanin	1	1	1	1	6
LLDPE	DHICA-melanin	<1	1	4	13	5
	DHI-melanin	1	1	3	12	6
	Sepia Melanin	1	2	9	47	23
EPC	DHICA-melanin	3	1	6	3	2
	DHI-melanin	6	3	17	4	2
	Sepia Melanin	2	2	9	8	8

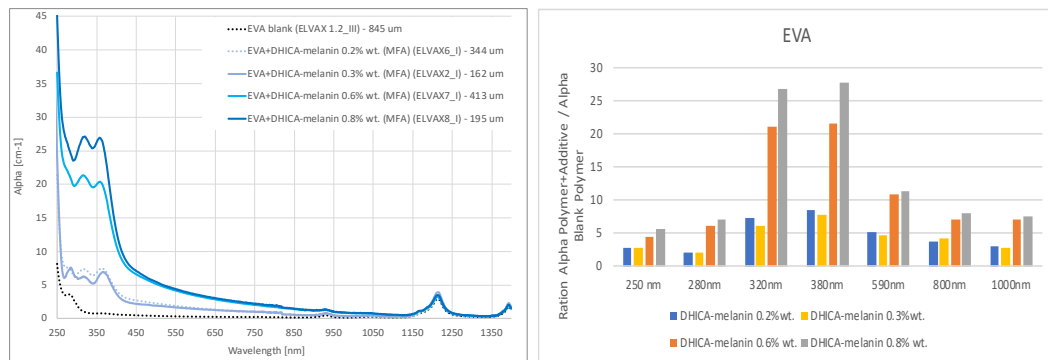
with no polar groups but relevant UV-absorption enhancement with melanin is EPC, which has 89% of Polypropylene, whose well interaction with melanin is already reported in literature.²⁶

Among the three types of additives, DHICA-melanin seems to provide the best compromise between UV-absorption improvement, leaving the visible spectra mostly unchanged. As reported in the Chapter 1.3 on page 29, DHICA-melanin displays poorer visible absorption and an intense absorption band in the UV region.⁴ While DHICA-melanin and DHI-melanin in general provide an absorption enhancement with its maximum in the near-UV, on the other hand Sepia Melanin leads to an increase of the coefficient of absorption which continues through the visible range, until the near-IR. Consequently, DHICA-melanin was considered interesting to be tested in percentage higher than 0.2% *wt.* (0.5% *wt.*/0.6% *wt.*, 0.8% *wt.*/1.2% *wt.*) for the three polymers for which the effect of DHICA-melanin 0.2% *wt.* was important (PCL, EVA and EPC) and for the three polymers for which the effect of DHICA-melanin 0.2% *wt.* was almost null (LLDPE, LLDPE-MA, LDPE-MA).

1. EVA: a four times increase of the DHICA-melanin amount (from 0.2% *wt.* to 0.8% *wt.*) brings about an higher absorption both in the UV and visible, showing the highest increase in the UVA range, as it is possible to see from Figure 3.15.
2. PCL: in this case a wider range of concentration was investigated, until six times the original one (from 0.2% *wt.* to 1.2% *wt.*). It is confirmed, as the Figure 3.16 on page 85 shows, an enhancement of absorption both in UV and visible range, however the relative increase is more pronounced in the near UV and visible (where the ratio $\alpha_{pol+add}/\alpha_{blank}$ is almost 16 times higher) than in UVB and UVC (for $\lambda < 380\text{ nm}$ the increase of the ratio is only 1 – 2 times), due to the presence of the the peak of the blank polymer between 320 *nm* and 280 *nm*.
3. EPC: it was examined with additive percentage from 0.2% *wt.* to 0.8% *wt.*. The absorption coefficient increase both in UV and visible as in the



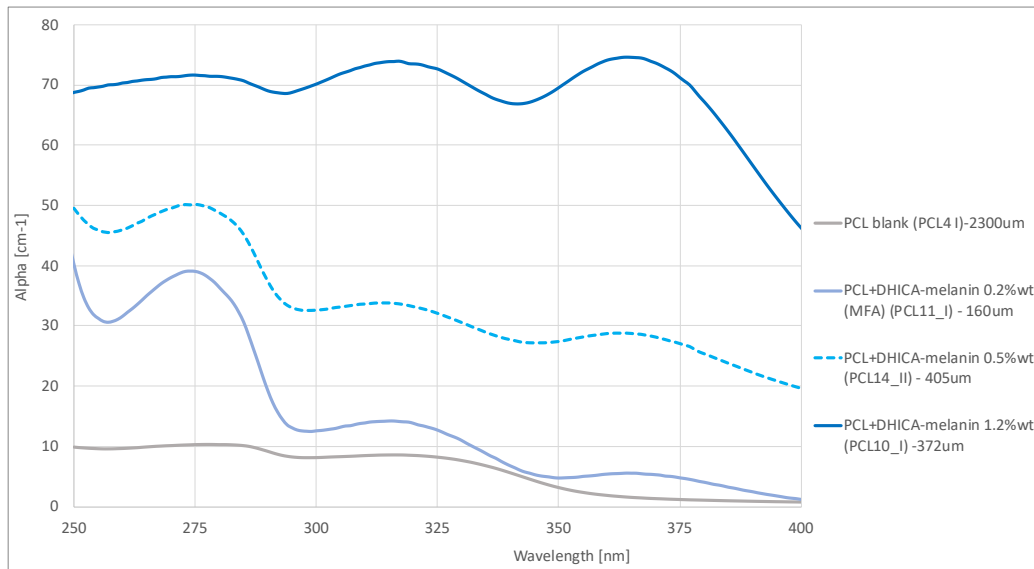
(a) Focus on UV range, 250 nm – 400 nm



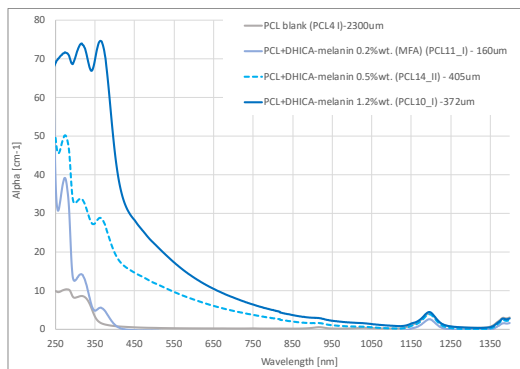
(b) Entire spectra

(c) Variation of the ratio $\alpha_{pol+add}/\alpha_{blank}$

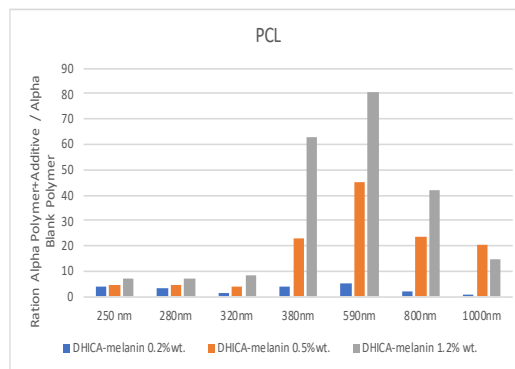
Figure 3.15: Influence on the coefficient of absorption as a function of the wavelength (a), focus on the UV range (b), and on the ratio $\alpha_{pol+add}/\alpha_{blank}$ (c) due to the different concentration values of DHICA-melanin in EVA



(a) Focus on UV range, 250 nm – 400 nm



(b) Entire spectra



(c) Variation of the ratio $\alpha_{pol+add}/\alpha_{blank}$

Figure 3.16: Influence on the coefficient of absorption as a function of the wavelength (a), focus on the UV range (b), and on the ratio $\alpha_{pol+add}/\alpha_{blank}$ (c) due to the different concentration values of DHICA-melanin in PCL

other polymer aforementioned. From the Figure 3.17 on the facing page is possible to observe that the highest increase is at 380 nm because the blank EPC has its own absorption peak between $315\text{ nm} - 280\text{ nm}$.

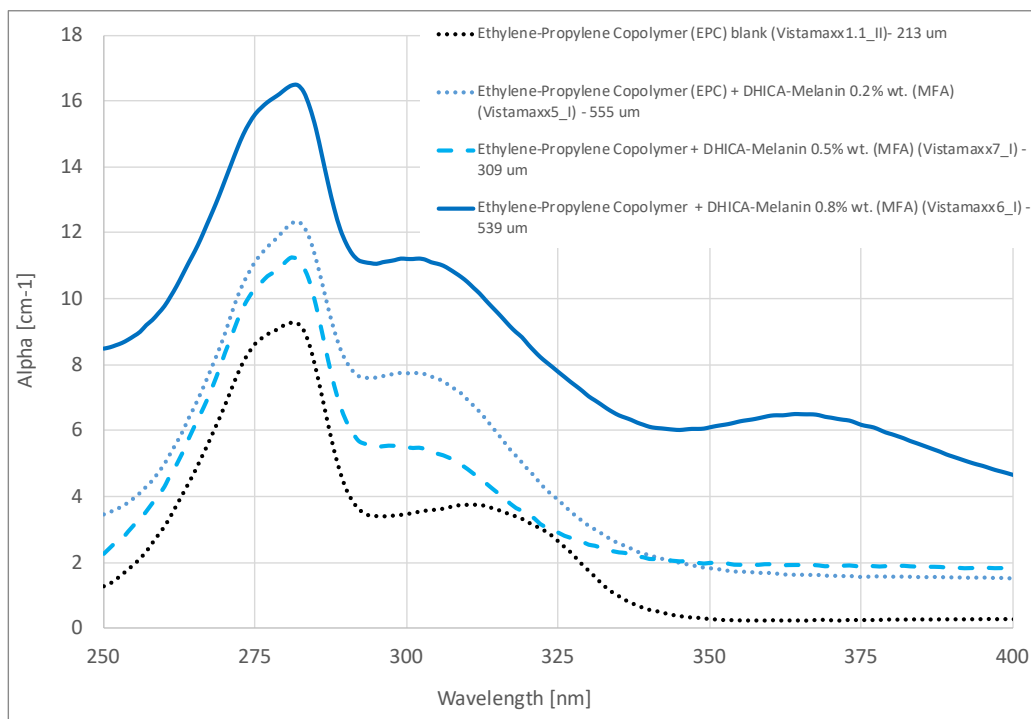
4. For LLDPE, LLDPE-MA and LDPE-MA the increase of the additive concentration gives a non-negligible enhancement of absorption both in UV and visible range, with a more significant relative increment in the visible as shown in Figure 3.18 on page 88.

It can be stated that the increasing of the additive percentage is worth for the polymers which did not evince a significant improvement with DHICA-melanin $0.2\% \text{ wt}$ in the UV-absorption (LLDPE and LDPE-MA). For the LLDPE-MA the increase of the concentration of the additive does not effect significantly the UV-absorption property with respect of $0.2\% \text{ wt}$.

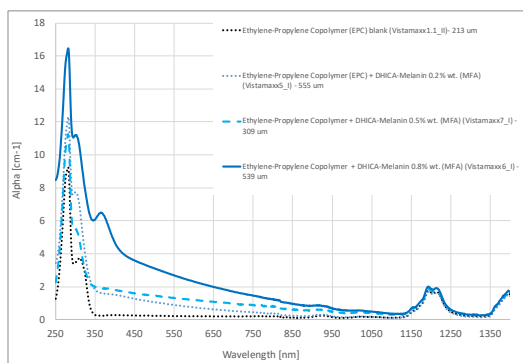
For EVA, PCL and EPC, for which the addition of $0.2\% \text{ wt}$. of DHICA-melanin causes a noticeable improvement in UV-absorption, it can be stated that the best performing percentage of additive remains $0.2\% \text{ wt}$. because higher concentration brings an enhancement more significant in the visible range than in the UV.

To confirm that DHICA-melanin was the only additive for which it was worth testing the effect of the concentration, Sepia Melanin $1\% \text{ wt}$. MFA was added to PCL: as shown in Figure 3.19 on page 89 the increase of absorption reaches one order of magnitude in the UV region, but in the visible range the ratio $\alpha_{pol+add}/\alpha_{blank}$ reaches two orders of magnitude of increase. Furthermore, the color of the sample turns to a completely black polymer (Figure 3.20 on page 89).

However, the performance of the three types of melanin additives tested are far from the commercial additive (benzophenone, $BLS^{\text{®}}531$), which manage to add one-two order of magnitude increase of the absorption coefficient in the UV region, leaving unchanged the α in the visible one as it is possible to observe in Figure 3.19.



(a) Focus on UV range, 250 nm – 400 nm



(b) Entire spectra

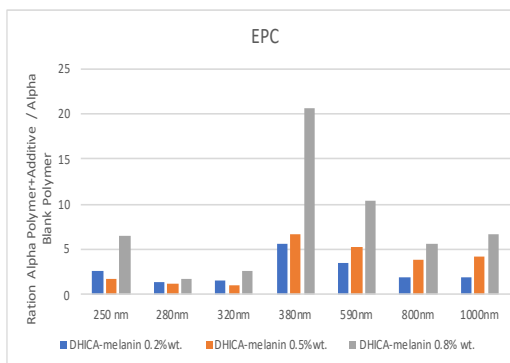
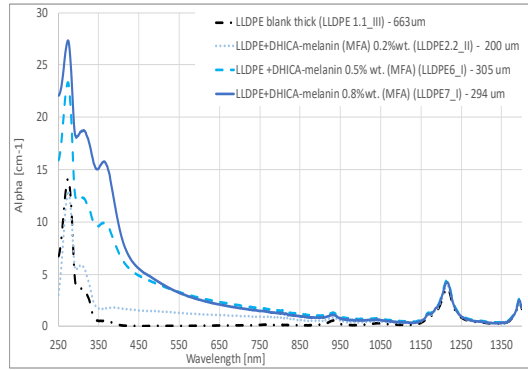
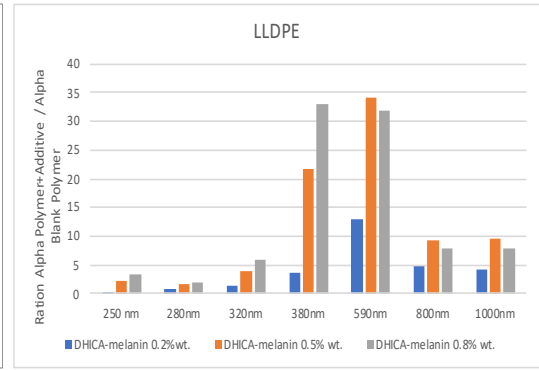
(c) Variation of the ratio $\alpha_{pol+add}/\alpha_{blank}$

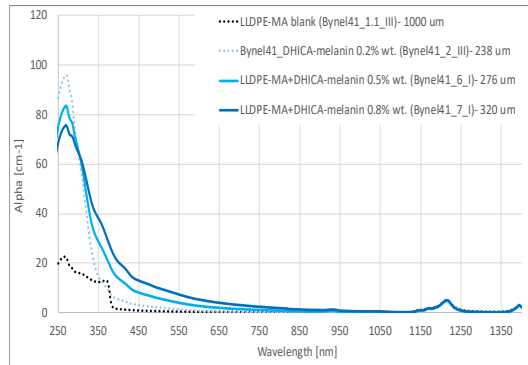
Figure 3.17: Influence on the coefficient of absorption as a function of the wavelength (a), focus on the UV range (b), and on the ratio $\alpha_{pol+add}/\alpha_{blank}$ (c) due to the different concentration values of DHICA-melanin in EPC



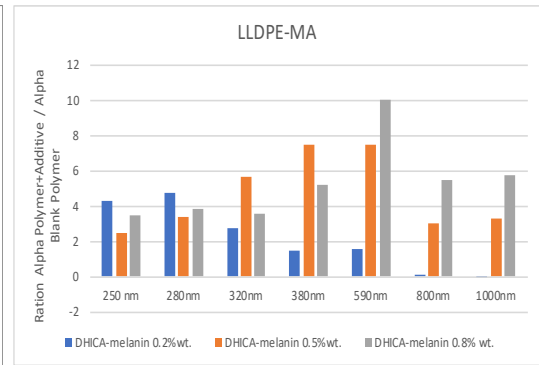
(a) DHICA-melanin influence on LLDPE



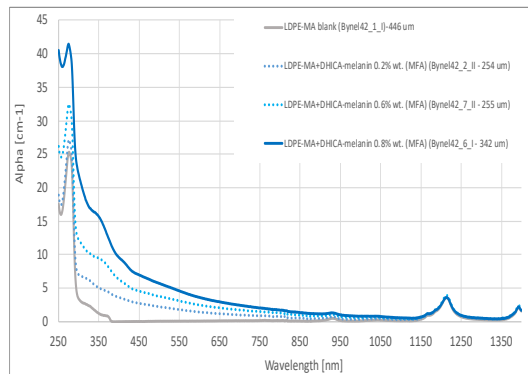
(b) Variation of the ratio $\alpha_{pol+add}/\alpha_{blank}$ in LLDPE



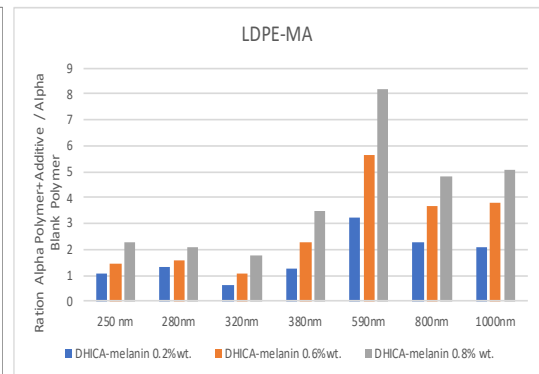
(c) DHICA-melanin influence on LLDPE-MA



(d) Variation of the ratio $\alpha_{pol+add}/\alpha_{blank}$ in LLDPE-MA



(e) DHICA-melanin influence on LDPE-MA



(f) Variation of the ratio $\alpha_{pol+add}/\alpha_{blank}$ in LDPE-MA

Figure 3.18: Influence on the coefficient of absorption and on the ratio $\alpha_{pol+add}/\alpha_{blank}$ for the different concentration in weight of DHICA-melanin.

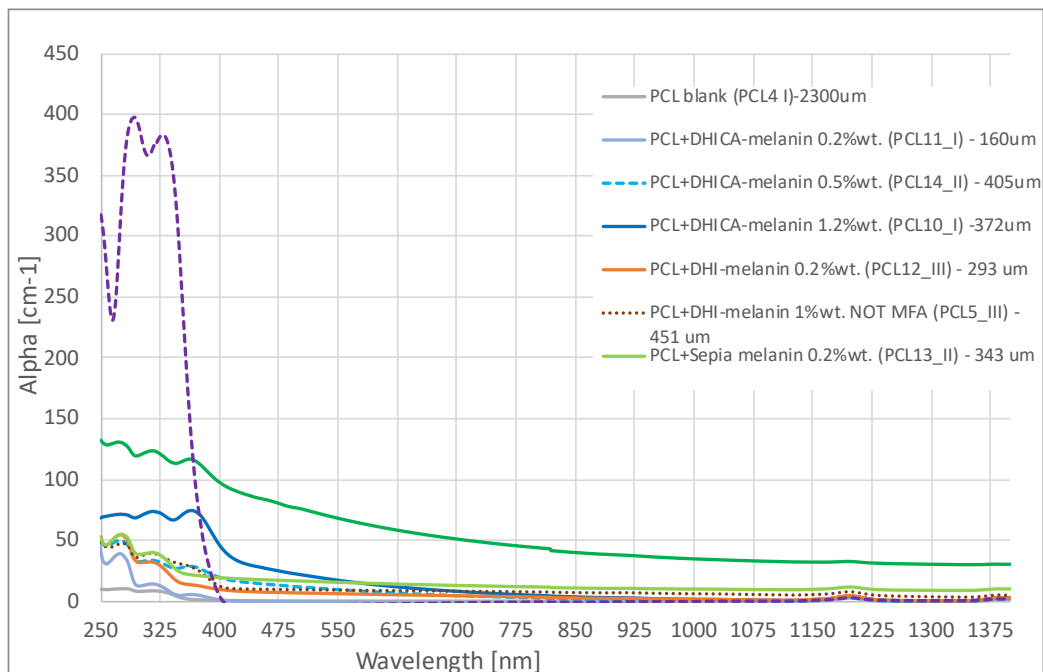


Figure 3.19: Comparison between all the additives tested on PCL

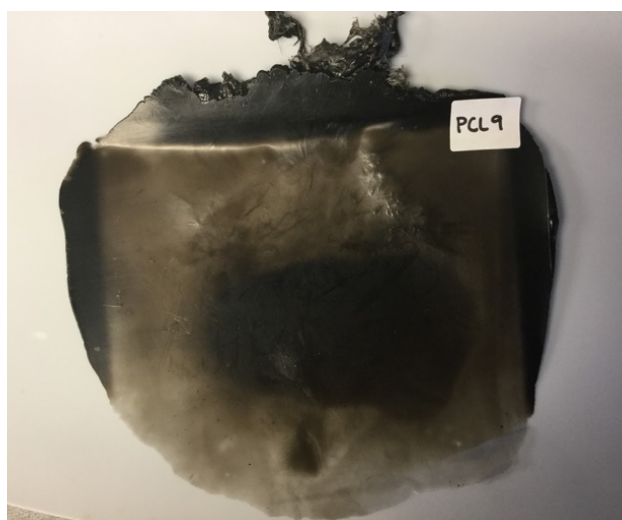


Figure 3.20: An example of how a PCL added with 1% wt. of Sepia Melanin looks like.

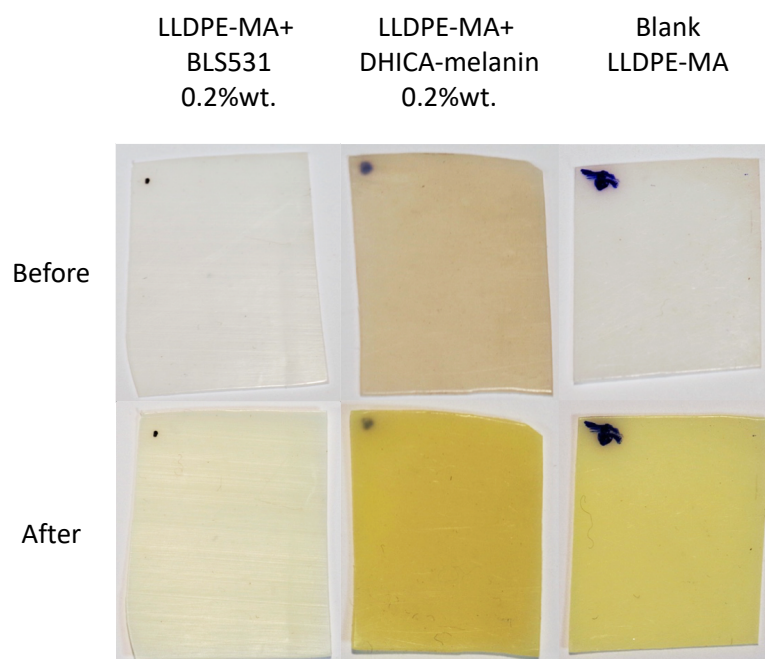


Figure 3.21: Comparison between the samples of LLDPE-MA before and after aging with different additives.

3.2.2 UV Exposure Effects

As mentioned in the Experimental Chapter 2.2.3 on page 54 the samples were aged in a UV chamber under the radiation from a lamp of 10 W/m^2 for 48 days. After that period, a detailed analysis was performed in order to understand the effects of the UV radiation on the polymers. Pictures before and after the aging test were taken to show if there would be a significant macroscopic visible effect on the color of the samples. It was observed that generally there was not a significant change of color of the exposed surfaces, with exception of the LLDPE-MA which clearly presented the typical yellow color of aged polymers, as can be seen from Figure 3.21. Only the commercial additive seems to preserve the initial color of the polymer under UV radiation for 48 days.

In order to obtain more specific and objective informations about the effect of the UV exposure, another data elaboration on the absorption with the spectrophotometer was performed. The elaboration on the *pseudo* α

showed that:

1. PCL: no improvement in the UVC region was detected. The peaks at 280 nm and 320 nm present before aging, disappeared. However, the samples with an higher percentage of melanin present a ratio between α after and before close to 1. The sample with commercial additive *BLS531* has no difference in wavelength of its peak, but the absolute value of *pseudo* α is shifted towards lower values.
2. EVA: also in this case, the peaks present before aging seems to disappear, but keeping the same absolute value. The sample with commercial additive presents the same behavior of the PCL and *BLS531*, shifting the peaks towards lower values in UV region (80 – 90%).
3. LLDPE: as in the previous cases, it was possible to notice the absence of the peaks observed in the analysis before aging, but the ratio between the coefficient of absorption after and before aging was getting closer to 1 : 1 increasing melanin content in the sample. *BLS531* presents again the same wavelength of the peak, but the absolute value of *pseudo* α is shifted towards lower values.
4. LLDPE-MA: the previous peaks at 270 nm and 315 nm disappear leaving a broad peak at 320 nm . A significative increase of the *pseudo* α in the UVA region is shown and, as aforementioned, it is the only polymer to turn into a yellow color, except for the sample with the commercial additive as shown in Figure 3.21.
5. LDPE-MA: in agreement with the other polymers, the peaks observed in the test before aging disappeared. With the increase of the melanin amount, the absolute value gets closer to the one before aging, or sometimes even higher. The commercial additive in this case has a reduction of absorption in the UV range and it seems that the cut-off point takes place earlier, so that there is a strong decrease of the absorption in UVA region.

6. EPC: again, the peaks at 270 nm and 315 nm of the case before aging disappeared. The increasing of melanin percentage brings the values of absorption closer to the before aging case. Furthermore, the *BLS531* shows a small reduction of *pseudo* α compared to the test before the aging.
7. PEMA: the blank polymer does not show the peak at 295 nm , but the absolute value remained the same. Also the samples with melanin present the same behavior, in which also the other peak that was present at 370 nm had a significant reduction. The additive *BLS531* manages to give a maximum reduction of *pseudo* α to 90% of its value before aging in the UV region.
8. PEEAMA: melanin seems to hinder the absorption reduction in the UVC and UVB regions. However, the samples with DHI-melanin and DHICA-melanin seem to have a decrease of the *pseudo* α in UVA region to the 50% and 40% of the previous values respectively for DHICA-melanin and DHI-melanin.

The FTIR analysis was performed on the same sample before and after the UV-Aging in order to evaluate if some surface modification occurred. This analysis is not finished yet, therefore just the graph for the LLDPE-MA, the only polymer clearly turned to yellow during the aging, with 0.2% *wt.* of DHICA is reported in Figure 3.22.

The spectra before aging is basically LLDPE, considering the low percentage of Maleic Anhydride (0.4 – 0.5%) and DHICA-melanin (0.2%). The spectra is not well understood yet, a process of identification of each peak is still requested. But, qualitatively, it is possible to identify some broad bands after the aging, mainly between $1800 - 700\text{ nm}$, which appears replacing sharper peaks. This behavior should indicate the presence of oxidation products due to the UV exposure, like the bonds $C = O$ or $C - O$.

This analysis is ongoing on all the samples in order to identify the aging functional groups and, furthermore, to verify the surface effect of aging, even if the external aspect is not significantly changed with respect of before aging case.

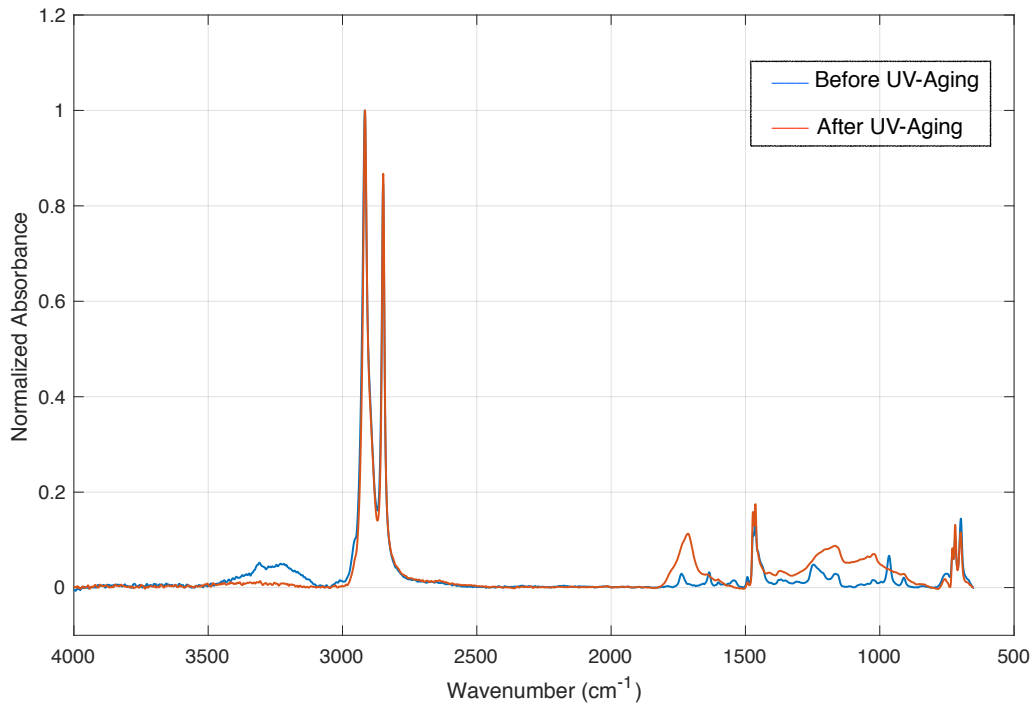


Figure 3.22: Comparison between the FTIR Absorbance spectra in LLDPE-MA polymer with 0.2% wt. DHICA-melanin before and after UV-Aging.

3.3 Biodegradability Analysis

As explained in the Chapter 2.3.1 on page 56, the results from the titration machine returns the volume of HCl needed to reach $pH = 7$ in the sample solution. In order to obtain data on the CO_2 evolved and on the mineralization, the following elaboration data procedure was performed.

According to the reaction 2.4 on page 57, the CO_2 evolved is in molar ratio 1 : 1 with the $Ba(OH)_2$ consumed. Hence, known the initial concentration, thus the moles (n), of barium hydroxide in the traps from the *As Prepared* solutions, it is easily computed the amount of the hydroxide consumed:

$$n_{(Ba(OH)_2)_{consumed}} = n_{(Ba(OH)_2)_{(t=0)}} - n_{(Ba(OH)_2)_{(t>0)}} \quad (3.3)$$

As just mentioned, the initial moles of barium hydroxide (at $t = 0$) are known. From the titration results it is possible to have information about the

last term of the formula 3.3: from the reaction 2.5 on page 60 it is possible to notice that the stoichiometry ration between $Ba(OH)_2$ and HCl is 1 : 2, thus it is easily deductible:

$$n_{(Ba(OH)_2)_{(t>0)}} = \frac{n_{HCl}}{2} \quad (3.4)$$

As aforementioned, the moles of CO_2 evolved are exactly the same of the moles of $Ba(OH)_2$ consumed, thus replacing it to the first term of Equation 3.3 and its last term with Equation 3.4, it is possible to obtain the moles (Equation 3.5) and the mass (Equation 3.6) of CO_2 evolved, knowing the molecular weight of CO_2 , 44 g/mol.

$$n_{(CO_2)_{evolved}} = n_{(Ba(OH)_2)_{(t=0)}} - \frac{n_{HCl}}{2} \quad (3.5)$$

$$m_{(CO_2)_{evolved}} = 44 * n_{(CO_2)_{evolved}} \quad (3.6)$$

The mass of CO_2 computed by Equation 3.6 refers to a single trap. Thus, the quantity of carbon anhydride evolved from a bioreactor will be the sum of the three values developed by the traps in series.

The value of percentage of biodegradation (called as aforementioned) is basically the ratio between the average of the grams of CO_2 evolved from the sample (the average between the triplicata of bioreactors containing the same material as explained in Chapter 2.3.1 on page 56) and the theoretical mass (in grams) of CO_2 evolved the same sample, as reported in Equation 3.7.

$$Mineralization (\%) = \frac{\overline{m_{(CO_2)_{evolved\ from\ the\ sample}}}}{m_{(CO_2)_{evolved\ theoretical}}} \quad (3.7)$$

It is important to notice that the numerator of the Equation 3.7 is referred only to the CO_2 developed from the sample: according to the reaction 2.3 on page 56, the CO_2 evolved from the vessel has two components: the one due the sample degradation but also the one evolved from the only compost. Thus, here it is the significance of testing bioreactors with only compost,

Table 3.2: % C in the structure of the molecules analyzed and their molecular weight

Name	Formula	% C
Poly(p-Phenylene Sulphide)	C ₆ H ₄ S	67
Copper (II) Phtalocyanine	C ₃₂ H ₁₆ CuN ₈	67
Polyethylene	CH ₂	94
Sepia Melanin(DHI 1.2 - DHICA)	(C ₈ H ₇ NO ₂)*1.2 + C ₉ H ₇ NO ₄	60
Cellulose	C ₆ H ₁₀ O ₅	44

from which it is possible to know the amount of CO_2 developed from the background (again, considering an average on the triplicata), which will be subtract from the values of carbon anhydride of the vessels in order to obtain the quantity effectively due to the degradation of the samples.

In order to have the value of the denominator, it is necessary to know the quantity of the carbon atoms in the molecule and the weight of material added, so the mass of carbons present in the samples is known. If this value is multiplied by 44/12 it is possible to obtain the theoretical vale of CO_2 evolved from the sample, considering the ideal reaction $C + O_2 \rightarrow CO_2$ in which 12 g of C yields 44 g of CO_2 . In the table 3.2 the percentage of carbon atoms and the molecular weight of each sample considered in the experiment is reported.

Therefore, the final formula to obtain the mineralization value is reported in Equation 3.8.

$$Mineralization (\%) = \frac{\overline{m(CO_2)}_{evolved\ from\ the\ vessel} - \overline{m(CO_2)}_{evolved\ from\ the\ blanks}}{(\% C) * m_{material} * \frac{44}{12}} \quad (3.8)$$

The graph of cumulative CO_2 evolved from the samples is shown in Figure 3.23, in which each trend is the result of the average between the values of the three bioreactors containing the same material. Regarding the Background and Sepia Melanin graphs, they were computed with an average between only two reactors after a certain point as one vessel for each batch had problems with the air flow which affected the cumulative production of

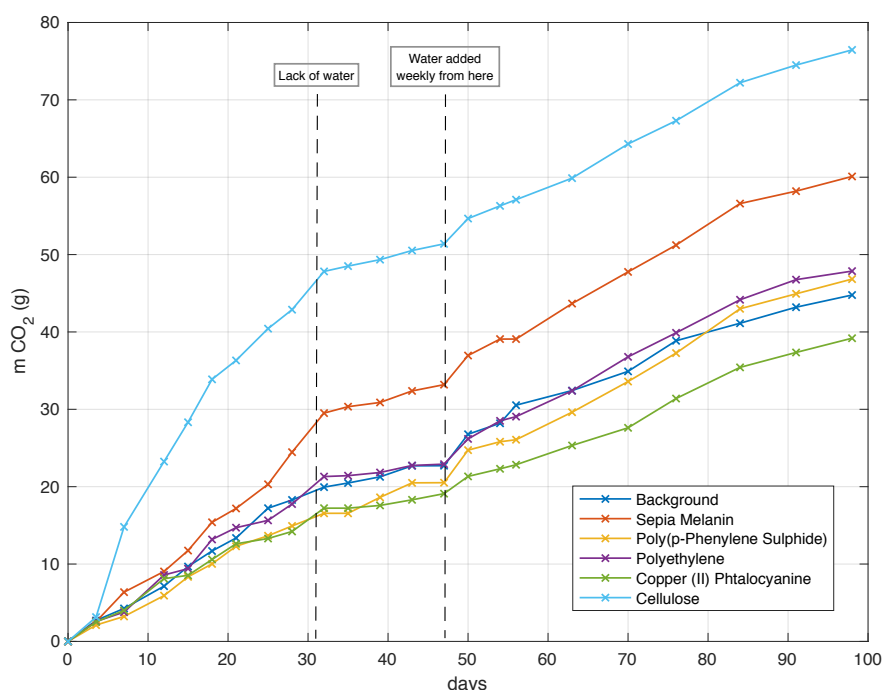


Figure 3.23: Cumulative CO_2 evolved from the reactors.

CO_2 .

It is evident from the Figure 3.23 how cellulose is the more “active” sample (as expected, it was chosen as positive control), reaching almost 80 g of CO_2 evolved in 100 days. Melanin it is not far, showing a production of carbon anhydride of 60 g during the experiment. However, the production of CO_2 cannot be considered alone as index of biodegradability, because it is strongly dependent on the percentage of carbon atoms in the structure of molecules (in fact, the mineralization considers in its formula this value).

If the biodegradation is not clearly evident yet, other features are noticeable: the trends of CO_2 evolved from the samples of Poly(p-Phenylene Sulphide) and Polyethylene are basically overlaid on the Background one. It clearly means that in those bioreactors the only contribution to the production of carbon dioxide is due to the microorganisms in the compost, therefore there is no degradation at all neither of Polyethylene (as expected, it was chosen as negative control), nor of Poly(p-Phenylene Sulphide).

Regarding Copper (II) Phtalocyanine, it shows a cumulative CO_2 lower than

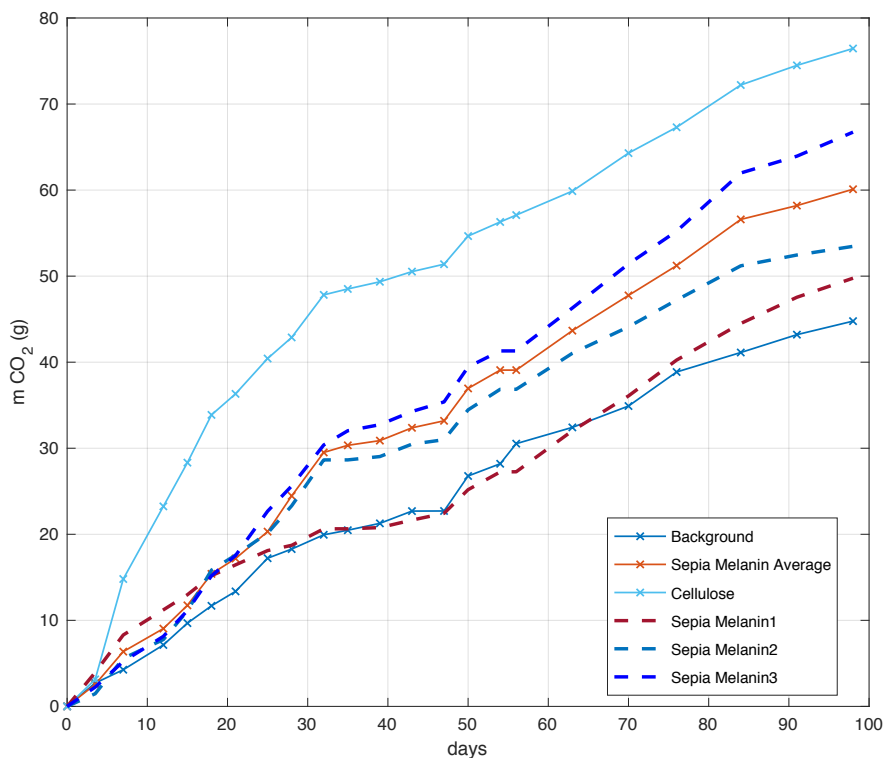


Figure 3.24: Focus on cumulative CO_2 evolved from the Sepia Melanin reactors compared to Cellulose and Background.

Background. This behavior is not well understood at the moment, but a first hypothesis could be that the copper in the molecule could have an inhibition effect on the microorganisms in the compost, hence their respiration will be slowed down. Other studies are required in order to understand if this hypothesis can be confirmed or refuted.

As pointed out in the Figure 3.23, between 30 and 50 *days* a plateau in the CO_2 evolution is evident. This characteristic is due to the lack of water in the bioreactors: around day 50 it was realized that a weekly insertion of water in the bioreactors was required, as mentioned in Chapter 2.3.2 on page 58, in order to guarantee the correct life conditions in the compost environment. After that, it is evident that the slope of the respiration started to increase again as expected.

The Figure 3.24 shows the aforementioned problem for the Sepia Melanin batch: one of the reactors with melanin had problems with the air flow

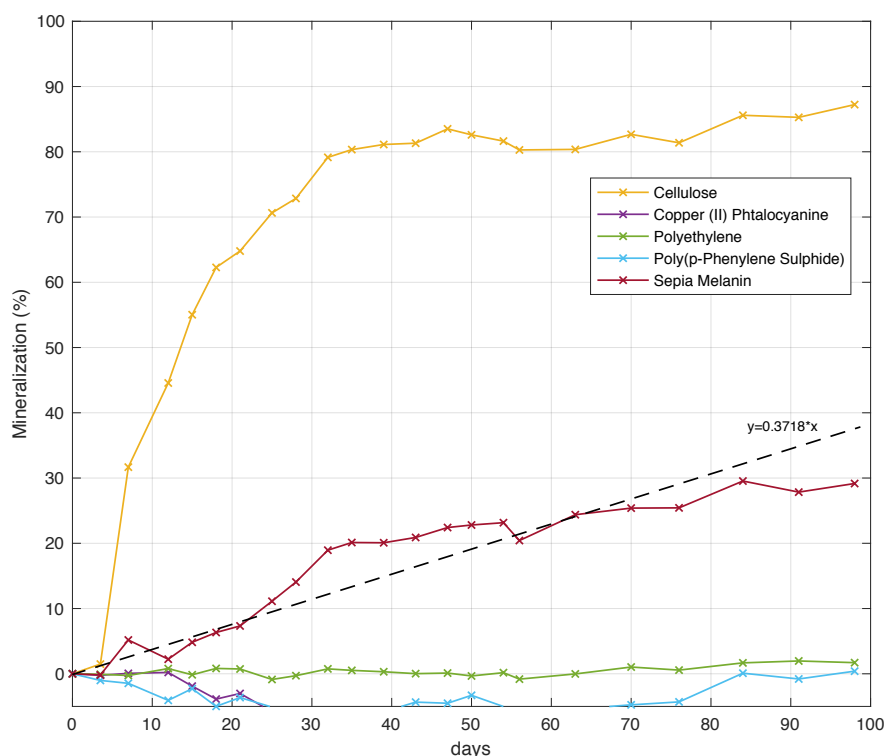


Figure 3.25: Mineralization of the samples.

system. Indeed, after 20 days it is possible to see that the trend of *Sepia Melanin1* is basically overlaid on the Background, thus it was excluded from the considerations on the *Sepia Melanin* behavior.

Therefore, in order to have information about the effective percentage of biodegradation of the samples, the graph is requested (Figure 3.25).

As aforementioned, the Cumulative CO_2 graph, Figure 3.23, does not give immediately information about biodegradability because it is not considering the percentage of carbon atoms in the molecules. On the other hand, the expression has at the denominator this information (Equation 3.8 on page 95): it is possible to observe how Cellulose, with the highest production of carbon dioxide during the experiment and the lowest % C in the molecule, reach the value of 87 % of degradation after 98 days and it seems to achieve a constant value around 90%, which agrees with the declared 90% of degradation in 180 days. In order to classify a material as *Biodegradable*, as mentioned in the Chapter 1.4 on page 31, it has to reach a certain threshold level in a cer-

tain time range. The threshold level is considered the 80% of the degradation of a reference material: in this case, the reference is the cellulose, therefore the other samples has to reach at least $0.8 * 90\% = 72\%$ of mineralization in 180 *days* to be considered biodegradable.

It is evident how Polyethylene, Poly(p-Phenylene Sulphide) and Copper (II) Phtalocyanine are not biodegradable: their mineralization level is zero in 98 *days*. According to the Equation 3.8 on page 95, negative values are possible only if the amount of CO_2 evolved from the bioreactors with only background is higher than the one from the vessels with the samples: as mentioned before, this is the case of Copper (II) Phtalocyanine, which presents in Figure 3.23 the cumulative CO_2 value lower than the background one. Regarding the Poly(p-Phenylene Sulphide) the assumes negative values, but they can be considered basically as zero considering the error that affects the measurements.

Regarding the samples of Sepia Melanin, a linear trend line with Excel was considered in order to fit the values of the average between the three bioreactors. The equation of linear fit of the Sepia Melanin Average is reported on the Figure 3.25: the slope of that line is 0.3718, which means that considering a period of 180 *days* is considered, the final value of mineralization would be $0.3718 * 180 = 66.92$ which would not be enough to reach the threshold level of 72%.

As already mentioned, the problem on the air flow in one Sepia Melanin bioreactor conditioned the average of the values of this sample. Therefore, again it was analyzed the behavior of each bioreactor separately (Figure 3.26) in order to verify the influence of that sample on the overall average. Following the same method adopted for the cumulative CO_2 graphs, a linear fit was applied to the data: as expected, the sample *Sepia Melanin1* has lost its significance after 20 *days*, therefore its data are useless for the global view. The best results are given by the sample *Sepia Melanin1*, whose linear fit has a value of slope of 0.4861, which means that in 180 *days* the mineralization level should be $180 * 0.4861 \approx 87.5\%$, hence it will be classified as biodegradable according to ASTM D5338. On the other hand, the sample *Sepia Melanin2* has not the same trend of the other one: indeed, the value expect-

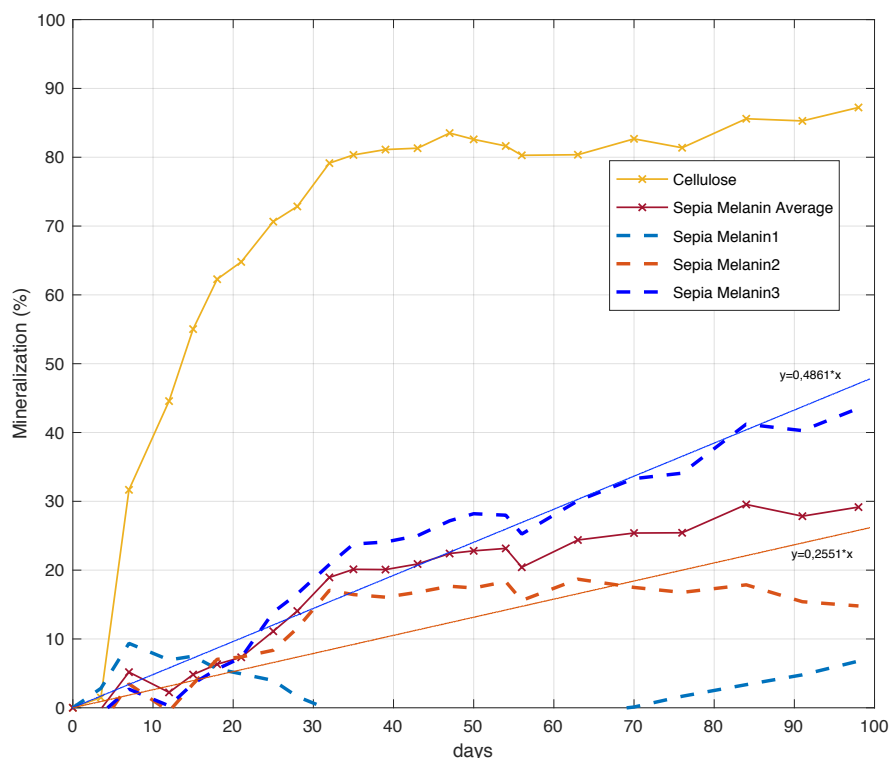


Figure 3.26: Focus on of the *Sepia Melanin* for each reactor.

ted with a linear approximation after 180 *days* should be $0.2551 * 180 \approx 46\%$, far from the target of 72%.

The key factors to understand how microorganisms digest eumelanin are the hygroscopic behavior of the pigment and its supramolecular structure²². The hydrophilicity of water allows an appropriate environment for the microorganisms to digest the material. But the stack of the oligomers of melanin in its supramolecular structure may not allow the enzymes of the organisms to reach all the levels of the molecule, so the process of degradation can occur only on the external part of each melanin particle. That phenomena could explain why melanin shows a constant rate of mineralization, differently from the cellulose, which reaches its maximum after 20 *days*, followed by a trend almost constant. The case of the curve *Sepia Melanin2* in Figure 3.26, in which it is possible to observe that the stopped after 30 *days*, could be explained with the presence of agglomerates of the pigment which prevented

the microorganisms to have access to the bulk of the structure.

Chapter 4

Conclusions and Perspectives

The properties of electrical conduction, in dark and under light conditions, UV-visible absorption and biodegradability of melanins were investigated in this project.

DHICA-melanin conductive behavior, polymerized directly on the substrate patterned with the electrodes, was investigated under different electrical bias, ambient and light conditions. Mostert¹³ and Wünsche¹⁴ results on conduction of hydrated melanin were confirmed immediately on DHICA-melanin film, because a current only with high water content in the film was observed. The charge transport mechanisms was identified with three main components: ionic conduction, electronic conduction whereas it cannot be excluded electrochemical processes.

The presence of a light source makes available a larger number of electrons by the excitation of the melanin molecules. The current under light conditions is between 4 – 5 times the one in dark conditions. Considering that the radiation spectra of the light source utilized in this experiment has a peak in the orange-red range, further tests in with a light source in the UV-blue visible range are suggested in order to evaluate the response of DHICA-melanin where this pigment has its peak of absorption of the radiation. Furthermore, the same test on DHI-melanin will be developed by other members in the group: the planar structure of the DHI-melanin is expected to give a better electron transport in the molecule, unlike the DHICA-melanin with

its disordinate organization. Nevertheless, on the other hand, the random placement of the monomers in DHICA-melanin is the responsible of a superior absorption behavior of the radiation. It will be interesting to understand if these preliminary hypothesis will be confirmed or not, and, if they are correct, which contribute is more significative.

The absorption properties of DHICA-melanin, DHI-melanin and Sepia Melanin were compared when used as additives in polymers with interest in packaging industry. The absorption of the radiation between 250 – 1400 *nm* was analyzed for eight different polymers (seven that are basically PE or copolymer of PE, and one PCL) with different percentages of the additives. A good enhancement of the UV-absorption properties of the polymers (between 2 – 20 times) was observed for the ones with polar groups in the structures (EVA, PCL, PEMA and PEEAMA), mainly with DHICA-melanin. The other polymers, with negligible or absent content of polar groups, did not show a significant enhancement of UV-absorption. Nevertheless, the ideal scenario of a strong enhancement in the only UV region in order to leave the visible region not affected, was achievable only with a commercial additive (BLS531), a benzophenone compound, classified dangerous for the health.

Possible improvements for this test regards both the sample fabrication, trying to produce more uniform samples with a better distribution, dispersion (MFA process developed to improve that), thickness, and the method for the characterization of the absorption spectra.

After that, a UV-chamber was used to understand the behavior of the polymers after 48 *days* of UV radiation. The expected situation of a decrease of the absorption coefficient (*pseudo* α) was generally true, but in any case the performance of the commercial additive *BLS531* seems to guarantee again a behavior closer to desired one, i.e. to keep the same absorption spectra before and after the UV-aging.

The great interest on melanin properties in green organic electronic was a motivation to start a biodegradability test on this molecule. In many articles it is possible to find a description of melanin as a *biodegradable pigment*, but actually nobody verified if melanin satisfies the standard requests (ASTM D5338-15) to be classified as biodegradable. Following the instructions in

the document ASTM D5338-15, which defines the test in controlled conditions, a system to test the biodegradability of Sepia Melanin and other two molecules with interest in green electronics (Copper (II) Phtalocyanine and Poly(p-Phenylene) Sulphide) were installed in order to capture the CO_2 developed by bioreactors, which contain compost and test material, in CO_2 traps in which $Ba(OH)_2$ captured the carbon dioxide.

After 98 *days* of test, it is difficult to give a conclusive response: the great difficulties in the management of the test lead to a significant error in the results. Only two samples of Sepia Melanin out of three could be analyzed due to technical problems to the air flow system of one bioreactor. One of them can be classified biodegradable, because it reaches the threshold percentage of mineralization (computed on the mineralization of cellulose, considered as positive control) in a certain time range. But the second one shows a different trend that doesn't allow to classify it as entirely biodegradable. This behavior can be explained with the high complexity of the molecule of melanin: it is not easy for the microorganisms to digest aggregates of molecules, in any case they need more time to do that. Another fundamental variable is the quantity of water in the compost: unfortunately it wasn't clear from the beginning that the bioreactors required a constant addition of water every week, leaving a dry compost for several days which is not ideal for the life of microorganisms.

The other two tested molecules (Copper (II) Phtalocyanine and Poly(p-Phenylene) Sulphide) were classified as non-biodegradable. Further studies are requested on Copper (II) Phtalocyanine to verify if there is the possibility that this molecule inhibits the organisms in the compost because it was noticed a cumulative CO_2 developed lower than the sample with only compost (Background).

In order to verify biodegradability also in ambient conditions, a Respirometry Test is actually ongoing.

Acknowledgements

Ringraziamenti

I want to express my gratitude to my supervisor and co-supervisor, Prof. Davide Fabiani and Prof. Clara Santato, for the incredible opportunity and for all the fundamental advices and lessons they gave me to write this thesis in the best way.

I want to express my gratitude also to Eduardo Di Mauro, to have taught me so many and for being a good friend both inside and outside the laboratory . I thank all the guys of the groups of research, Julien, Manuel, Abdelaziz, Xu, Tian, Dominic, Zhaojing, Ben, Nicolò, Côme, Tom, Yang and Arun for the great workplace I found.

I thank Dr. Denis Rho for all the biology lessons he gave me and for the interesting discussions.

Dedico questo lavoro alla mia famiglia, a mamma, babbo e a mia sorella Chiara, che mi hanno sempre sostenuto in tutti questi anni di studio e per avermi trasmesso la mentalità di impegno, serietà e umiltà sia nel mondo del lavoro che fuori fin da piccolo. È innegabile che gran parte del raggiungimento dei miei risultati siano frutto del loro sostegno, per il quale non li ringrazierò mai abbastanza.

Lo dedico alla mia Chiara, che mi ha sempre incitato a fare le mie esperienze, seppur mi abbiano portato lontano per un bel periodo, supportandomi con amore e comprensione nei momenti di difficoltà e di stress nello studio.

Bibliography

1. N. G. Jablonski, G. Chaplin, Human skin pigmentation as an adaptation to UV radiation. *PNAS* **107**, 8962–8968 (2010).
2. M. d’Ischia, et al., Melanins and melanogenesis: methods, standards, protocols. *Pigment Cell & Melanoma Research* **26**, 616–633 (2013).
3. E. Di Mauro, et al., Natural melanin pigments and their interfaces with metal ions and oxides: emerging concepts and technologies. *MRS Communications* **7**, 141–151 (2017).
4. L. Panzella, et al., Atypical Structural and π -Electrons Features of a Melanin Polymer that Lead to Superior Free-Radical-Scavenging Properties. *Angewandte* **52**, 12684–12687 (2013).
5. A. Pezzella, et al., Stem cell-compatible eumelanin biointerface fabricated by chemically controlled solid state polymerization. *Mater. Horiz.* **2**, 212–220 (2015).
6. P. Laube, *Semiconductor Technology from A to Z* (<https://www.halbleiter.org/en/>).
7. D. Fabiani, *Tecnologie Elettriche Innovative per allievi Ingegneri Elettrici ed Energetici*.
8. M. Graetzel, B. O’Regan, A low-cost, high efficiency solar cell based on dye-sensitized colloidal TiO₂ films. *Letters to Nature* **353**, 737–740 (2001).
9. M. Nazeeruddin, E. Baranoff, M. Graetzel, Dye-sensitized solar cells: A brief overview. *Solar Energy* **85**, 1172–1178 (2011).

10. J. Gong, K. Sumathy, Q. Qiao, Z. Zhou, Review on dye-sensitized solar cells (DSSCs): Advanced techniques and research trends. *Renewable and Sustainable Energy Reviews* **68**, 234–256 (2017).
11. J. E. McGinness, Mobility Gaps: A Mechanism for Band Gaps in Melanins. *Science* **177**, 896–897 (1972).
12. J. E. McGinness, et al., Amorphous Semiconductor Switching in Melanins. *Science* **183**, 853–855 (1974).
13. A. B. Mostert, et al., Role of semiconductivity and ion transport in the electrical conduction of melanin. *PNAS* **109**, 8943–8947 (2012).
14. W. Julia, et al., Eumelanin thin films: solution-processing, growth, and charge transport properties. *J. Mater. Chem. B* **1**, 3836–3842 (2013).
15. M. Jastrzebska, et al., Photoconductivity of synthetic dopa-melanin polymer. *Photochemistry and Photobiology B: Biology* **66**, 201–206 (2002).
16. M. L. Tran, et al., Chemical and structural Disorder in Eumelanins: A Possible Explanation for Broadband Absorbance. *Biophysical Journal* **90**, 743–752 (2006).
17. J.-W. Lee, et al., Dye-sensitized solar cells using purified squid ink nanoparticles coated on TiO_2 nanotubes/nanoparticles. *The Ceramic Society of Japan* **121** [1], 123–127 (2013).
18. Y. Wang, et al., Simultaneous Enhancement of UV-Shielding Properties and Photostability of Poly(vinyl alcohol) via Incorporation of Sepia Eumelanin. *ACS Sustainable Chemistry and Engineering* **4**, 2252–2258 (2016).
19. ASTM D5338, *Standard Test Method for Determining Aerobic Biodegradation of Plastic Materials Under Controlled Composting Conditions, Incorporating Thermophilic Temperatures*.
20. ASTM D6400, *Standard Specification for Labeling of Plastic Designed to be Aerobically Composted in Municipal or Industrial Facilities*.
21. ASTM 883, *Standard Terminology Relating to Plastics*.

22. L. G. Albano, et al., Novel insights on the physicochemical proprieties of eumelanins and their DMSO derivatives. *Society of Chemical Industry* **65**, 1315–1322 (2016).
23. G. Wypych, *Handbook of Polymers* (ChemTec Publishing, 2016).
24. M. Magarelli, et al., Purification, characterization and analysis of sepia melanin from commercial sepia ink (*Sepia Officinalis*). *Rev CES Med Vet Zootec* **5 (2)**, 18–28 (2010).
25. L. J. Wolfram, et al., The Mechanism of Hair Bleaching. *J. Soc. Cosmet. Chem.* **21**, 875–900 (1970).
26. K. Shanmuganathan, et al., Thermooxidative Stabilization of Polymers Using Natural and Synthetic Melanins. *Macromolecules* **44**, 9499–9507 (2011).